9-25-2020

# New Approaches for Isolation and Characterization of Extracellular Vesicles

Mehdi Dehghani
md3826@rit.edu

RIT

# New Approaches for Isolation and Characterization of Extracellular Vesicles

by
Mehdi Dehghani

A dissertation submitted in partial fulfillment of the requirements
for the degree of Doctorate of Philosophy in Microsystems Engineering

Microsystems Engineering Program
Kate Gleason College of Engineering

Rochester Institute of Technology
Rochester, New York
September 25, 2020

**New Approaches for Isolation and Characterization of Extracellular Vesicles**
**by**
**Mehdi Dehghani**

**Committee Approval:**

We, the undersigned committee members, certify that we have advised and/or supervised the candidate on the work described in this dissertation. We further certify that we have reviewed the dissertation manuscript and approve it in partial fulfillment of the requirements of the degree of Doctor of Philosophy in Microsystems Engineering.

_____

Dr. Thomas Gaborski — Date
Associate Professor, Biomedical Engineering

_____

Dr. Blanca Lapizco-Encinas — Date
Professor, Biomedical Engineering

_____

Dr. Michael Schertzer — Date
Associate Professor, Mechanical Engineering

_____

Dr. Vinay Abhyankar — Date
Assistant Professor, Biomedical Engineering

**Certified by:**

_____

Dr. Bruce Smith — Date
Director, Microsystems Engineering Program

_____

Typed Dean's Name — Date
Dean, Kate Gleason College of Engineering

# ABSTRACT

Kate Gleason College of Engineering
Rochester Institute of Technology

**Degree**: Doctor of Philosophy **Program**: Microsystems Engineering
**Author's Name: Mehdi Dehghani** **Advisor's Name: Dr. Thomas Gaborski**
**Dissertation Title:** New Approaches for Isolation and Characterization of Extracellular Vesicles

Extracellular vesicles (EVs) are membrane vesicles secreted by cells and distributed widely in all biofluids. Extracellular vesicles can modulate the biological activities of the recipient cells. Due to their role in intercellular communication, they are receiving attention for therapeutic and diagnostic applications. The first step to better understand EVs and to utilize them as therapeutic and diagnostic tools is to purify them from a variety of biofluids. Membranes have been extensively used for purification of different biological species from biological fluids. **As the first aim**, a novel microfluidic system, termed as tangential flow for analyte capture (TFAC) was developed to isolate nanoparticles and EVs using ultrathin nanomembranes. Ultrathin nanomembranes were found well-suited for TFAC system when compared with conventional thickness membranes. TFAC also proved feasible for capturing of EVs from undiluted plasma.

Fluorescent labeling of EVs has been employed for studying uptake and biodistribution of EVs. However, far too little attention has been paid to the effect of the fluorescent labeling on the size of EVs. **In the second aim**, the effect of PKH labeling, the most commonly used dye, on the size of EVs was systematically evaluated by nanoparticle tracking analysis (NTA). PKH labeling did not preserve the size of EVs and caused a size increase in all the PKH labeling conditions tested. The observed size shift may alter the uptake and biodistribution of EVs, suggesting that PKH labeling is not a reliable technique.

Precise quantification and characterization of EVs is an important step towards utilizing them as therapeutic and diagnostic tools. EVs have been analyzed using bulk techniques such as western blot which is challenging due to the heterogeneity of EVs. Therefore, a robust and well-established technique for quantification and characterization of individual EVs is required. **As the third aim**, the efficacy of a virus detection technology for EVs was evaluated. Virus Counter 3100 (VC3100) is a fluorescence-based technique with similar principles as flow cytometry and was purpose-built for detection of small nanoparticles such as viruses. Due to the similarity in size and density of viruses and EVs in many biofluids, it was hypothesized that the VC3100 could detect EVs similarly to flow cytometry characterization of cells. Fluorescently labeled EVs from different sources were successfully quantified by the VC3100. Furthermore, VC3100 was also used to determine the expression level of target protein markers. Therefore, VC3100 is a powerful technique for precise quantification and protein profiling of EVs.

# ACKNOWLEDGMENTS

First and foremost, I would like to express my special appreciation and thanks to my advisor, Dr. Thomas Gaborski who has been tremendous mentor for me. Dr. Gaborski has guided and pushed me every day to learn and achieve more from the first day. Ever since, Dr. Gaborski has supported me not only by providing a research assistantship, but also personally and emotionally through the rough road of my Ph.D. and away from my family for the last 5 years. I am always grateful for what he has done for me professionally and personally and will never forget that none of these would have been possible without him.

I would also like to thank Microsystems Engineering and Biomedical Engineering programs at RIT, especially Dr. Bruce Smith who introduced me to the program and helped me decide to pursue my Ph.D. and Lisa Zimmerman for all the help and support. I also appreciate the guidance of my committee members, Dr. Blanca Lapizco-Encinac, Dr. Michael Schertzer, and Dr. Vinay Abhyankar.

I would also like to acknowledge our collaborators, Dr. James McGrath group at University of Rochester. I have learned significantly from colleagues, particularly Henry Chung, Marcela Mireles, Kilean Lucas, and Stephanie Casilo. Additionally, Dr. James Roussie from SiMPore Inc. who helped me to find an amazing industrial internship position.

I would particularly like to thank Dr. David Pollard, Dr. Michael Olszowy and Dr. Rebecca Montange from Sartorius Stedim North America for their supports during my internship and the last aim of my thesis.

I would like to thank my parents, Sima Ghavami and Mohammad Karim Dehghani and my brothers, Ali, Reza, and Arash for their supports during all these 5 years of being away. And many thanks to my wonderful friends that I met during this journey who always cheered me up and were there for me when I needed them.

# Table of Contents

# List of Figures

# Chapter 1

## 1 Introduction and General Background

## 1.1 Extracellular Vesicles

All cell types are capable of shedding membrane-enclosed vesicles called extracellular vesicles (EVs) which were initially proposed as a means of discarding a cell's garbage [1]. However, two decades of research have provided evidence that EVs play a key role in intercellular communication and are more than just waste carriers [2]. EVs have been found from diverse bodily fluids including blood, urine, saliva, amniotic fluids, ascites, cerebrospinal fluid and breast milk [3,4]. Extracellular vesicles can be divided into three categories based on the current state of knowledge of their biogenesis; (i) Exosomes (ii) Microvesicles (iii) Apoptotic Bodies. A lipid bilayer membrane which encapsulates a cargo of biomolecules is the common feature in all the EV subtypes [2,5]. Exosomes (30-150 nm) are released via exocytosis from multivesicular bodies (MVBs) of the late endosome. Microvesicles (100 nm to 1 μm) directly bud from the cell's plasma membrane. Apoptotic bodies (50 nm to 1 μm) are released by cells undergoing apoptosis [2,6,7]. However, EV subtypes cannot be solely discriminated on the basis of intrinsic properties such as size, buoyant density and protein composition.

Extracellular vesicles (EVs) have received significant attention in recent decades due to their roles in physiological, therapeutic and pathological processes. EVs are known to be functionally involved in intercellular communications by various signaling pathways including delivery of cargo (RNA and proteins) into the recipient cells [2,8–10]. EVs in both unmodified and modified states have also been investigated as candidates for therapeutic agents in drug delivery applications [11,12]. From a clinical and diagnostic prospective, EVs are of interest as novel biomarkers for noninvasive detection and monitoring of diseases, since they are secreted in all

biological fluids such as blood, semen, urine, saliva and milk [5,13,14]. A comprehensive understanding of the EV properties will benefit their development as diagnostic and therapeutic tools.

## 1.2 Purification of Extracellular Vesicles

Interest in extracellular vesicles (EVs) for diagnostic and therapeutic applications has seen a meteoric rise in the past decade from biomarkers for breast, lung, and bladder cancer to drug delivery vehicles that can transport drugs across the blood-brain barrier [7,15–18]. Extracellular vesicles are found in all bodily fluids as well as cell culture supernatant [19]. However, in order to study these vesicles they must first be isolated. Despite the increasing clinical importance of EVs, current methods of EV isolation suffer from complicated procedures with long processing time [20]. The isolation of a pure population of EVs would facilitate studies regarding their physiological functions and their roles in various pathologies [21]. Additionally, contamination of EV preparations with non-EV proteins can lead to incorrect conclusions about their biological activities [22].

The “gold standard” method for isolating EVs from biofluids is ultracentrifugation, which requires large volumes of biofluids (>25 mL), long processing times, expensive instrumentation and trained technicians. In order to eliminate the requirements of ultracentrifugation, commercial EV isolation kits have been developed (e.g. ExoQuick® or Total Exosome Isolation™). These precipitation based techniques are hydrogel net based methods that are useful for isolating EVs in small volumes. However, these nets are non-specific and will co-precipitate proteins with the EVs [23]. Additionally, having intact EVs is very important for therapeutic applications, but these residual precipitation matrices could influence EVs biological activities [24,25]. Microfluidic devices have been developed to minimize the material

cost, energy consumption, sample sizes, and reaction time for isolation of EVs. The microfluidic-based platforms for EV isolation can be divided into three categories;

**Immunoaffinity-based Techniques**

Immunoaffinity-based techniques use antibody coated “capture surfaces” or “capture beads” to target specific surface markers of EV subpopulations [26]. Two main types of platforms for EV isolation have been developed based on functionalizing the surface including devices with coated inner surface [27–29] and devices that use capture beads [30–32] with great advantages such as reduced isolation time and high purity. However, these techniques suffer from major limitations such as cost, sample pretreatment, and non-specific sorption of nontarget EVs. Furthermore, affinity-based methods are not suitable for diagnostic applications because of isolating only known surface antigens (not all the EVs) as well as concerns regarding having intact EVs after elution off the complexes with antibodies [33–35].

**Contact-free Techniques**

Contact-free isolation of EVs has been demonstrated with many different mechanisms such as acoustic microfluidics [36–38] and nanoscale deterministic lateral displacement (nDLD) [39,40]. Both acoustic and nDLD sorting techniques have been successfully used for size separation of micron scale particles. Breakthroughs from the micro [41,42] to nanoscale using these technologies have been recently reported with promising potential in separation of nanoparticles and EVs. Precise separation of cancer-derived microvesicles from EVs [39] as well as separation of colloids and EVs [40] have been demonstrated using nDLD technology. However, these fabricated dense nanostructures may also result in blockage and decrease the throughput of the device and further studies are needed [26,33,34]. Separation of EVs from

whole blood was observed in acoustic-based microfluidics in two steps; the cell-removal step to first remove larger blood components followed by the EV-isolation step to purify EVs [38]. However, higher throughput and evaluation of the robustness of acoustic-based platforms with various bodily fluids are necessary. Furthermore, the purification of EVs from proteins is still challenging and requires further studies [26,33,34].

**Filtration-based Techniques**

These techniques use membranes with different pore size to allow smaller particles to pass through the membrane and particles larger than selected pore size to be retained and isolated. Filtration-based microfluidics have been recently developed for EV isolation and analysis featuring at least double filtration [43–45]. Larger EVs and impurities from urine samples were retained by a 200 nm membrane while small EVs were enriched by a 30 nm membrane which allows the proteins to pass through [44]. The ExoDisc system employed 20 and 600 nm pore sizes which could decrease the purity due to co-isolation of larger EVs [45]. Both systems achieved high throughput and good recovery. However, filtration based separations have disadvantages such as blockage of the membrane by protein molecules and formed aggregates which are hard to remove and potential deformation of EVs while passing through the membrane due to pressure [34,46]. Membranes used in filtration systems are often 'track-etch' membranes [43–45] which are made of a polymer (e.g. PET, PTFE, polycarbonate) and the pores are generated using a charged particle etching technique. While these membranes are widely used, their thickness (often > 6 μm) means that they have high transmembrane pressures under flow conditions and they also have very low permeabilities [47,48].

## 1.3 Fluorescent Labeling of Extracellular Vesicles

Since EVs are highly heterogeneous in their size, cargo, functional role and cells of origin, precise characterization and accurate imaging techniques are crucial for their diagnostic and therapeutic applications [49,50]. Advanced imaging and characterization technologies such as electron microscopy (EM) and atomic force microscopy (AFM) have been used for studying EVs, however challenges still exist due to the small size and complex nature of EVs [8,10]. Real-time imaging and tracking of EVs as well as direct and high throughput characterization are crucial and can provide valuable information in understanding the mechanisms at play during uptake and biodistribution. Fluorescent labeling of EVs has been employed to assist researchers in identifying and monitoring EVs both *in vitro* and *in vivo*.

### 1.3.1 Applications of Fluorescent Labeling of EVs

Using recent advances in fluorescent dyes for labeling EVs combined with high resolution characterization and imaging techniques, fluorescent labeling can be applied in the following studies:

#### 1.3.1.1 Uptake Studies

Since cellular functions can be modulated by EVs under both physiological and pathological conditions, the distinct mechanisms and pathways associated with the uptake of EVs by recipient cells needs to be explored [8,51]. Moreover, EVs can also be utilized to increase functional cargo delivery for therapeutic and drug delivery applications [10,11]. In order to understand the role of EVs in intercellular communication by transporting cargo between close and distant cells, uptake studies are crucial. Uptake studies have been performed by studying co-localization of labeled EVs with fluorescently labeled plasma membranes or intracellular components such as endosome and nuclei of the recipient cells [52]. Using fluorescent labeling, the internalization of EVs has been reported by a wide range of recipient cells such as dermal fibroblasts [53], dendritic cells [54], macrophages [14], myocardial cells and endothelial cells [55]. Furthermore, It has been shown that EVs can be internalized through multiple routes including, phagocytosis, macropinocytosis, and receptor-mediated endocytosis and fusion using fluorescent labeling [9,12].

#### 1.3.1.2 Biodistribution Studies

Secreted EVs by various cell types can be found in secreted biological fluids as well as the circulation system [13,49]. Studying the fate of EVs in circulation can provide valuable

information about the dynamic biological behavior of EVs such as determining whether EVs are targeting specific tissues and subsequently being internalized by their recipient cells or are getting cleared in the blood [49,56]. Furthermore, recent studies have provided evidence that EVs can promote tumor progression which also shows the importance of evaluating distribution and clearance of tumor-derived EVs [10,11,15]. EVs have also received attention as therapeutic agents due to their inherent ability to carry various biomolecules (e.g. RNA and proteins), their effective transport of their cargo to recipients cells, and their reduced toxicity and immunogenicity compared to artificial delivery vehicles [12,49,57]. Therefore, investigating the *in vivo* distribution, accumulation and tracking of therapeutic EVs is desired for their safety and efficacy in therapeutic and drug delivery applications of EVs [56,58].

#### 1.3.1.3 Characterization Studies

The abundance of a specific EVs in biological fluids has been linked with various diseases and cancers such as and cardiovascular disease [59], lung [60], ovarian cancer [61], kidney and breast cancers [62], which makes them attractive candidates for biomarkers in non-invasive liquid biopsies [63,64]. Moreover, therapeutic applications of EVs have received significant attention by researchers recently to develop new treatments for cancer [13,65]. For both therapeutic and diagnostic applications of EVs, better understanding and knowledge of different subclasses and functional differences is required [12,13,65].

Molecular composition of EVs has been analyzed using bulk based techniques such as proteomics, lipidomics and western blot. However, small size and heterogeneity of EVs hamper these quantitative analyses [57,66]. Alternatively, single EV analysis techniques such as immunoelectron microscopy and atomic force microscopy have been applied to study

biomarker profiling and their potential clinical applications, but are still time consuming [64]. High-resolution flow cytometry has also been used for analyzing single EVs [67,68]. Small size and low refractive index of EVs is problematic in scattering based flow cytometry, which results in low sensitivity of the system [64,69,70]. Moreover, High background signal due to using sheath and sample buffers as well as the presence of non-EV artifacts is another challenge to resolve true biological EVs from instrument noise [13,71]. As an alternative, fluorescent based detection of EVs has been employed to analyze EVs which is independent of size, refractive index and is less affected by the background signal [63,65,71]. Nanoparticle tracking analysis (NTA) as a single EV analysis technique, has been applied to determine the size and concentration of EVs [63,65,71]. However, NTA quantitative analysis is less accurate in heterogeneous samples in terms of concentration and has limited ability to characterize different parameters simultaneously [57,64,66,70].

### 1.3.2 EV Labeling Approaches

EVs can be fluorescently labeled for uptake, biodistribution and characterization studies of EVs by different fluorescent dyes such as:

#### 1.3.2.1 Surface marker labeling of EVs:

Proteins on the membrane surface can be fluorescently labeled to track cell-cell communication, determine their biodistribution and identify the phenotype subset of EVs by flow cytometry. Tetraspanins such as CD9, CD63 and CD81 are abundant on the surface of many EV types and are known as common markers of EVs, which have been labeled fluorescently using primary and secondary antibodies [72]. In addition, surface proteins on membranes of EVs can be also fluorescently labeled non-specifically by conjugating fluorophores with different functional groups such as TAMARA and Alexa Flour bound with N-hydroxy succinimidyl (NHS) ester which covalently bond with amine groups on proteins [73,74]. In addition to flow cytometry for identifying the phenotype subset of EVs, other techniques have been developed for single EV analysis [75]. Using a microfluidic device, the authors first captured EVs on the device surface coated with neutravidin. Then, captured EVs were labeled by fluorescent antibodies such as CD9, CD63 and CD81 and then imaged to identify their marker expression profile [75].

#### 1.3.2.2 Lipid Membrane Labeling of EVs:

The plasma membrane of EVs can be labeled using lipophilic dyes. PKH family [64,76,77], DiI/DiR/DiD dyes [52,56,78], and FM dye [79], are commonly used lipid membrane dyes to label EVs due to their stable fluorescent signal and simple labeling process. Among lipid membrane

dyes, the PKH family has been the most extensively used dye for labeling EVs in uptake, biodistribution and flow cytometry characterization of EVs. PKH dyes are lipophilic long-chain carbocyanine dyes that rapidly intercalate into lipid structures (biological and artificial) and form noncovalent interactions leading to a bright and stable labeling [50,80].

One study reported biochemical evidences that the internalization of EVs derived from glioblastoma multiforme (GBM) cell line depends on cell-surface heparan sulfate proteoglycans [81]. The authors labeled GBM derived EVs with PKH26 and found a dose dependent and saturable internalization of EVs using flow cytometry and confocal fluorescence microscopy [81]. In another study, PKH labeling was employed to evaluate the interaction of platelet derived EVs with human brain endothelial cells using confocal microscopy and reported that the internalization is driven by endocytosis [76]. Moreover, The transfer mechanism of EVs was addressed from oligodendroglia cells to target cells and confocal microscopy analysis of PKH labeled EVs showed their internalization and transfer to late endosome and lysosome of microglia cells [82].

PKH labeling was also applied to investigate the effect of EVs derived from MSCs on an immune-induced liver model [83]. The authors observed co-localization of PKH and CD81 in the injured liver specimen and showed promising therapeutic potentials of MSC derived EVs [83]. Furthermore, therapeutic potentials of EVs were investigated as drug delivery carriers in a cancer model by labeling EVs with PKH67 and showed the uptake of EVs by breast cancer cell lines for 4 hours using flow cytometry and confocal electron microscopy [77]. Biodistribution of human cancer has been characterized by PKH labeling of cell-line-derived E in the lung and liver

of mice [84]. The authors used near infrared (NIR) whole-lung imaging of lung and fluorescent microscopy of lung, liver and brain to trace PKH-labeled EVs [84].

PKH labeling has been also used for characterization of EVs using flow cytometry. A novel flow cytometry-based method was developed to quantify nanosized particles like EVs derived from Dendritic and T cells [64]. PKH family was also used to demonstrate the effect of non-EV particles in plasma which can lead to false positive signals using light scattering and even fluorescent detection of low-abundance PKH67 labeled EVs due to coincidence and swarm by fluorescence-based flow cytometry [71]. However, the authors identified potential solutions by monitoring the undesired particles in serial dilutions [71]. Another study provided a step by step protocol for quantitative and qualitative analysis of EVs by high resolution microscopy. The authors reported that PKH67 dye brightly labels EVs and can be detected above a fluorescent threshold that eliminates non-fluorescent noise [85].

#### 1.3.2.3 Luminal labeling of EVs:

The lumen of EVs can be fluorescently labeled using membrane permeable dyes such as the acetomethoxy derivative of calcein (Calcein AM) and carboxyfluorescein diacetate succinimidyl ester (CFDA-SE, hereinafter CFSE). These chemical compounds become fluorescent and EV-impermeable in their hydrolyzed forms. Similar to cells, the presence of esterases inside EVs catalyzes the cleavage of CFSE acetate groups leading to fluorescent labeling of EVs [86].

CFSE labeling has been used to study the effect of lung derived EVs in the development of marrow cell-based cellular therapies, internalization of CFSE labeled EVs has been shown by stem/progenitor cells and different differentiated cell types such as granulocytes, B cells and erythroid cells using fluorescent microscopy [87]. In another study, CFSE labeled EVs were

incubated with prostate PC-3 tumor cells to investigate the effect of human bone marrow-derived EVs on prostate cancer [88]. The authors observed localization of CFSE-labeled EVs in the cytoplasm of cancer cells in a time dependent manner suggesting uptake of EVs [88]. Different uptake mechanisms of labeled EVs has been also studied using immunofluorescence microscopy and flow cytometry analysis using CFSE labeled EVs derived from ovarian cancer cells [89]. Another group determined the target organelle after EV internalization by confocal microscopy and found colocalization of CFSE labeled EVs with endosomes and lysosomes suggesting their involvement in an endocytic pathway [52]. In another study, a novel and fast protocol was presented for quantification and characterization of EVs using CFSE labeling by a flow cytometer specifically designed for small particles [79]. Furthermore, the effect of particles concentration on the performance of the high resolution flow cytometry for EVs characterization was explored by CFSE as a generic labeling of EVs [13].

### 1.3.3 Post-labeling Clean-up

In fluorescent based studies of EVs, there is always a concern that the signal detected is from unbound dye and not labeled EVs [78]. In uptake studies, the excess dye can interact with the recipient cells, which increases the background signal and can result in false positive events affecting the accuracy of the uptake studies [8,80,81,90]. A common approach to study the possibility of false positive signals from free dye is to process a dye-only control (without EVs) and observe the fluorescent intensity in the recipient cell [90]. In biodistribution studies, especially using lipophilic dyes, free dye can non-specifically bind to non-EV lipid structures leading to false positive signals. Additionally, since lipophilic dyes are estimated to have a longer half-life compared to EVs, they can remain in tissue even after the clearance of EVs [15,51]. In characterization studies of EVs using flow cytometry, unbound dye can contribute to the background signal and decrease the signal to noise ratio resulting in inaccurate analysis of EV samples [16,71,91]. Moreover, given the fact that the EV samples are not completely pure and contain proteins, protein aggregates and other contaminants, free dye can interact with these non-EV complexes and interfere with fluorescent labeled EVs. Therefore, in order to make a reliable conclusion in uptake, biodistribution and characterization studies of EVs by fluorescent labeling, a post-labeling step for removing the unbound fluorescent dye is required. Different techniques have been employed to separate labeled EVs from unincorporated dye including differential ultracentrifugation, density gradient centrifugation, size exclusion chromatography, and filtration.

#### 1.3.3.1 Differential Ultracentrifugation:

Ultracentrifugation has been widely used for isolation of EVs in biological fluids and cell culture conditioned media [20]. Using the same principle, It has been reported that labeled EVs can be separated from free dye by ultracentrifugation (~100,000 g and for at least an hour) [80,92]. The time of centrifugation is defined by properties of the rotor used and needs to be adjusted to achieve similar results between studies [93]. For example, removing of unbound dyes has been reported using differential ultracentrifugation from PKH26 labeled EVs at 100,000 g for 70 minutes [80] and from DiO, DiR and FM labeled EVs at 120,000 g for 90 minutes [92].

#### 1.3.3.2 Density Gradient Centrifugation:

Similarly, density gradient centrifugation can be applied to separate labeled EVs from protein aggregates, free dyes and antibodies based on their buoyant density [20]. Density gradient technique requires 14 – 20 hours centrifugation at high forces (~ 200,000 g) to separate labeled EVs from free dyes [13,64,71,78]. Fluorescently labeled EVs equilibrate and can be collected at representative sucrose density of EVs (1.11 – 1.2 g/mL) without free dyes which have a lower buoyant density [64]. For instance, PKH67 labeled EVs have been successfully separated from free dyes and protein aggregates by overnight density gradient centrifugation at 270,000 g to demonstrate how non-EV particles in plasma can affect the fluorescent detection of EVs using high resolution flow cytometry [71]. DiR labeled EVs have also been purified from unbound dyes using sucrose gradient ultracentrifugation at 200,000 g for 16 hours [78].

#### 1.3.3.3 Size Exclusion Chromatography:

Size exclusion chromatography (SEC) is a powerful technique to enrich and isolate EVs from non-EV contaminates such as proteins and subsets of plasma lipoproteins based on size differences [20]. SEC has also been widely applied to remove free dye and unincorporated fluorophore conjugated antibodies from fluorescently labeled EVs [16,73,94,95]. For example, labeled EVs have been successfully separated from free Alexa Fluor 488 NHS [73] and DiR dyes [95] using SEC packed with Sepharose CL-4B. Unbound CFSE dyes have been also removed using PD-10 columns to detect tumor derived EVs with nanoscale fluorescent based flow cytometry [16,96]. The authors reported a detectable background noise from CFSE-alone controls due to spontaneous hydrolysis of CFSE dye. However, after removal of free CFSE using SEC, they observed an increase in the signal to noise ratio of EVs labeled with CFSE [16].

#### 1.3.3.4 Filtration:

Filtration has been used for separation of different size particles including EVs [20,97]. Filtration combined with low speed centrifugation has been also used for removing free dye from labeled EVs [13,14,52,74]. For example, PKH67 labeled EV samples at 4000 g has been removed the excess PKH dye by centrifugation through 300 KDa Viva-spin filters to study the uptake of EVs derived from human saliva, plasma and breast milk by macrophage [14]. The free dyes have been also filtered from R18 and TAMRA-NHS labeled EVs using 300 KDa [52] and 100 KDa [74] ultrafiltration membranes, respectively. In another study, 0.2 μm centrifugal filters were used to remove unbound antibodies by centrifugation at 600 g for 2-5 minutes [65].

Each of these techniques for removing unbound dye has their own advantages and disadvantages and few studies have paid attention to the efficiency and purity of these techniques. The differential ultracentrifugation has been reported not sufficient to remove free dye aggregates whereas a density gradient was found necessary to remove free dye and dye aggregates from PKH67 labeled EVs [64,85]. In another study, higher removal efficiency of unbound CFSE dyes using SEC was reported compared to differential and density gradient ultracentrifugation [16]. These post labeling techniques are usually time and sample consuming, expensive and can cause undesired variation in the EV samples such as aggregation [57], which can be problematic for biodistribution, uptake and characterization studies. Filtration is a relatively fast and low-cost technique for removing excess dye, but has a low yield especially since EVs that are smaller than the pore size of the membranes can be lost and dye and protein aggregates larger than EVs can be retained [65]. In summary, the efficiency and yield of these techniques still need to be systematically explored and compared.

### 1.3.4 Pros and Cons of Fluorescent Labeling Approaches

#### 1.3.4.1 Surface Marker Labeling

Affinity-based labeling is the only labeling technique that can be considered 100% specific to EVs expressing the protein of interest. Combing surface marker labeling with a generic label can be used to identify the marker expression level of EVs using flow cytometry. However, the fluorescent intensity due to surface marker labeling depends on *(i)* the expression level of the target proteins, *(ii)* the efficiency of the labeling process, *(iii)* the light source excitation strength and the fluorescent dye quantum yield [90,98,99]. Additionally, the effect of labeling surface proteins on the uptake of EVs needs to be investigated since surface proteins are involved in the internalization of EVs [50,66]. Also, the surface protein labeling is limited in biodistribution studies since they tend to have a lower signal compared to other labeling techniques [15]. One other challenge with protein labeling of EVs is that antibodies tend to aggregate, therefore, removal of these antibody aggregates is crucial before labeling EVs. Removal of antibody aggregates has been reported by centrifugation at 16,000 g for 2-20 minutes [57,85,100].

#### 1.3.4.2 Lipid Membrane Labeling:

Membrane dyes can be considered as generic markers since all EVs are membrane-enclosed vesicles. Due to the number of incorporated dye molecules, lipid-labeled EVs are also relatively bright and stable with a simple labeling process. However, recent studies have shown that lipophilic dyes tend to form aggregation and micelle formation which are in the same size range as EVs and are indistinguishable from EVs and can result in false positive results. Membrane dyes are not specific to EVs, since they can also label lipoproteins or even debris. Also, a higher

signal from labeling cell-free culture medium (as a negative control) compared to PKH-labeled EVs has been reported [99]. Similarly, specificity of lipophilic dyes for labeling EVs and contaminant artifacts such as lipoproteins and free proteins has been evaluated by fractionating rat blood plasma or conditioned cell culture media using size exclusion chromatography (SEC) [90]. The authors reported the significant contribution of non-EV contaminants in uptake studies suggesting that lipophilic dyes are not specific to EVs and not ideal unless a completely pure population of EVs is labeled [90]. Non-specificity of lipophilic dyes can also result in labeling the target cells in uptake studies [2,15].

One other challenge of lipophilic dyes is their long *in vivo* half-life (5-100 days for PKH and 4 weeks for DiR) for biodistribution studies. The long half-life of lipophilic dyes results in the persistence of lipophilic dyes in tissues for long periods even after the clearance and degradation of EVs leading to inaccurate determination of EV fate [15,49,50,74]. The effect of lipophilic dyes on surface properties of EVs also needs to be explored which could lead to changes in EV internalization [66].

#### 1.3.4.3 Luminal Labeling:

As opposed to lipophilic dyes, luminal dyes like CFSE do not tend to aggregate and form micelles. Another luminal dye, Calcein, has been used to differentiate between intact EVs and membrane fragments or other debris using flow cytometry [100]. In order to do so, they used Triton 100-X and saponin to permeabilize EVs derived from human plasma, red blood cells and conditioned media of human aortic endothelial cells. The authors found that calcein AM does not label permeabilized/lysed EVs as opposed to PKH67 lipophilic labeling [100].

However, it is important to note that esterase activity in all subtypes of EVs needs to be explored to determine the typical efficiency to hydrolyze the markers within EVs. In fact, a study on different generic markers for labeling EVs from breast cancer cells using flow cytometry revealed low sensitivity of calcein AM which could be due to insufficient esterase activity or low brightness of the labeled EVs for the system used [91]. Additionally, the authors were not able to study CFSE due to the swarm detection and insufficient event rates even after removal of excess dye using size exclusion chromatography [91]. Moreover, another study found that CFSE dye might also label lipoproteins and lipoproteins-like particles in complex fluids and recommended a combination of CFSE with a surface marker of EVs to enhance the specificity of the characterization of EVs using flow cytometry [101].

## 1.4 Thesis Outline and Research Objectives

In this work, following aims were defined and achieved focusing on isolation and characterization of extracellular vesicles;

#### 1.4.1.1 Aim 1 – Tangential Flow for Analyte Capture of Extracellular Vesicles

A novel microfluidic based method, termed as tangential flow for analyte capture (TFAC), was developed for purification of extracellular vesicles using ultrathin nanomembranes. EVs from undiluted plasma were successfully captured using nanoporous silicon nitride (NPN) membranes. The performance of ultrathin nanomembranes was compared with conventional thickness membranes in this technique. NPN membranes were found ideal for this technique with higher capturing and releasing efficiency compared to conventional thickness membranes such as polycarbonate membranes.

#### 1.4.1.2 Aim 2 – Systematic Evaluation of PKH labeling on Extracellular Vesicles Size by Nanoparticle Tracking Analysis

In this aim, the effect of PKH labeling, as the most commonly used dye, on the size of extracellular vesicles was systematically evaluated using nanoparticle tracking analysis (NTA). A size shift towards larger particles was found after PKH labeling of EVs, which could affect their uptake and biodistribution efficiency and mechanism. As opposed to PKH labeling, the size of EVs was preserved suggesting that CFSE is a more reliable dye for labeling EVs without affecting their size.

#### 1.4.1.3 Aim 3 – The efficacy of the Virus Counter 3100 for detection of EVs

In the last aim, precise quantification and characterization of EVs was performed using the virus counter 3100. The performance of VC3100 was compared with NTA and VC3100 was found ideal for precise quantification of nanoparticles in heterogenous samples such as EVs. Furthermore, single EVs from six different sources were successfully quantified by VC3100 using CellMask Orange dye. Protein profiling of EVs by VC3100 was also shown using PE conjugated CD9, CD63, and CD81 which are common exosome markers.

## 1.5 References


[1] R.M. Johnstone, M. Adam, J.R. Hammond, L. Orr, C. Turbide, Vesicle formation during reticulocyte maturation. Association of plasma membrane activities with released vesicles (exosomes)., J. Biol. Chem. 262 (1987) 9412–9420. doi:10.1016/j.biocel.2011.10.005.

[2] G. Van Niel, G. D'Angelo, G. Raposo, Shedding light on the cell biology of extracellular vesicles, Nat. Rev. Mol. Cell Biol. 19 (2018) 213–228. doi:10.1038/nrm.2017.125.

[3] J. Kowal, M. Tkach, C. Théry, Biogenesis and secretion of exosomes, Curr. Opin. Cell Biol. 29 (2014) 116–125. doi:10.1016/j.ceb.2014.05.004.

[4] M. Colombo, G. Raposo, C. Théry, Biogenesis, Secretion, and Intercellular Interactions of Exosomes and Other Extracellular Vesicles, Annu. Rev. Cell Dev. Biol. 30 (2014) 255–289. doi:10.1146/annurev-cellbio-101512-122326.

[5] H. Kalra, G.P.C. Drummen, S. Mathivanan, Focus on extracellular vesicles: Introducing the next small big thing, Int. J. Mol. Sci. 17 (2016). doi:10.3390/ijms17020170.

[6] L. Urbanelli, A. Magini, S. Buratta, A. Brozzi, K. Sagini, A. Polchi, B. Tancini, C. Emiliani, Signaling pathways in exosomes biogenesis, secretion and fate, Genes (Basel). 4 (2013) 152–170. doi:10.3390/genes4020152.

[7] S. Roy, F.H. Hochberg, P.S. Jones, Extracellular vesicles: the growth as diagnostics and therapeutics; a survey, J. Extracell. Vesicles. 7 (2018). doi:10.1080/20013078.2018.1438720.

[8] A. Mondal, K.A. Ashiq, P. Phulpagar, D.K. Singh, A. Shiras, Effective Visualization and Easy Tracking of Extracellular Vesicles in Glioma Cells, Biol. Proced. Online. 21 (2019) 1–12. doi:10.1186/s12575-019-0092-2.

[9] L.A. Mulcahy, R.C. Pink, D.R.F. Carter, Routes and mechanisms of extracellular vesicle uptake, J. Extracell. Vesicles. 3 (2014) 1–14. doi:10.3402/jev.v3.24641.

[10] and R.D. Pauline Carnell-Morris, Dionne Tannetta, Agnieszka Siupa, Patrick Hole, Extracellular Vesicles, Methods and Protocols - Chapter 13; Analysis of Extracellular Vesicles Using Fluorescence Nanoparticle Tracking Analysis., 2017. doi:10.1016/j.semcdb.2017.05.016.

[11] R. Kalluri, V.S. LeBleu, The biology, function, and biomedical applications of exosomes., Science. 367 (2020). doi:10.1126/science.aau6977.

[12] D.E. Murphy, O.G. de Jong, M. Brouwer, M.J. Wood, G. Lavieu, R.M. Schiffelers, P. Vader, Extracellular vesicle-based therapeutics: natural versus engineered targeting and trafficking, Exp. Mol. Med. 51 (2019). doi:10.1038/s12276-019-0223-5.

[13] T.G. Kormelink, G.J.A. Arkesteijn, F.A. Nauwelaers, G. van den Engh, E.N.M. Nolte-'t Hoen, M.H.M. Wauben, Prerequisites for the analysis and sorting of extracellular vesicle subpopulations by high-resolution flow cytometry, Cytom. Part A. 89 (2016) 135–147. doi:10.1002/cyto.a.22644.

[14] C. Lässer, V. Seyed Alikhani, K. Ekström, M. Eldh, P. Torregrosa Paredes, A. Bossios, M. Sjöstrand, S. Gabrielsson, J. Lötvall, H. Valadi, Human saliva, plasma and breast milk exosomes contain RNA: Uptake by macrophages, J. Transl. Med. 9 (2011) 1–8. doi:10.1186/1479-5876-9-9.

[15] P. Gangadaran, C.M. Hong, B.C. Ahn, An update on in vivo imaging of extracellular vesicles as drug delivery vehicles, Front. Pharmacol. 9 (2018) 1–14. doi:10.3389/fphar.2018.00169.

[16] A. Morales-Kastresana, B. Telford, T.A. Musich, K. McKinnon, C. Clayborne, Z. Braig, A. Rosner, T. Demberg, D.C. Watson, T.S. Karpova, G.J. Freeman, R.H. Dekruyff, G.N. Pavlakis, M. Terabe, M. Robert-Guroff, J.A. Berzofsky, J.C. Jones, Labeling extracellular vesicles for nanoscale flow cytometry, Sci. Rep. 7 (2017) 1–10. doi:10.1038/s41598-017-01731-2.

[17] K.O. Jung, H. Youn, C.H. Lee, K.W. Kang, J.K. Chung, Visualization of exosome-mediated miR-210 transfer from hypoxic tumor cells, Oncotarget. 8 (2017) 9899–9910. doi:10.18632/oncotarget.14247.

[18] D. Ha, N. Yang, V. Nadithe, Exosomes as therapeutic drug carriers and delivery vehicles across biological membranes: current perspectives and future challenges, Acta Pharm. Sin. B. 6 (2016) 287–296. doi:10.1016/j.apsb.2016.02.001.

[19] M.I. Ramirez, M.G. Amorim, C. Gadelha, I. Milic, J.A. Welsh, V.M. Freitas, M. Nawaz, N. Akbar, Y. Couch, L. Makin, F. Cooke, A.L. Vettore, P.X. Batista, R. Freezor, J.A. Pezuk, L. Rosa-Fernandes, A.C.O. Carreira, A. Devitt, L. Jacobs, I.T. Silva, G. Coakley, D.N. Nunes, D. Carter, G. Palmisano, E. Dias-Neto, Technical

challenges of working with extracellular vesicles, Nanoscale. 10 (2018) 881–906. doi:10.1039/c7nr08360b.
[20] M.I. Ramirez, M.G. Amorim, C. Gadelha, I. Milic, J.A. Welsh, V.M. Freitas, M. Nawaz, N. Akbar, Y. Couch, L. Makin, F. Cooke, A.L. Vettore, P.X. Batista, R. Freezor, J.A. Pezuk, L. Rosa-Fernandes, A.C.O. Carreira, A. Devitt, L. Jacobs, I.T. Silva, G. Coakley, D.N. Nunes, D. Carter, G. Palmisano, E. Dias-Neto, Technical challenges of working with extracellular vesicles, Nanoscale. 10 (2018) 881–906. doi:10.1039/c7nr08360b.
[21] A. Rana, Y. Zhang, L. Esfandiari, Advancements in microfluidic technologies for isolation and early detection of circulating cancer-related biomarkers., Analyst. (2018) 2971–2991. doi:10.1039/c7an01965c.
[22] F. Liu, O. Vermesh, V. Mani, T.J. Ge, S.J. Madsen, A. Sabour, E.C. Hsu, G. Gowrishankar, M. Kanada, J. V. Jokerst, R.G. Sierra, E. Chang, K. Lau, K. Sridhar, A. Bermudez, S.J. Pitteri, T. Stoyanova, R. Sinclair, V.S. Nair, S.S. Gambhir, U. Demirci, The Exosome Total Isolation Chip, ACS Nano. 11 (2017) 10712–10723. doi:10.1021/acsnano.7b04878.
[23] D.D. Taylor, S. Shah, Methods of isolating extracellular vesicles impact down-stream analyses of their cargoes, Methods. 87 (2015) 3–10. doi:10.1016/j.ymeth.2015.02.019.
[24] L. Paolini, A. Zendrini, G. Di Noto, S. Busatto, E. Lottini, A. Radeghieri, A. Dossi, A. Caneschi, D. Ricotta, P. Bergese, Residual matrix from different separation techniques impacts exosome biological activity, Sci. Rep. 6 (2016) 1–11. doi:10.1038/srep23550.
[25] A. Gámez-Valero, M. Monguió-Tortajada, L. Carreras-Planella, M. Franquesa, K. Beyer, F.E. Borràs, Size-Exclusion Chromatography-based isolation minimally alters Extracellular Vesicles' characteristics compared to precipitating agents, Sci. Rep. 6 (2016) 1–9. doi:10.1038/srep33641.
[26] J.C. Contreras-Naranjo, H.-J. Wu, V.M. Ugaz, Microfluidics for exosome isolation and analysis: Enabling liquid biopsy for personalized medicine, Lab Chip. (2017). doi:10.1039/C7LC00592J.
[27] S.S. Kanwar, C.J. Dunlay, D.M. Simeone, S. Nagrath, Microfluidic device (ExoChip) for on-chip isolation, quantification and characterization of circulating exosomes, Lab Chip. 14 (2014) 1891–1900. doi:10.1039/c4lc00136b.
[28] C. Chen, J. Skog, C.H. Hsu, R.T. Lessard, L. Balaj, T. Wurdinger, B.S. Carter, X.O. Breakefield, M. Toner, D. Irimia, Microfluidic isolation and transcriptome analysis of serum microvesicles, Lab Chip. 10 (2010) 505–511. doi:10.1039/b916199f.
[29] P. Zhang, M. He, Y. Zeng, Ultrasensitive microfluidic analysis of circulating exosomes using a nanostructured graphene oxide/polydopamine coating, Lab Chip. 16 (2016) 3033–3042. doi:10.1039/c6lc00279j.
[30] J.C. Mallinson, On the preservation of human- and machine-readable records, Inf. Technol. Libr. 7 (1988) 19–23.
[31] Z. Zhao, Y. Yang, Y. Zeng, M. He, A microfluidic ExoSearch chip for multiplexed exosome detection towards blood-based ovarian cancer diagnosis, Lab Chip. 16 (2016) 489–496. doi:10.1039/c5lc01117e.
[32] J.S. Dudani, D.R. Gossett, H.T.K. Tse, R.J. Lamm, R.P. Kulkarni, D. Di Carlo, Rapid inertial solution exchange for enrichment and flow cytometric detection of microvesicles, Biomicrofluidics. 9 (2015) 1–9. doi:10.1063/1.4907807.
[33] S.-C. Guo, S.-C. Tao, H. Dawn, Microfluidics-based on-a-chip systems for isolating and analysing extracellular vesicles, J. Extracell. Vesicles. 7 (2018) 1508271. doi:10.1080/20013078.2018.1508271.
[34] M.Y. Konoshenko, E.A. Lekchnov, A. V. Vlassov, P.P. Laktionov, Isolation of Extracellular Vesicles: General Methodologies and Latest Trends, Biomed Res. Int. 2018 (2018) 1–27. doi:10.1155/2018/8545347.
[35] A. Liga, A.D.B. Vliegenthart, W. Oosthuyzen, J.W. Dear, M. Kersaudy-Kerhoas, Exosome isolation: a microfluidic road-map, Lab Chip. 15 (2015) 2388–2394. doi:10.1039/C5LC00240K.
[36] K. Lee, H. Shao, R. Weissleder, H. Lee, Acoustic purification of extracellular microvesicles, ACS Nano. 9 (2015) 2321–2327. doi:10.1021/nn506538f.
[37] P. Sehgal, B.J. Kirby, Separation of 300 and 100 nm Particles in Fabry-Perot Acoustofluidic Resonators, Anal. Chem. 89 (2017) 12192–12200. doi:10.1021/acs.analchem.7b02858.
[38] M. Wu, Y. Ouyang, Z. Wang, R. Zhang, P.-H. Huang, C. Chen, H. Li, P. Li, D. Quinn, M. Dao, S. Suresh, Y. Sadovsky, T.J. Huang, Isolation of exosomes from whole blood by integrating acoustics and microfluidics, Proc. Natl. Acad. Sci. 114 (2017) 10584–10589. doi:10.1073/pnas.1709210114.
[39] S.M. Santana, M.A. Antonyak, R.A. Cerione, B.J. Kirby, Microfluidic isolation of cancer-cell-derived microvesicles from hetergeneous extracellular shed vesicle populations, Biomed. Microdevices. 16 (2014) 869–877. doi:10.1007/s10544-014-9891-z.

[40] B.H. Wunsch, J.T. Smith, S.M. Gifford, C. Wang, M. Brink, R.L. Bruce, R.H. Austin, G. Stolovitzky, Y. Astier, Nanoscale lateral displacement arrays for the separation of exosomes and colloids down to 20nm, Nat. Nanotechnol. 11 (2016) 936–940. doi:10.1038/nnano.2016.134.
[41] X. Ding, Z. Peng, S.-C.S. Lin, M. Geri, S. Li, P. Li, Y. Chen, M. Dao, S. Suresh, T.J. Huang, Cell separation using tilted-angle standing surface acoustic waves, Proc. Natl. Acad. Sci. 111 (2014) 12992–12997. doi:10.1073/pnas.1413325111.
[42] M. Jiang, A.D. Mazzeo, G. Drazer, Centrifugal deterministic lateral displacement separation system, (2014).
[43] M.L. Heinemann, M. Ilmer, L.P. Silva, D.H. Hawke, A. Recio, M.A. Vorontsova, E. Alt, J. Vykoukal, Benchtop isolation and characterization of functional exosomes by sequential filtration, J. Chromatogr. A. 1371 (2014) 125–135. doi:10.1016/j.chroma.2014.10.026.
[44] L.G. Liang, M.Q. Kong, S. Zhou, Y.F. Sheng, P. Wang, T. Yu, F. Inci, W.P. Kuo, L.J. Li, U. Demirci, S.Q. Wang, An integrated double-filtration microfluidic device for isolation, enrichment and quantification of urinary extracellular vesicles for detection of bladder cancer, Sci. Rep. 7 (2017) 1–10. doi:10.1038/srep46224.
[45] H.K. Woo, V. Sunkara, J. Park, T.H. Kim, J.R. Han, C.J. Kim, H. Il Choi, Y.K. Kim, Y.K. Cho, Exodisc for Rapid, Size-Selective, and Efficient Isolation and Analysis of Nanoscale Extracellular Vesicles from Biological Samples, ACS Nano. 11 (2017) 1360–1370. doi:10.1021/acsnano.6b06131.
[46] M.F. Peterson, N. Otoc, J.K. Sethi, A. Gupta, T.J. Antes, Integrated systems for exosome investigation, Methods. 87 (2015) 31–45. doi:10.1016/j.ymeth.2015.04.015.
[47] J.D. Winans, K.J.P. Smith, T.R. Gaborski, J.A. Roussie, J.L. McGrath, Membrane capacity and fouling mechanisms for ultrathin nanomembranes in dead-end filtration, J. Memb. Sci. 499 (2016) 282–289. doi:10.1016/j.memsci.2015.10.053.
[48] T.R. Gaborski, J.L. Snyder, C.C. Striemer, D.Z. Fang, M. Hoffman, P.M. Fauchet, J.L. McGrath, High-performance separation of nanoparticles with ultrathin porous nanocrystalline silicon membranes, ACS Nano. 4 (2010) 6973–6981. doi:10.1021/nn102064c.
[49] H. Choi, D.S. Lee, Illuminating the physiology of extracellular vesicles, Stem Cell Res. Ther. 7 (2016) 1–7. doi:10.1186/s13287-016-0316-1.
[50] S.T.Y. Chuo, J.C.Y. Chien, C.P.K. Lai, Imaging extracellular vesicles: Current and emerging methods, J. Biomed. Sci. 25 (2018) 1–10. doi:10.1186/s12929-018-0494-5.
[51] B. Balachandran, Y. Yuana, Extracellular vesicles-based drug delivery system for cancer treatment, Cogent Med. 6 (2019). doi:10.1080/2331205x.2019.1635806.
[52] T. Tian, Y.L. Zhu, F.H. Hu, Y.Y. Wang, N.P. Huang, Z.D. Xiao, Dynamics of exosome internalization and trafficking, J. Cell. Physiol. 228 (2013) 1487–1495. doi:10.1002/jcp.24304.
[53] N. Bakhtyar, M.G. Jeschke, E. Herer, M. Sheikholeslam, S. Amini-nik, Exosomes from acellular Wharton ' s jelly of the human umbilical cord promotes skin wound healing, (2018) 1–14. doi:10.1186/s13287-018-0921-2.
[54] A.E. Morelli, A.T. Larregina, W.J. Shufesky, M.L.G. Sullivan, D.B. Stolz, G.D. Papworth, A.F. Zahorchak, A.J. Logar, Z. Wang, S.C. Watkins, L.D. Falo, A.W. Thomson, Endocytosis, intracellular sorting, and processing of exosomes by dendritic cells, Blood. 104 (2004) 3257–3266. doi:10.1182/blood-2004-03-0824.
[55] G. Di Noto G., M. Chiarini, L.L. Paolini, E.L. Mazzoldi, V. Giustini, A. Radeghieri, L. Caimi, D. Ricotta, Immunoglobulin free light chains and GAGs mediate multiple myeloma extracellular vesicles uptake and secondary NfκB nuclear translocation, Front. Immunol. 5 (2014). doi:10.3389/fimmu.2014.00517.
[56] J.Z. Nordin, Purification and Biodistribution of Extracellular Vesicles, 2017.
[57] N. Arraud, C. Gounou, D. Turpin, A.R. Brisson, Fluorescence triggering: A general strategy for enumerating and phenotyping extracellular vesicles by flow cytometry, Cytom. Part A. 89 (2016) 184–195. doi:10.1002/cyto.a.22669.
[58] P. Vader, E.A. Mol, G. Pasterkamp, R.M. Schiffelers, Extracellular vesicles for drug delivery, Adv. Drug Deliv. Rev. 106 (2016) 148–156. doi:10.1016/j.addr.2016.02.006.
[59] J.M. Sinning, J. Losch, K. Walenta, M. Böhm, G. Nickenig, N. Werner, Circulating CD31 +/Annexin V + microparticles correlate with cardiovascular outcomes, Eur. Heart J. 32 (2011) 2034–2041. doi:10.1093/eurheartj/ehq478.
[60] T. Fleitas, V. Martínez-Sales, V. Vila, E. Reganon, D. Mesado, M. Martín, J. Gómez-Codina, J. Montalar, G. Reynés, Circulating Endothelial Cells and Microparticles as Prognostic Markers in Advanced Non-Small Cell Lung Cancer, PLoS One. 7 (2012) 1–6. doi:10.1371/journal.pone.0047365.

[61] L.E. Graves, E. V. Ariztia, J.R. Navari, H.J. Matzel, M.S. Stack, D.A. Fishman, Proinvasive properties of ovarian cancer ascites-derived membrane vesicles, Cancer Res. 64 (2004) 7045–7049. doi:10.1158/0008-5472.CAN-04-1800.
[62] F.F. Van Doormaal, A. Kleinjan, M. Di Nisio, H.R. Büller, R. Nieuwland, Cell-derived microvesicles and cancer, Neth. J. Med. 67 (2009) 266–273.
[63] S.A. Stoner, E. Duggan, D. Condello, A. Guerrero, J.R. Turk, P.K. Narayanan, J.P. Nolan, High sensitivity flow cytometry of membrane vesicles, Cytom. Part A. 89 (2016) 196–206. doi:10.1002/cyto.a.22787.
[64] E.N.M.N. t. Hoen, E.J. van der Vlist, M. Aalberts, H.C.H. Mertens, B.J. Bosch, W. Bartelink, E. Mastrobattista, E.V.B. van Gaal, W. Stoorvogel, G.J.A. Arkesteijn, M.H.M. Wauben, Quantitative and qualitative flow cytometric analysis of nanosized cell-derived membrane vesicles, Nanomedicine Nanotechnology, Biol. Med. 8 (2012) 712–720. doi:10.1016/j.nano.2011.09.006.
[65] H.C. Inglis, A. Danesh, A. Shah, J. Lacroix, P.C. Spinella, P.J. Norris, Techniques to improve detection and analysis of extracellular vesicles using flow cytometry, Cytom. Part A. 87 (2015) 1052–1063. doi:10.1002/cyto.a.22649.
[66] V. Sunkara, H. Woo, Y. Cho, Characterization of Extracellular Vesicles and, 2016. doi:10.1039/c5an01775k.
[67] E. van der Pol, F.A.W. Coumans, A.E. Grootemaat, C. Gardiner, I.L. Sargent, P. Harrison, A. Sturk, T.G. van Leeuwen, R. Nieuwland, Particle size distribution of exosomes and microvesicles determined by transmission electron microscopy, flow cytometry, nanoparticle tracking analysis, and resistive pulse sensing, J. Thromb. Haemost. 12 (2014) 1182–1192. doi:10.1111/jth.12602.
[68] W.L. Chandler, W. Yeung, J.F. Tait, A new microparticle size calibration standard for use in measuring smaller microparticles using a new flow cytometer, J. Thromb. Haemost. 9 (2011) 1216–1224. doi:10.1111/j.1538-7836.2011.04283.x.
[69] J.P. Nolan, S.A. Stoner, A trigger channel threshold artifact in nanoparticle analysis, Cytom. Part A. 83 A (2013) 301–305. doi:10.1002/cyto.a.22255.
[70] A. Görgens, M. Bremer, R. Ferrer-Tur, F. Murke, T. Tertel, P.A. Horn, S. Thalmann, J.A. Welsh, C. Probst, C. Guerin, C.M. Boulanger, J.C. Jones, H. Hanenberg, U. Erdbrügger, J. Lannigan, F.L. Ricklefs, S. El-Andaloussi, B. Giebel, Optimisation of imaging flow cytometry for the analysis of single extracellular vesicles by using fluorescence-tagged vesicles as biological reference material, J. Extracell. Vesicles. 8 (2019). doi:10.1080/20013078.2019.1587567.
[71] S.F.W.M. Libregts, G.J.A. Arkesteijn, A. Németh, E.N.M. Nolte-'t Hoen, M.H.M. Wauben, Flow cytometric analysis of extracellular vesicle subsets in plasma: impact of swarm by particles of non-interest, J. Thromb. Haemost. 16 (2018) 1423–1436. doi:10.1111/jth.14154.
[72] J. Lötvall, A.F. Hill, F. Hochberg, E.I. Buzás, D. Di Vizio, C. Gardiner, Y.S. Gho, I. V. Kurochkin, S. Mathivanan, P. Quesenberry, S. Sahoo, H. Tahara, M.H. Wauben, K.W. Witwer, C. Théry, Minimal experimental requirements for definition of extracellular vesicles and their functions: A position statement from the International Society for Extracellular Vesicles, J. Extracell. Vesicles. 3 (2014) 1–6. doi:10.3402/jev.v3.26913.
[73] S.A.A. Kooijmans, J.J.J.M. Gitz-Francois, R.M. Schiffelers, P. Vader, Recombinant phosphatidylserine-binding nanobodies for targeting of extracellular vesicles to tumor cells: A plug-and-play approach, Nanoscale. 10 (2018) 2413–2426. doi:10.1039/c7nr06966a.
[74] T. Tian, Y. Wang, H. Wang, Z. Zhu, Z. Xiao, Visualizing of the cellular uptake and intracellular trafficking of exosomes by live-cell microscopy, J. Cell. Biochem. 111 (2010) 488–496. doi:10.1002/jcb.22733.
[75] K. Lee, K. Frase, B. Ghaddar, K. Yang, E. Kim, L. Balaj, E.A. Chiocca, X.O. Breakefield, H. Lee, Ralph Weissleder, Multiplexed Profiling of Single Extracellular Vesicles, Physiol. Behav. 176 (2017) 139–148. doi:10.1016/j.physbeh.2017.03.040.
[76] D. Faille, F. El-Assaad, A.J. Mitchell, M.C. Alessi, G. Chimini, T. Fusai, G.E. Grau, V. Combes, Endocytosis and intracellular processing of platelet microparticles by brain endothelial cells, J. Cell. Mol. Med. 16 (2012) 1731–1738. doi:10.1111/j.1582-4934.2011.01434.x.
[77] S.I. Ohno, M. Takanashi, K. Sudo, S. Ueda, A. Ishikawa, N. Matsuyama, K. Fujita, T. Mizutani, T. Ohgi, T. Ochiya, N. Gotoh, M. Kuroda, Systemically injected exosomes targeted to EGFR deliver antitumor microrna to breast cancer cells, Mol. Ther. 21 (2013) 185–191. doi:10.1038/mt.2012.180.
[78] O.P.B. Wiklander, J.Z. Nordin, A. O'Loughlin, Y. Gustafsson, G. Corso, I. Mäger, P. Vader, Y. Lee, H. Sork, Y. Seow, N. Heldring, L. Alvarez-Erviti, C.I. Edvard Smith, K. Le Blanc, P. Macchiarini, P. Jungebluth, M.J.A.

Wood, S. El Andaloussi, Extracellular vesicle in vivo biodistribution is determined by cell source, route of administration and targeting, J. Extracell. Vesicles. 4 (2015) 1–13. doi:10.3402/jev.v4.26316.
[79] V. Pospichalova, J. Svoboda, Z. Dave, A. Kotrbova, K. Kaiser, D. Klemova, L. Ilkovics, A. Hampl, I. Crha, E. Jandakova, L. Minar, V. Weinberger, V. Bryja, Simplified protocol for flow cytometry analysis of fluorescently labeled exosomes and microvesicles using dedicated flow cytometer, J. Extracell. Vesicles. 4 (2015) 1–15. doi:10.3402/jev.v4.25530.
[80] P. Pužar Dominkuš, M. Stenovec, S. Sitar, E. Lasič, R. Zorec, A. Plemenitaš, E. Žagar, M. Kreft, M. Lenassi, PKH26 labeling of extracellular vesicles: Characterization and cellular internalization of contaminating PKH26 nanoparticles, Biochim. Biophys. Acta - Biomembr. 1860 (2018) 1350–1361. doi:10.1016/j.bbamem.2018.03.013.
[81] H.C. Christianson, K.J. Svensson, T.H. Van Kuppevelt, J.P. Li, M. Belting, Cancer cell exosomes depend on cell-surface heparan sulfate proteoglycans for their internalization and functional activity, Proc. Natl. Acad. Sci. U. S. A. 110 (2013) 17380–17385. doi:10.1073/pnas.1304266110.
[82] D. Fitzner, M. Schnaars, D. Van Rossum, G. Krishnamoorthy, P. Dibaj, M. Bakhti, T. Regen, U.K. Hanisch, M. Simons, Selective transfer of exosomes from oligodendrocytes to microglia by macropinocytosis, J. Cell Sci. 124 (2011) 447–458. doi:10.1242/jcs.074088.
[83] R. Tamura, S. Uemoto, Y. Tabata, Immunosuppressive effect of mesenchymal stem cell-derived exosomes on a concanavalin A-induced liver injury model, Inflamm. Regen. 36 (2016) 1–11. doi:10.1186/s41232-016-0030-5.
[84] A. Hoshino, B. Costa-Silva, T.L. Shen, G. Rodrigues, A. Hashimoto, M. Tesic Mark, H. Molina, S. Kohsaka, A. Di Giannatale, S. Ceder, S. Singh, C. Williams, N. Soplop, K. Uryu, L. Pharmer, T. King, L. Bojmar, A.E. Davies, Y. Ararso, T. Zhang, H. Zhang, J. Hernandez, J.M. Weiss, V.D. Dumont-Cole, K. Kramer, L.H. Wexler, A. Narendran, G.K. Schwartz, J.H. Healey, P. Sandstrom, K. Jørgen Labori, E.H. Kure, P.M. Grandgenett, M.A. Hollingsworth, M. De Sousa, S. Kaur, M. Jain, K. Mallya, S.K. Batra, W.R. Jarnagin, M.S. Brady, O. Fodstad, V. Muller, K. Pantel, A.J. Minn, M.J. Bissell, B.A. Garcia, Y. Kang, V.K. Rajasekhar, C.M. Ghajar, I. Matei, H. Peinado, J. Bromberg, D. Lyden, Tumour exosome integrins determine organotropic metastasis, Nature. 527 (2015) 329–335. doi:10.1038/nature15756.
[85] E.J. van der Vlist, E.N.M. Nolte-'t Hoen, W. Stoorvogel, G.J.A. Arkesteijn, M.H.M. Wauben, Fluorescent labeling of nano-sized vesicles released by cells and subsequent quantitative and qualitative analysis by high-resolution flow cytometry., Nat. Protoc. 7 (2012) 1311–1326. doi:10.1038/nprot.2012.065.
[86] L. De Rond, E. Van Der Pol, C.M. Hau, Z. Varga, A. Sturk, T.G. Van Leeuwen, R. Nieuwland, F.A.W. Coumans, Comparison of generic fluorescent markers for detection of extracellular vesicles by flow cytometry, Clin. Chem. 64 (2018) 680–689. doi:10.1373/clinchem.2017.278978.
[87] J.M. Aliotta, M. Pereira, E.H. Sears, M.S. Dooner, S. Wen, L.R. Goldberg, P.J. Quesenberry, Lung-derived exosome uptake into and epigenetic modulation of marrow progenitor/stem and differentiated cells, J. Extracell. Vesicles. 4 (2015). doi:10.3402/jev.v4.26166.
[88] Y. Che, X. Shi, Y. Shi, X. Jiang, Q. Ai, Y. Shi, F. Gong, W. Jiang, Exosomes Derived from miR-143-Overexpressing MSCs Inhibit Cell Migration and Invasion in Human Prostate Cancer by Downregulating TFF3, Mol. Ther. - Nucleic Acids. 18 (2019) 232–244. doi:10.1016/j.omtn.2019.08.010.
[89] P.A. and J.C. Cristina Escrevente, Sascha Keller, Interaction and uptake of exosomes by ovarian cancer cells, Nat. Commun. 11 (2015) 883–91. doi:10.1016/j.bbrc.2014.12.015.
[90] K. Takov, D.M. Yellon, S.M. Davidson, Confounding factors in vesicle uptake studies using fluorescent lipophilic membrane dyes, J. Extracell. Vesicles. 6 (2017). doi:10.1080/20013078.2017.1388731.
[91] L. De Rond, E. Van Der Pol, C.M. Hau, Z. Varga, A. Sturk, T.G. Van Leeuwen, R. Nieuwland, F.A.W. Coumans, Comparison of generic fluorescent markers for detection of extracellular vesicles by flow cytometry, Clin. Chem. 64 (2018) 680–689. doi:10.1373/clinchem.2017.278978.
[92] Y. Tian, S. Li, J. Song, T. Ji, M. Zhu, G.J. Anderson, J. Wei, G. Nie, A doxorubicin delivery platform using engineered natural membrane vesicle exosomes for targeted tumor therapy, Biomaterials. 35 (2014) 2383–2390. doi:10.1016/j.biomaterials.2013.11.083.
[93] A. Cvjetkovic, J. Lo, C. La, The influence of rotor type and centrifugation time on the yield and purity of extracellular vesicles, 1 (2014) 1–11.
[94] A. Montecalvo, A.T. Larregina, W.J. Shufesky, D.B. Stolz, M.L.G. Sullivan, J.M. Karlsson, C.J. Baty, G.A. Gibson, G. Erdos, Z. Wang, J. Milosevic, O.A. Tkacheva, S.J. Divito, R. Jordan, J. Lyons-Weiler, S.C. Watkins,

A.E. Morelli, Mechanism of transfer of functional microRNAs between mouse dendritic cells via exosomes, Blood. 119 (2012) 756–766. doi:10.1182/blood-2011-02-338004.
[95] T. Smyth, M. Kullberg, N. Malik, P. Smith-jones, M.W. Graner, T.J. Anchordoquy, Biodistribution and delivery ef fi ciency of unmodi fi ed tumor-derived exosomes, 199 (2015) 145–155.
[96] A. Morales-Kastresana, T.A. Musich, J.A. Welsh, W. Telford, T. Demberg, J.C.S. Wood, M. Bigos, C.D. Ross, A. Kachynski, A. Dean, E.J. Felton, J. Van Dyke, J. Tigges, V. Toxavidis, D.R. Parks, W.R. Overton, A.H. Kesarwala, G.J. Freeman, A. Rosner, S.P. Perfetto, L. Pasquet, M. Terabe, K. McKinnon, V. Kapoor, J.B. Trepel, A. Puri, H. Kobayashi, B. Yung, X. Chen, P. Guion, P. Choyke, S.J. Knox, I. Ghiran, M. Robert-Guroff, J.A. Berzofsky, J.C. Jones, High-fidelity detection and sorting of nanoscale vesicles in viral disease and cancer, J. Extracell. Vesicles. 8 (2019) 1–14. doi:10.1080/20013078.2019.1597603.
[97] M. Mireles, C.W. Soule, M. Dehghani, T.R. Gaborski, Use of nanosphere self-assembly to pattern nanoporous membranes for the study of extracellular vesicles, Nanoscale Adv. (2020). doi:10.1039/d0na00142b.
[98] L. Chen, Z. Xie, T. Gan, Y. Wang, G. Zhang, C.A. Mirkin, Z. Zheng, Biomimicking Nano-Micro Binary Polymer Brushes for Smart Cell Orientation and Adhesion Control, (2016) 3400–3406. doi:10.1002/smll.201600634.
[99] C.P. Lai, E.Y. Kim, C.E. Badr, R. Weissleder, T.R. Mempel, B.A. Tannous, X.O. Breakefield, Visualization and tracking of tumour extracellular vesicle delivery and RNA translation using multiplexed reporters, Nat. Commun. 6 (2015) 1–12. doi:10.1038/ncomms8029.
[100] W.D. Gray, A.J. Mitchell, C.D. Searles, An accurate, precise method for general labeling of extracellular vesicles, MethodsX. 2 (2015) 360–367. doi:10.1016/j.mex.2015.08.002.
[101] A. Milasan, N. Tessandier, S. Tan, A. Brisson, E. Boilard, C. Martel, Extracellular vesicles are present in mouse lymph and their level differs in atherosclerosis, J. Extracell. Vesicles. 5 (2016). doi:10.3402/jev.v5.31427.

# Chapter 2

## 2 Tangential Flow for Analyte Capture of Extracellular Vesicles

## 2.1 Abstract

Membranes have been used extensively for the purification and separation of biological species. A persistent challenge is the purification of species from concentrated feed solutions such as extracellular vesicles (EVs) from biological fluids. We investigated a new method to isolate micro- and nano-scale species termed tangential flow for analyte capture (TFAC), which is an extension of traditional tangential flow filtration (TFF). Initially, EV purification from plasma on ultrathin nanomembranes was compared between both normal flow filtration (NFF) and TFAC. NFF resulted in rapid formation of a protein cake which completely obscured any captured EVs and also prevented further transport across the membrane. On the other hand, TFAC showed capture of CD63 positive small EVs (sEVs) with minimal contamination. We explored the use of TFAC to capture target species over membrane pores, wash and then release in a physical process that does not rely upon affinity or chemical interactions. This process of TFAC was studied with model particles on both ultrathin nanomembranes and conventional thickness membranes (polycarbonate track-etch). Successful capture and release of model particles was observed using both membranes. Ultrathin nanomembranes showed higher efficiency of capture and release with significantly lower pressures indicating that ultrathin nanomembranes are well-suited for TFAC of delicate nanoscale particles such as EVs.

## 2.2 Introduction

Tangential flow filtration (TFF) is used extensively in bioprocessing [1]. In this method, a feed solution containing a species of interest flows tangentially over a selective membrane with some fraction of the flow also passing through the membrane. If the species of interest is to be retained behind the membrane, TFF can be used to remove impurities or to concentrate the species in the feed solution [2, 3]. If the volume lost through transmembrane flow is resupplied to the feed channel as fresh buffer (diafiltration), TFF can be used for buffer exchange [4, 5]. TFF can also be used to partially purify a species that emerges in the filtrate, although the product typically requires final purification by column or membrane chromatography [6-10].

The advantage of TFF over normal flow filtration (NFF) is that the tangential flow component disrupts the formation of a concentration polarization layer that builds as species are rejected by the membrane [11]. Without a tangential component, this polarization layer will eventually form a 'cake' layer on the membrane with its own separation properties and significantly reduced permeate flux [12]. With TFF filtration however, it is possible to identify conditions for which both the flux and transmembrane pressure (TMP) are steady with time [13]. Under these conditions filtration can, in principle, continue indefinitely.

Our laboratories develop ultrathin porous membranes for a range of applications including separations [14-17]. Ultrathin membranes are best defined as materials with pores on the same order as, or larger than, the membrane thickness [18]. These have been made with a variety of materials including silicon, silicon-nitride, silicon dioxide, graphene, and graphene-oxide [19-24]. We have recently demonstrated that the high permeability of ultrathin membranes causes

them to foul rapidly in NFF, with initial pore blockage events quickly followed by cake filtration [25]. We showed the same fouling phenomena occurs with both particle and protein solutes when used in NFF [25, 26].

To extend the capacity of ultrathin membranes in separations, we have recently examined their performance in TFF. Working with undiluted serum and nanoporous silicon nitride (NPN) membranes, we made the surprising discovery, reported here for the first time, that 60 - 100 nm extracellular vesicles (EVs), are captured in the pores of ultrathin membranes with little evidence of protein fouling [27]. Our discovery inspired a closer look at the mechanisms and potential utility of capturing nanoparticle-sized analytes from biofluids in the pores of ultrathin membranes.

Extracellular vesicles (EVs) are secreted from tissue cells into all body fluids, and EVs that are < 100 nm are typically, but not exclusively, exosomes. Exosomes contain the largest pool of extracellular RNA (exRNA) in biofluids, and are thus valued both for their diagnostic and therapeutic potential [28-33]. The conventional method for exosome purification is ultracentrifugation although many alternative strategies have been proposed, including TFF [34-37]. Out of respect for the careful criterion used to define exosomes, we will refer to < 100 nm EVs as small EVs (sEVs) rather than exosomes [38].

We propose a novel method for the extraction of nanoparticle species from biofluids which we call tangential flow for analyte capture (TFAC). In this method, sEVs and similarly-sized analytes are captured in the pores of an ultrathin membrane where they can be washed and released with additional flows. TFAC resembles bind/elute purification strategies although it distinguishes itself from affinity chromatography because the binding is purely physical. TFAC

does not require engineered surface chemistries for capture or chemical treatments for elution. The purpose of the current report is to demonstrate the basic principles of TFAC using model particles. We also test the hypothesis that ultrathin membranes are ideally suited for TFAC because they facilitate capture and release at lower pressures than conventional thick membranes.

## 2.3 Materials and Methods

### Fabrication of NPN Membranes

The fabrication steps for nanoporous silicon nitride nanomembranes (NPN) have been published previously [19]. Briefly, a silicon wafer is coated with a three layer stack of silicon nitride (SiN), amorphous silicon, and silicon dioxide. A porous nanocrystalline silicon (pnc-Si) layer is formed on top of SiN via rapid thermal annealing. The nanopores present in the pnc-Si are transferred into the SiN layer by reactive ion etching. In order to create the freestanding membranes, the back side of the silicon wafer is etched to the silicon nitride layer using ethylene diamine pyrocatechol.

### NPN Device Fabrication

Polydimethylsiloxane (PDMS) sheets (Trelleborg Sealing Solutions Americas, Fort Wayne, IN) were used to create microfluidic devices. Custom ordered 100 μm and 300 μm thick restricted grade sheets were patterned using a Silhouette Cameo digital craft cutter (Silhouette America, Oren, UT) [39]. The patterned silicone sheets were assembled into layer stack devices by aligning the patterned layers. NPN membrane chips (300 μm thick) were sandwiched between stacked layers and the final device was clamped to seal it for flow.

### PCTE Device Fabrication

As a representative of conventional thickness membranes, commercial polycarbonate track-etch (PCTE) membranes with pore sizes of 8 μm and 80 nm were utilized (Sterlitech, WA, USA). In order to have a sealed system for track-etch membranes, the above described microfluidic

device was modified. Holes were drilled in polycarbonate slabs for accessing the bottom channel of the device, while the PDMS slabs were punched for flowing to the top channel. We used 100 µm and 300 µm thick patterned PDMS sheets for bottom and top channels, respectively. In order to prevent leaking in the system, the PCTE membranes covering the entire device were sandwiched between the top and bottom layers using a clamp.

## sEV CAPTURE FROM PLASMA

**Normal Flow Filtration:** Small extracellular vesicle experiments were performed using purified human plasma (Equitech-Bio, Inc., Kerrville, TX). NFF experiments were performed using NPN chips with 50 nm thick freestanding membranes, with an average pore diameter of 50 nm and a porosity of 15% in a SepCon™ centrifuge cup (SiMPore Inc., Rochester, NY). A 500 µL sample of undiluted plasma was spun at 1500 *x g* through the membrane and the chip was extracted from the device. The chip was allowed to dry and was then imaged by scanning electron microscopy as described below.

**Tangential Flow for Analyte Capture:** Nanoporous silicon nitride microfluidic devices were fabricated as described above. The NPN chip used had a 50 nm thick freestanding membrane with a 50 nm average pore diameter and a 15% porosity. 1 mL of plasma was passed tangential to the membrane surface at a rate of 10 µL/min using a syringe pump (Chemyx Fusion 200, Chemyx Inc., Stafford, TX), while fluid was actively pulled through the membrane at a rate of 2 µL/min. After processing the full 1 mL volume, the device was unclamped and the chip extracted. Captured sEVs were labeled for CD63 (Abcam, Cambridge, MA) and imaged via scanning electron microscopy as outlined below.

## Capture and Release of Nanoparticles

**Microscale Experiments:** Flow experiments were performed using two Chemyx Fusion 200 syringe pumps (Chemyx Inc., Stafford, TX). Micron scale experiments with 10 µm polystyrene green fluorescent particles (Thermo Scientific, USA) were conducted on 8 µm track-etch membranes. Capturing step was performed using a sample supply flow rate of 90 µL/min and an ultrafiltration/pulling rate of 10 µL/min. Captured particles were released by reversed flow of 10 µL/min through the membrane.

**Nanoscale Experiments:** These experiments were conducted using 100 nm polystyrene green fluorescent particles (Thermo Scientific, USA) on PCTE or NPN membranes with 80 nm median pore size. Nanoparticles were captured by supply flow rate of 5 µL/min and the ultrafiltration/pulling flow rate of 2 µL/min. Input channel was then cleaned by rinsing buffer to wash away the floating particles under the same flow condition as the capturing step. Finally, captured particles were released by reversed flow of 2 µL/min through the membranes.

## Time-Lapse Video Microscopy

Devices were illuminated with metal halide lamp source (LE6000 Leica) through DIC and FITC (488 nm Ex/525 nm Em) filter sets on a Leica DM16000 microscope (Leica Microsystems, Buffalo Grove, IL) using the 10X objective. Images were collected using MetaMorph software with a Rolera em- camera (QImaging, Surrey, BC Canada) for 50 ms exposure time for FITC and 10 ms for DIC. The measuring and merging channel tool in NIH ImageJ were used for quantifying the average intensity values and making videos by merging DIC with FITC images,

respectively. Images were taken every minute for nanoscale experiments and every second for microscale experiments.

## Electron Microscopy

After the completion of experiments, the PCTE and NPN membranes were imaged via electron microscopy. Samples were prepared for electron microscopy by first removing the membranes from the device and then allowing them to air dry. Samples were then mounted and sputter coated with ~3-10 nm of gold. Scanning electron micrographs were taken at an accelerating voltage of 10 kV using either a Hitachi S-4000 scanning electron microscope (SEM) or a Zeiss AURIGA scanning electron microscope.

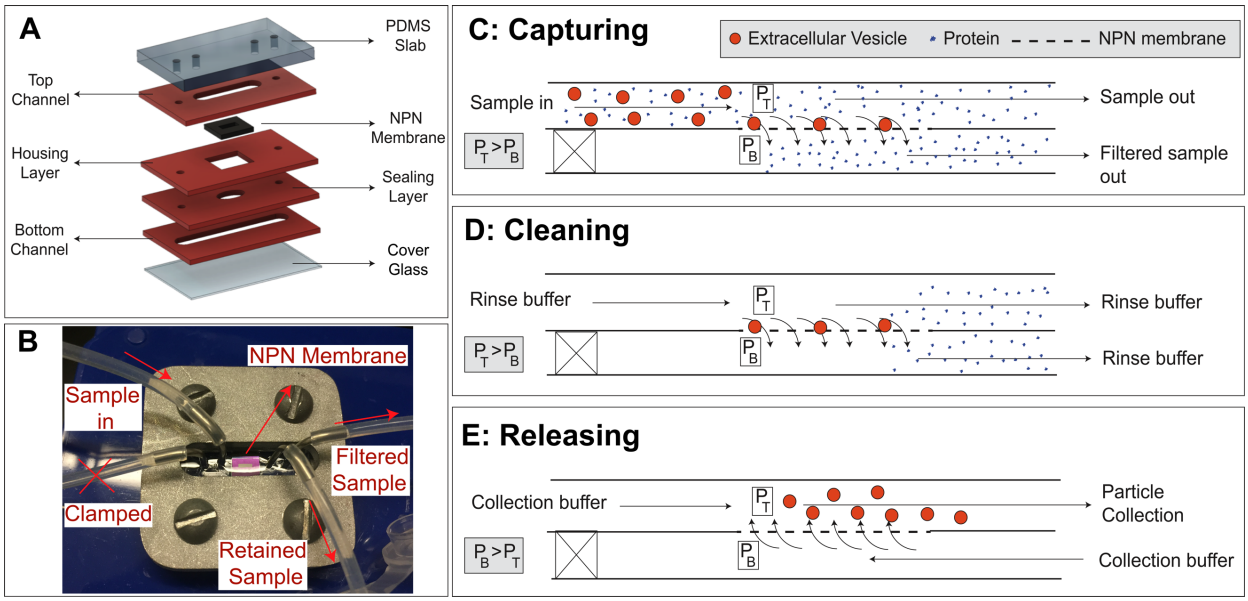


**Figure 2.1 – Tangential Flow Analyte Capture (TFAC) Technique for Isolation of Particles.**

**(A)** Microfluidic devices are assembled through a layer stack process, in which channels and other featured are patterned into PDMS sheets. **(B)** These layers are then formed into the device through thermal bonding or stacking and clamping. **(C)** The sample is passed across the surface of the membrane and a transmembrane pressure generated by syringe pumps drives particle motion towards the membrane. Contaminating particles pass through pores or are swept downstream while the particles are retained on the membrane surface. **(D)** The cleaning buffer is then passed through the input channel under the same flow condition as the capturing step to wash the channel and membrane surfaces of any remaining contaminants. **(E)** The transmembrane pressure is then reversed, releasing the particles from the membrane where they are then swept downstream and collected.

## 2.4 Results

### 2.4.1 Tangential Flow for Particle Capture

The system and scheme for particle capture and release is shown in **Figure 2.1**. As in our prior work [40-43], we used layer-by-layer assembly (**Figure 2.1-A**) to construct microfluidic devices (**Figure 2.1-B**) with membranes separating top and bottom flow channels. The only difference is that we used a clamped system for both PCTE systems and NPN systems instead of a fully bonded devices. This enables the removal and inspection of PCTE membranes or NPN chips by SEM after use. Particle capture (**Figure 2.1-C**) was performed using two syringe pumps: a positive pressure pump providing a constant sample supply flow rate into the input channel of the device, and a negative pressure pump at the output channel exit side controlling a smaller, steady rate of ultrafiltration through the membrane. The difference between the supply and ultrafiltration rates exited the top channel as waste and provided the tangential flow needed to prevent fouling [11, 13]. The inlet port on the bottom channel was blocked for all experiments. After capture, non-adsorbed contaminants could be cleared by replacing the sample with a rinse buffer while maintaining the transmembrane pressure (**Figure 2.1-D**) and captured analytes could be released by operating both pumps under positive pressure (**Figure 2.1-E**).

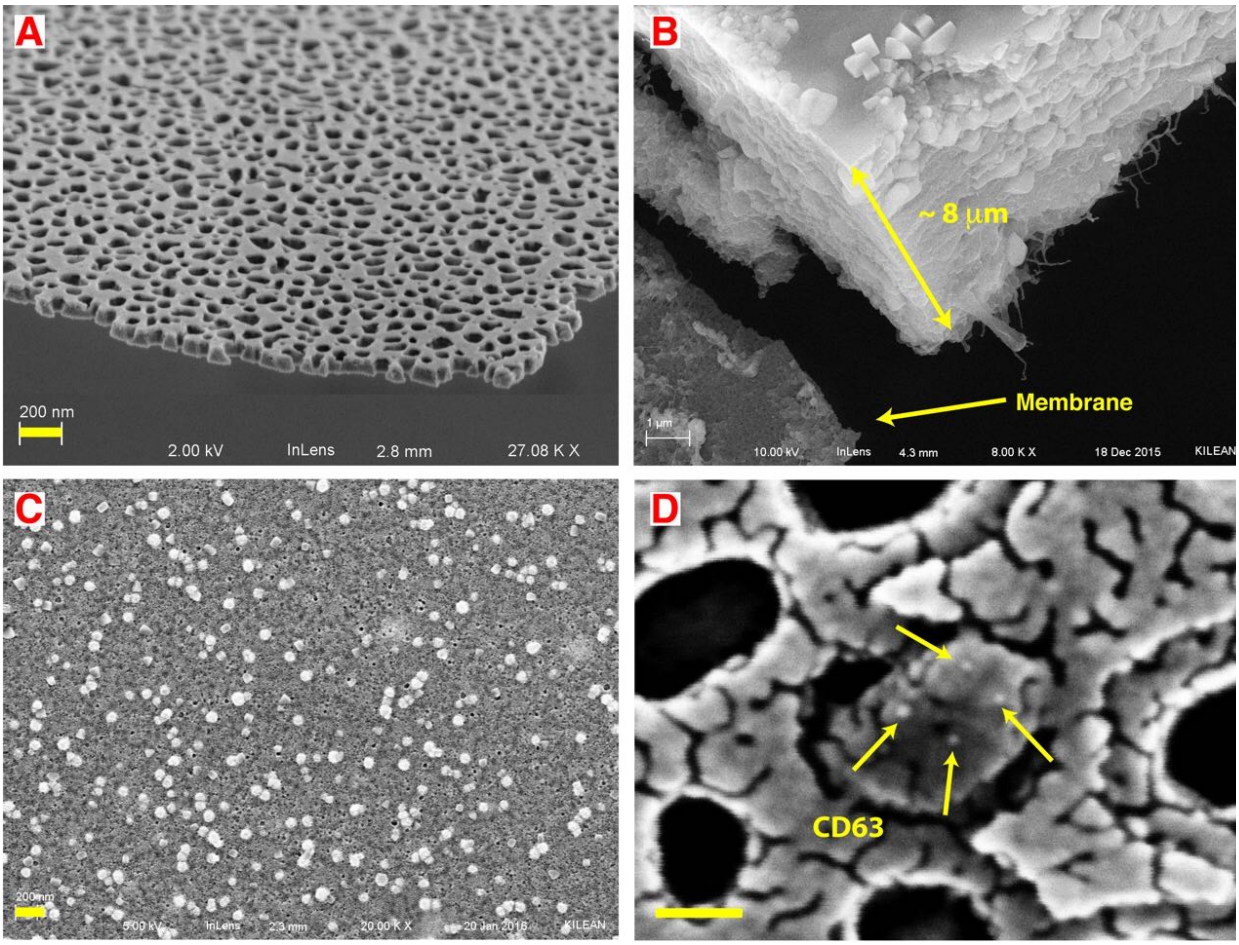


**Figure 2.2 - Small Extracellular Vesicles (sEV) Captured from Undiluted Blood Plasma.**

**(A)** SEM images showing the thinness and high porosity of nanoporous silicon nitride (NPN). **(B)** In normal flow filtration (NFF) a protein cake of ~8 µm cake rapidly builds up on the membrane surface. **(C)** After capturing and cleaning steps of TFAC, small vesicles are captured on the membrane surface with minimum fouling. **(D)** Nanogold conjugated anti-CD63 antibody labels an EV captured in a pore multiple times, indicating it is likely a CD63 positive sEV. Note: the fragmented appearance of the surface results from the use of a limited amount of gold (3 nm) to avoid obscuring the gold label on the antibody (18 nm). By contrast 10 nm of gold was sputtered on the samples to avoid charging effects in SEM in both B and C. Scale bar = 200 nm for A, B and C. Scale bar = 50 nm for D.

### 2.4.2 Small EV capture from Undiluted Serum

The initial discovery of analyte capture occurred with experiments on undiluted serum (**Figure 2.2**). The scanning electron microscopy (SEM) image of the membrane can be seen in **Figure 2.2-A**. In these experiments, we showed that the filtration of undiluted serum is difficult in NFF (**Figure 2.2-B**), causing an 8 µm cake of serum protein and salts to foul the membrane and allowing the passage of only 10 µL of a 1 mL sample. However, upon passing the undiluted serum across the membrane in tangential flow, we observed a significant reduction in the protein build-up on the membrane, showing captured particles (**Figure 2.2-C**).

Human plasma and serum contain different types of particles including EVs and lipoproteins. Lipoproteins and EVs cannot be distinguished only by their physical properties since their size and density closely overlap [44, 45]. However, further analysis of the captured particles with immunostaining showed that some of the particles were positive for CD63 which is a common sEV surface protein and is not expressed on lipoproteins (**Figure 2.2-D**). We did not attempt rinse or release steps with undiluted serum, instead we turned to the following experiments with model systems to confirm and study the capture phenomena under defined conditions.

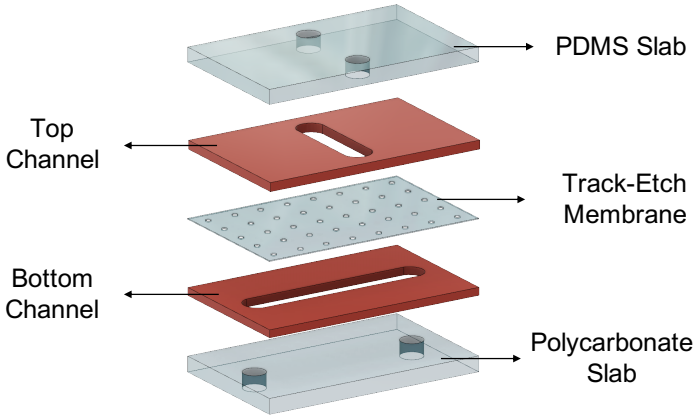


**Figure 2.3 - Microfluidic Device for PCTE Membranes.**

### 2.4.3 Microporous Track-Etch Capture of Fluorescent Particles

We first explored the particle capture phenomena at the microscale using microporous polycarbonate track-etched (mPCTE) membranes with 8 µm pores and 10 µm particles. The schematic of the microfluidic device for PCTE membranes can be found in **Figure 2.3**. Polycarbonate and PDMS slabs with holes were used to have access to the bottom and top channels respectively. Top and bottom channels were patterned into PDMS sheets, and PCTE membrane was sandwiched between the channels. In order to make sure that the system is sealed, a plus sign design for channels were used and the PCTE was covering the entire device. At this scale we were able to image individual particle capture events in fluorescence microscopy (**Figure 2.4**). Before flow ($T_0$; **Figure 2.4-B)** there were no particles on the membrane. With a steady supply rate of 90 µL/min and ultrafiltration rate of 10 µL/min particles began to accumulate on the membrane, primarily drawn directly to the pores (see electron micrograph in **Figure 2.4-C**, bottom panel), and the fluorescence steadily increased over time (red line in **Figure 2.4-A**). The capturing process was then stopped at $T_1$ resulting in

immediate release of particles loosely held on the membrane and a distinct, sudden drop in fluorescence (light blue line **Figure 2.4-A**). Finally, the flow was reversed by switching the ultrafiltration pump to infusion mode, resulting in a directional shift for the bottom flow. The bottom flow rate was then increased to provide a high transmembrane pressure in an attempt to fully release the remaining particles, although a fraction remained irreversibly bound resulting in a residual fluorescence after the experiment $T_2$ (**Figure 2.4-D**). Electron microscopy (**Figure 2.4-D, bottom panel**) shows that most of these particles were not associated with pores and thus were non-specifically adhered to the surface of the membrane through surface interactions.

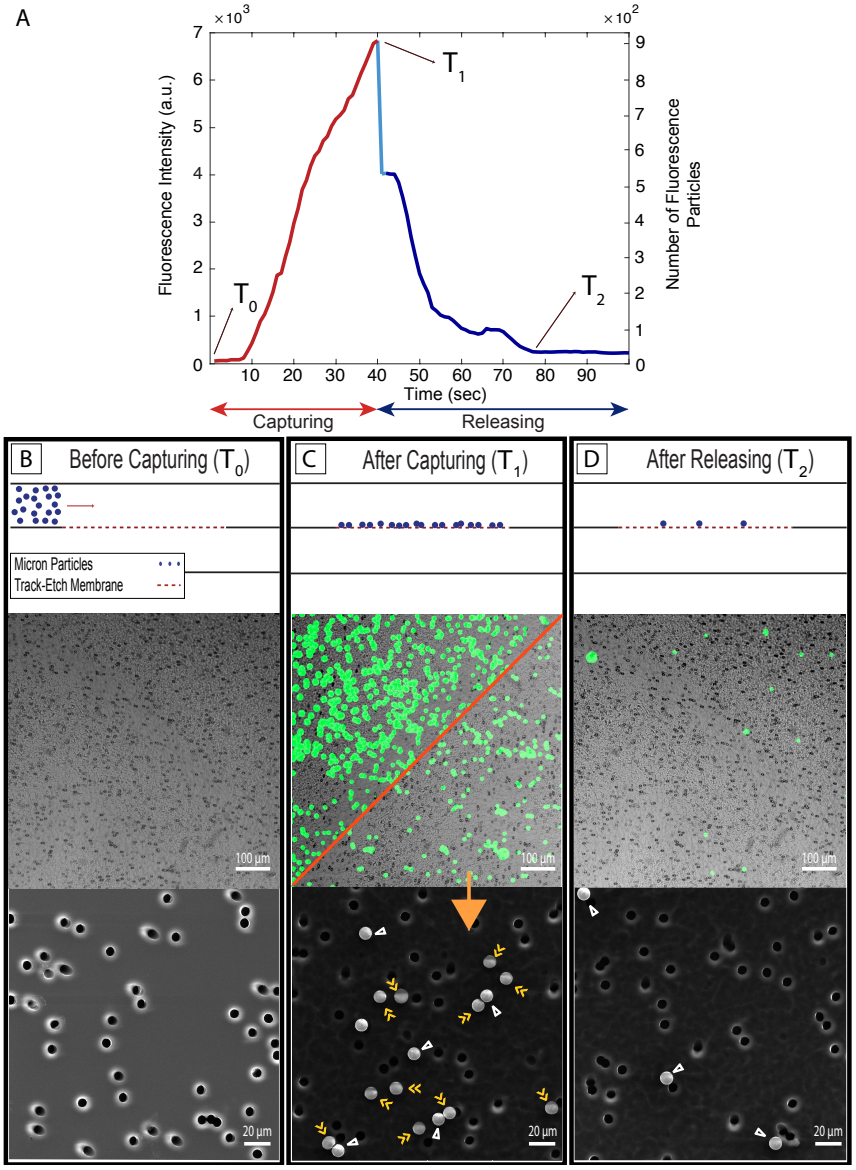


**Figure 2.4 - Microscale Experiments with 10 µm Fluorescent Particles and 8 µm Median Pore Size Polycarbonate Track-etch (mPCTE) Membranes.**

*(***A)** SEM images showing the thinness and high porosity of nanoporous silicon nitride (NPN). **(B)** In normal flow filtration (NFF) a protein cake of ~8 µm cake rapidly builds up on the membrane surface. **(C)** After capturing and cleaning steps of TFAC, small vesicles are captured on the membrane surface with minimum fouling. **(D)** Nanogold conjugated anti-CD63 antibody labels an EV captured in a pore multiple times, indicating it is likely a CD63 positive sEV. Note: the fragmented appearance of the surface results from the use of a limited amount of gold (3 nm) to avoid obscuring the gold label on the antibody (18 nm). By contrast 10 nm of gold was sputtered on the samples to avoid charging effects in SEM in both B and C. Scale bar = 200 nm for A, B and C. Scale bar = 50 nm for D.

MATLAB code was generated to count the number of micron particles being captured and released over time. All the images in the time lapse series were binarized and summed over time to create the residence time map as it can be seen in **Figure 2.5**. The color indicates the residence time of the particles on the membrane (where yellow indicates longer residence time). In order to ensure that floating particles were not counted as a captured particle, a threshold of 3 images was applied so that particles that were in the field of view for less than 3 images were excluded (**Figure 2.5-A**). Then, the images were binarized to yellow for the captured particles and blue colors for the membrane (**Figure 2.5-B**). Number of particles was calculated by dividing the yellow colored area by the area of a single particle for every single image during the experiment (**Figure 2.5-C**). More than 90% of the particles captured were released (**Figure 2.4-A and Figure 2.5-C**) suggesting this method has promise for the purification of microscale particles.

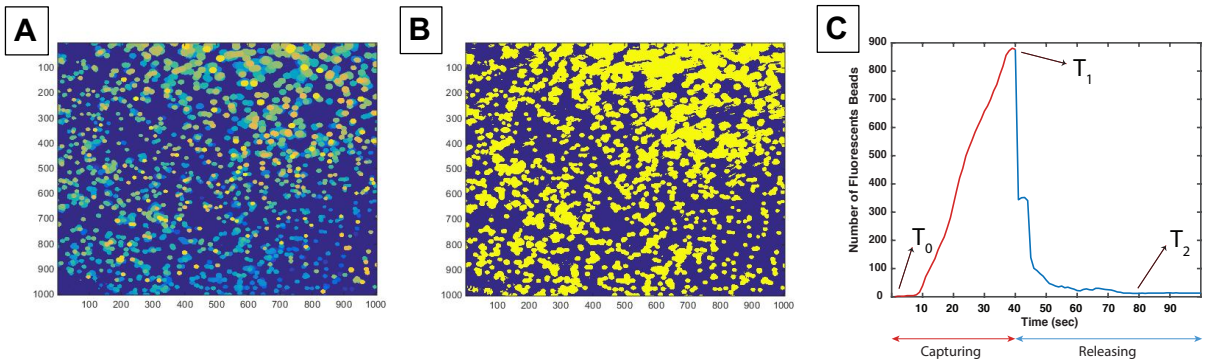


**Figure 2.5 - Counting of 10 Micron Fluorescent Particles.**

**(A)** Residence time map, **(B)** Binarized residence time map, and **(C)** Number of fluorescent particles - time plot showing capturing and releasing of micron particles over the experiment.

### 2.4.4 Nanoporous Track-Etch Capture of Fluorescent Nanoparticles

Having demonstrated capture using modified tangential flow in a microscale system, experiments were performed to show capture and release at the nanoscale (**Figure 2.6**). Track-etch membranes with 80 nm pores (nPCTE) were used to capture 100 nm fluorescent nanoparticles. Because of the significant increase in membrane resistance compared to mPCTE, flow rates of 5 µL/min (sample supply) and 2 µL/min (ultrafiltration) were now used for capture. This was followed by washing with clean buffer to remove any non-specifically bound particles before the releasing in a backwash step (5 µL/min backflow).

During the capture phase of the experiments, the fluorescence intensity curves displayed similar behavior to the microscale experiments, with a steady increase throughout the capture period (**Figure 2.6-A**). Unlike the mPCTE experiments however, there was no observable loss of fluorescence after the release of transmembrane pressure at the end of the capture phase. A fraction of loosely-associated particles, either on the surface or in suspension above the surface (**Figure 2.6-C**), were removed with a wash step.

During the capture phase of the experiments, the fluorescence intensity curves displayed similar behavior to the microscale experiments, with a steady increase throughout the capture period (**Figure 2.6-A**). Unlike the mPCTE experiments however, there was no observable loss of fluorescence after the release of transmembrane pressure at the end of the capture phase. A fraction of loosely-associated particles, either on the surface or in suspension above the surface (**Figure 2.6-C**), were removed with a wash step.

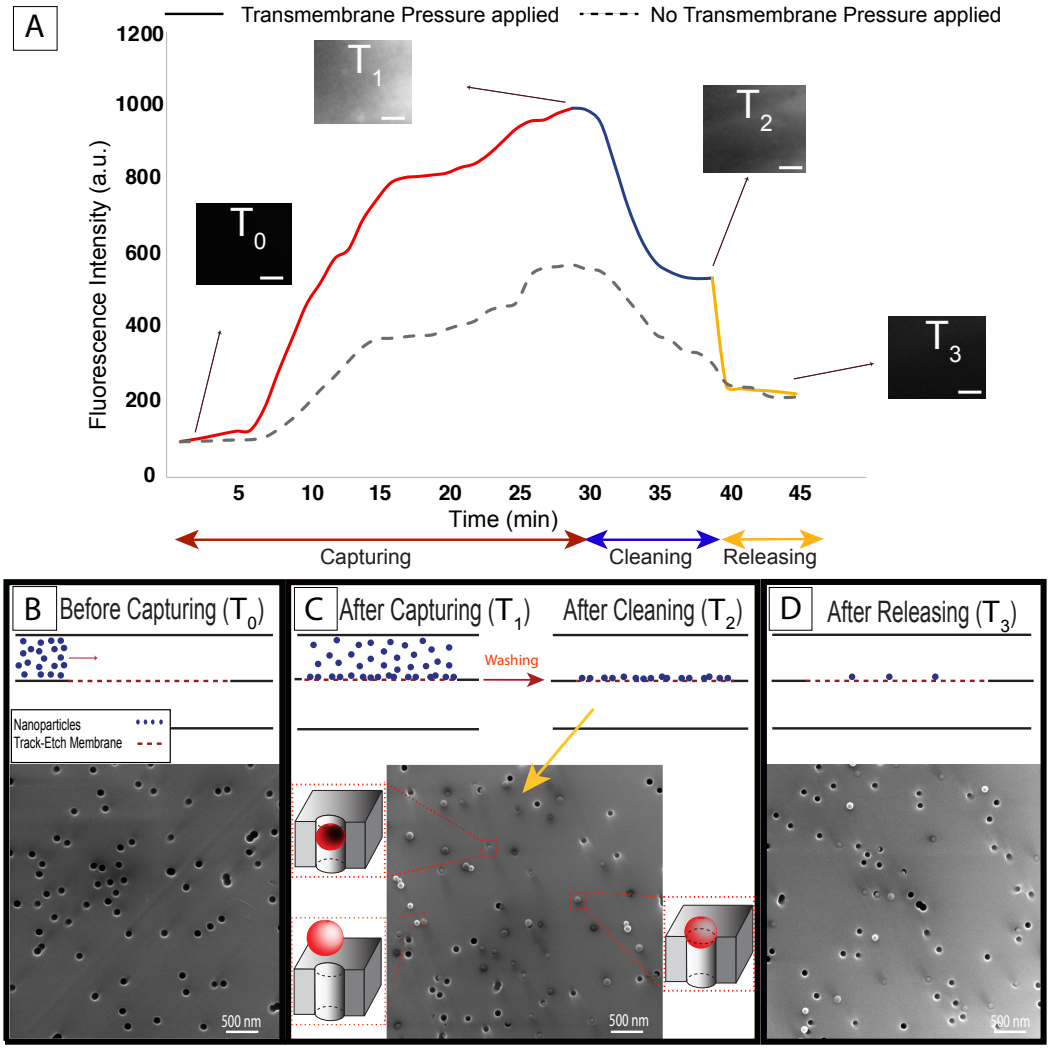


**Figure 2.6 - Nanoscale Experiments with 100 nm Fluorescent Particles and 80 nm Median Pore Size Polycarbonate Track-etch (nPCTE) Membranes.**

**(A)** Fluorescent intensity analysis (solid line) showing the gradual increasing and decreasing in the fluorescent signal during the capturing step and cleaning step, respectively, followed by a sharp drop as nanoparticles were released (the dash line shows the intensity change during the experiment in the absence of the transmembrane pressure). Scale bar on fluorescence image insets = 50 µm. **(B, C and D)** Electron micrographs showing before capturing, after capturing-cleaning, and after releasing panels, respectively.

SEM images after capturing-cleaning step suggested capturing of nanoparticles on the pores, inside the pore channels and on the surface of the membranes. In order to determine the capturing sites on the membranes, samples were gradually tilted and imaged as it can be seen in **Figure 2.7**. High magnification SEM image of $60^{o}$ tilted sample showed captured particles on the pores, inside the pores, and on the surface of the membranes due to the charge interaction (**Figure 2.7**). Flow reversal did not fully remove all the particles captured on the membrane as some were lodged deep within pores (**Figure 2.6-D and Figure 2.7**), but the system did return to within ~85% of the baseline fluorescence value.

In order to assess the role of the applied transmembrane pressure on capturing, experiments were performed in the absence of active transmembrane pressure (dashed line, **Figure 2.6-A**). To achieve this, supply flow was performed as before, but the ultrafiltration pump was not used to generate active transmembrane flow. While the change in fluorescence intensity showed an increase in particles, the maximum measured intensity was only 50% of the system with active transmembrane pressure which indicates that transmembrane pressure is the driving force of particle capture.

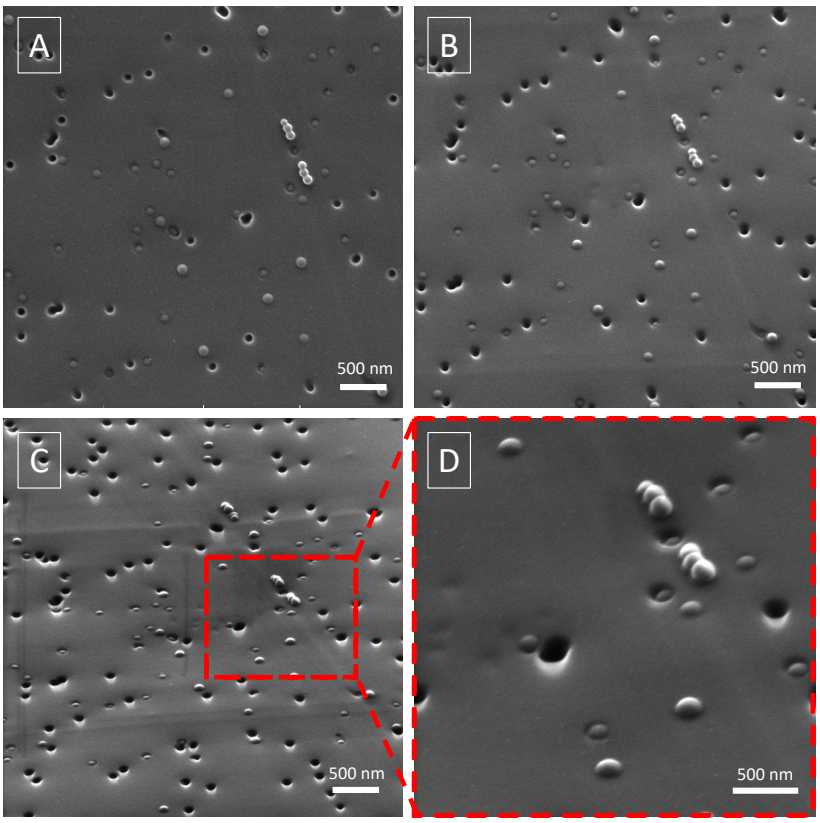


**Figure 2.7 - Characterization of Nanoparticles Capturing Sites of nPC-TE Membranes Using SEM Images.**

Micrographs were taken at different stage positions to show different perspectives. **(A)** Top down view, **(B)** 30° tilt, **(C)** 60° tilt, and **(D)** High magnification image of 60° tilt sample.

### 2.4.5 Nanoporous Silicon Nanomembrane Capture of Fluorescent Nanoparticles

Our original observations of EV capture from serum (**Figure 2.2**) were obtained with 100 nm thick nanoporous silicon-nitride (NPN) membranes [27]. It is important to note that PCTE membranes used are approximately 60 times thicker compared to ultrathin nanomembranes. Thus, our next set of studies replicated the experimental conditions used with nPCTE on NPN (5 µL/min supply; 2 µL/min ultrafiltration) with similar pore sizes (80 nm median) and total number of pores actively filtering materials were of the same order (nPCTE = 4 x $10^7$ pores/$mm^2$; NPN = 9.2 x $10^7$ pores/$mm^2$), which resulted in a slightly larger membrane area for the nPCTE membranes (4 $mm^2$) compared to the NPN membranes (1.4 $mm^2$). Therefore, membrane thickness and membrane surface chemistry are the key parametric differences between experiments on nPCTE vs. NPN.

Similar set of experiments as nanoporous track etch membranes under the same operating condition was performed to evaluate capturing and releasing of 100 nm fluorescent nanoparticles using NPN membranes (**Figure 2.8**). The capture and release intensity curves (**Figure 2.8-A**) with NPN show similar trends to nPCTE with some interesting differences. There is again an increase in fluorescence intensity on the membrane during the capture phase followed by a sudden loss of particles when the flows are stopped. After a rinse with clean buffer, the intensity returns to within ~95% of the baseline, which is slightly better than that seen with nPCTE (**Figure 2.8-A**, inset). A control in the absence of transmembrane pressure (**Figure 2.8-A**, dashed line) showed once more that the capture process is driven by transmembrane pressure.

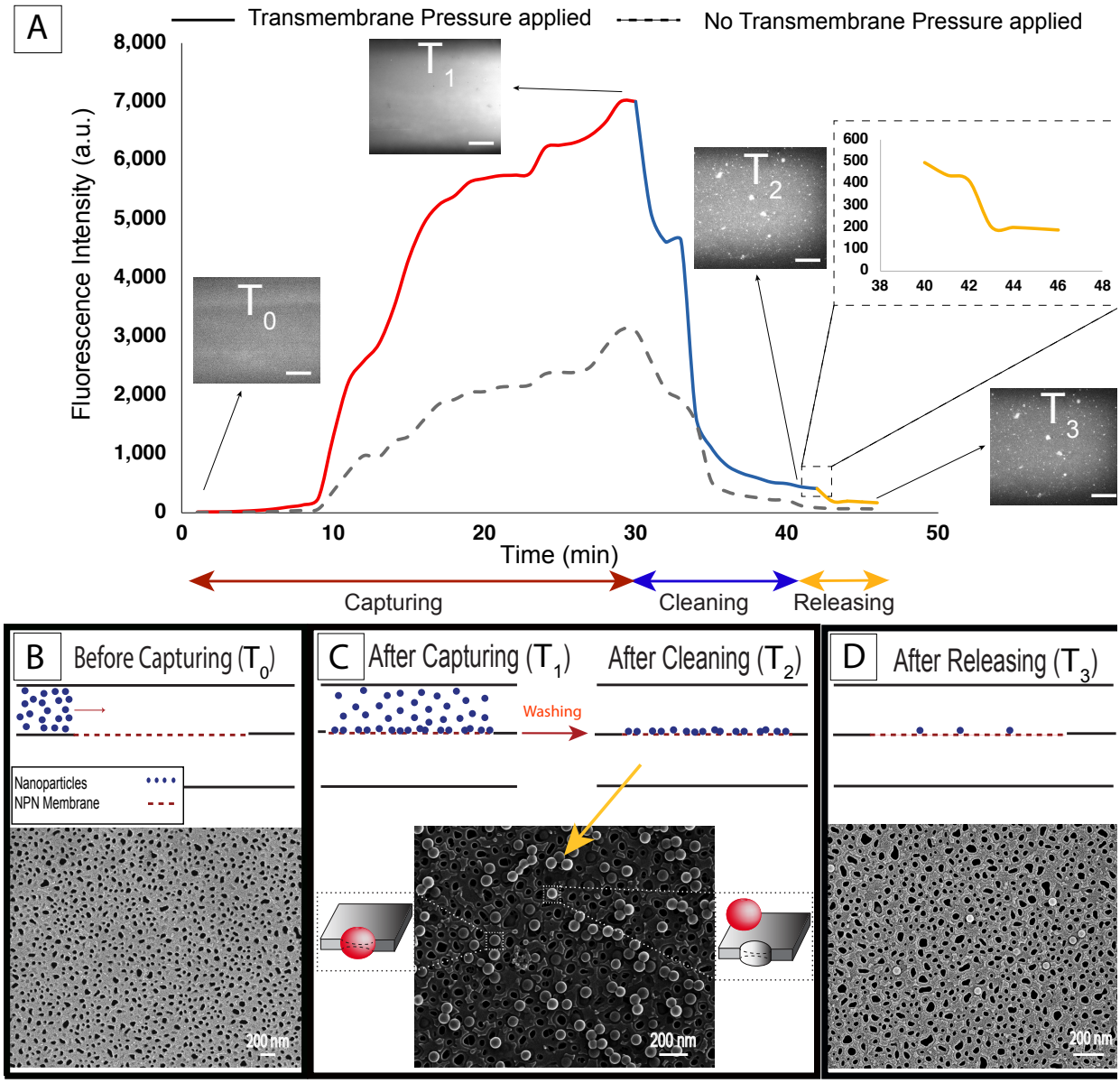


**Figure 2.8 - Nanoscale Experiments with 100 nm Fluorescent Particles and 80 nm Median Pore Size NPN membranes.**

**(A)** Fluorescent intensity analysis (solid line) showing the gradual increasing and decreasing in the fluorescent signal during the capturing step and cleaning step, respectively, followed by a sharp drop as nanoparticles were released (the dash line shows the intensity change during the experiment in the absence of the transmembrane pressure). Scale bar on fluorescence image insets = 50 µm. **(B, C and D)** Electron micrographs showing before capturing, after capturing-cleaning, and after releasing panels, respectively.

Electron microscopy was again performed to better understand the capture process. The membrane showed high pore density (**Figure 2.8-B**), in contrast with track-etch membranes (**Figure 2.8-B**), and a distribution of pore sizes with median of 80 nm (**Figure 2.9**). As expected, the majority of the 100 nm particles captured remained on top of the pores (**Figure 2.8-C**). A small proportion of particles persisted on the membrane after the releasing step, and these all appeared to be captured within pores (**Figure 2.8-D**).

In order to estimate particle concentrations throughout the capture and release process, calibration curves for both NPN and nPCTE experiments were made by correlating the fluorescent intensity to the number of particles on the membrane (**Figure 2.10**).

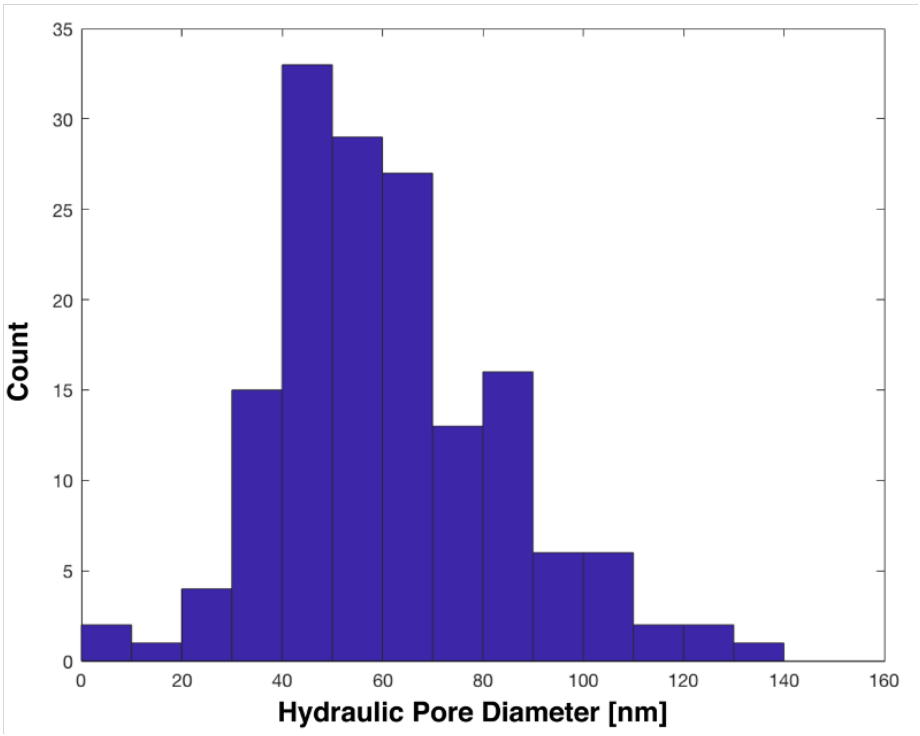


**Figure 2.9 - Pore Size Distribution for Nanoporous Silicon Nitride Membrane Chips.**

The pore distribution of NPN chips is heterogeneous, but the median diameter is 80 nm. The etching process produces random, large pores, but these would improve the capture of a heterogeneous particle population such as EVs.

Calibration curves for both PCTE and NPN membranes were obtained by correlating the fluorescent intensity with the number of fluorescent particles dried on the membrane. In order to avoid a coffee-ring effect during the drying process, water drops containing 100 nm monodispersed particles were dried on PCTE and NPN membranes at 80°C [46]. Drying the drop at higher degrees allowed the particles to accumulate at the air-liquid interface rather than at the drop edge leading to uniform deposition of particles [47].

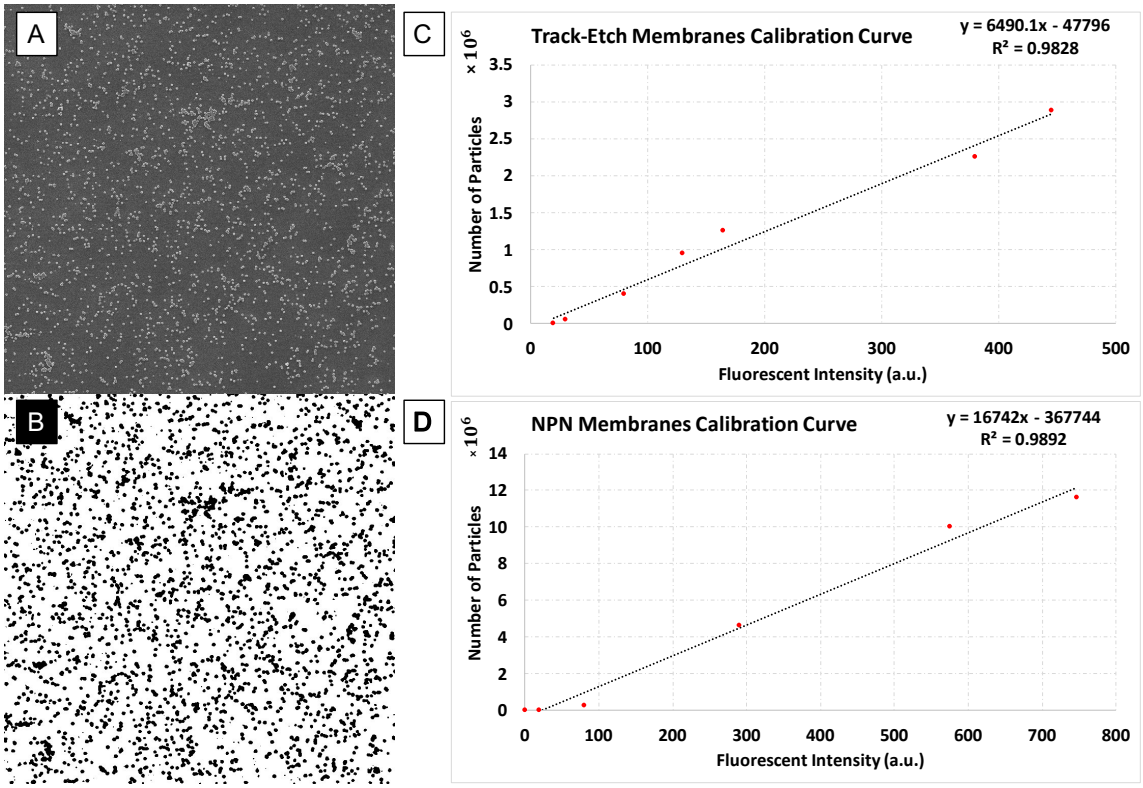


**Figure 2.10 - Calibration Curves Correlating the Fluorescent Intensity to the Number of Particles on TE and NPN Membranes.**

**(A)** SEM image of a uniform deposition of fluorescent nanoparticles, **(B)** Binarized image, **(C)** TE membranes calibration curve, and **(D)** NPN membranes calibration curve

The dried membranes were then placed back into the microfluidic devices and the channels were primed. Fluorescent images were taken using the Leica microscope and the intensity values were measured using ImageJ. Scanning electron microscopy was used to count the number of particles on the surface of the membranes. SEM images were binarized to black and white using ImageJ and number of particles in binarized SEM images was calculated by dividing the total area of particles by the area of a single particle. The best linear fit and the equation correlating the concentration of particles and the fluorescent signal were obtained and further used for analyzing the experimental data on PCTE and NPN.

These curves allowed for the direct comparison of membrane performance for particle capture and release (**Table 2-1**). We estimate that track-etch membranes capture ~2.6 x $10^6$ particles from an available population of 5 x $10^7$ and released 60% of the particles captured. By contrast, silicon nanomembranes captured ~8.6 x $10^6$ particles from the same solution and released 68% of the captured population.

These curves allowed for the direct comparison of membrane performance for particle capture and release (**Table 2-1**). We estimate that track-etch membranes capture ~2.6 x $10^6$ particles from an available population of 5 x $10^7$ and released 60% of the particles captured. By contrast, silicon nanomembranes captured ~8.6 x $10^6$ particles from the same solution and released 68% of the captured population.

**Table 2-1 - Nanoporous Track-etch (nPCTE) *vs.* Silicon Nanomembrane (NPN) Captured and Released Particle Counts.**

| Membrane | Captured Particles | Released Particles |
|---|---|---|
| TE Membranes | $(2.58 \pm 0.24) \times 10^6$ | $(1.56 \pm 0.43) \times 10^6$ |
| NPN Membranes | $(8.64 \pm 3.15) \times 10^6$ | $(5.89 \pm 1.98) \times 10^6$ |

### 2.4.6 Pressure Modeling of Track-Etch and Ultrathin Silicon Nitride Nanomembranes

We explored the effect of the membrane thickness on transmembrane pressure in our studies both analytically and experimentally. Experiments were conducted with nanoporous track-etch membranes and ultrathin nanoporous silicon nitride nanomembranes (**Figure 2.11**). Pressure sensors were placed upstream and downstream on either side of the membrane (**Figure 2.11-A**) and the pressures were monitored under flow conditions equivalent to the capture experiments (5 µL/min supply, 2 µL/min ultrafiltration). Results for both nPCTE and NPN compared favorably to predictions of the Dagan equation – a modified Hagen-Poiseuille equation that also applies to ultrathin membranes.[14, 41, 48] The Dagan equation gives the pore resistance as:

$$R_{pore} = \frac{\mu}{r^3}\left[3 + \frac{8}{\pi}\left(\frac{L}{r}\right)\right] \qquad (2.1)$$

where $\mu$ is the fluid viscosity [Pa $s^{-1}$], $r$ is the pore radius [m], and $L$ is the pore length [m]. The total membrane resistance $R$ is calculated by adding the resistance for each pore in the membrane in parallel (9.2 x $10^7$ pores for NPN and 4 x $10^7$ pores for nPCTE) and the anticipated pressure drop is then found by multiplying by the flow rate:

$$\Delta P = Q \cdot R \qquad (2.2)$$

The comparison of this estimate with experimental results (**Figure 2.11-B**) showed that a simple analytical approximation is sufficient for predicting the transmembrane pressure drop that could be experienced in the system. These results were compared to an analytical model of

pressure drop (**Figure 2.11-B**) as well as COMSOL Multiphysics simulations (**Figure 2.11-C** and **2.11-D**) to illustrate the pressure gradients and streamlines in the system.

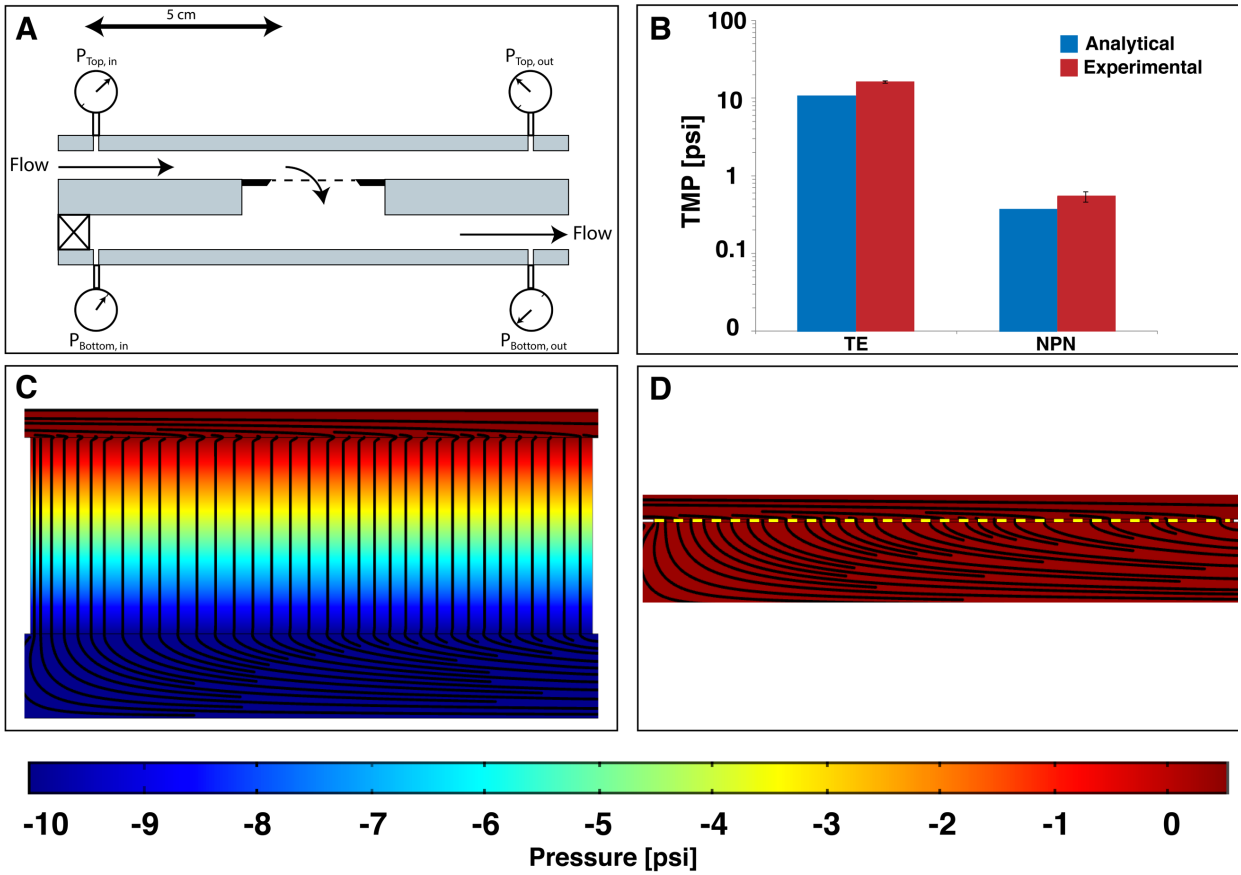


**Figure 2.11 - Theoretical and Experimental Pressure Drops Across Nanoporous Polycarbonate Track-etch Membranes (nPCTE) and Nanoporous Silicon Nitride (NPN) Membranes.**

**(A)** Diagram of the pressure monitoring system showing the position of the pressure sensors and the direction of flow. All flow was performed at 10 µL/min through the membrane with a syringe pump pushing on the top channel and a syringe pump pulling on the bottom channel. The pressure sensors were positioned 5 cm above and below the membrane. **(B)** Comparison of pressure drops across the track-etch and NPN membranes. Blue = Dagan predicted, homogeneous distribution pressure drop. Red = experimental data. Logarithmic scale used for comparison. **(C)** COMSOL model of pressure in a track-etch system showing a large pressure drop across the membrane. **(D)** COMSOL model of pressure in an NPN system showing almost no pressure drop across the membrane, in stark contrast to the track etch system. COMSOL simulations were performed using the Free and Porous Flow toolbox with a Darcy's permeability calculated for this system.

## 2.5 Discussion

In this work, we introduced a new method for sample purification in which particles are captured on the surface of a membrane in tangential flow, washed to remove contaminants, and then released in a controlled fashion where they can be further analyzed, concentrated or processed.

We call this process tangential flow for analyte capture (TFAC) and while the process resembles bind and elute strategies found in column or membrane chromatography, it relies on physical interaction, rather than chemical affinity, for capture. Similarly, TFAC requires physical release through back-flow for elution, rather than chemically treatments to disassociate chemical bonds formed during capture. As the release of chemical bonds in affinity schemes can often be destructive and incomplete, there are clear advantages for physical capture and release.

Proof of concept experiments using fluorescent particles on both PCTE and NPN membranes showed successful capture and release of particles. We have shown that NPN membranes outperform PCTE membranes for capture and release with polystyrene nanoparticles. Our analytical and experimental comparison showed that the greater thickness of PCTE compared to NPN caused higher transmembrane pressure. This high pressure drives nanoparticles into the membrane bulk where they disappear from view and are more difficult to recover (**Figure 2.8**).

One potential application of TFAC utilizing ultrathin membranes as a microfluidic based technique would be isolation of extracellular vesicles. Studies have indicated that not only the RNA content of these vesicles, but also their protein varies by cell of origin as well as by the pathologic state of these cells [49-53]. This differential cell state specific and cellular origin-

based content indicates that EVs could serve as biomarkers of disease. These biomarkers could be used for a range of clinical purposes including disease screening, predicting *a priori* disease responsiveness to treatment, and monitoring response to treatment. Currently, the "gold standard" method for isolating extracellular vesicles from biofluids is ultracentrifugation, which requires large volumes of biofluid (> 25 ml), long processing times, expensive instrumentation and trained technicians. Gel precipitation and size exclusion chromatography and have been developed that remove the need for ultracentrifugation and allow extracellular vesicle isolation in a benchtop centrifuge, but these methods suffer from low yield and/or contamination with co-precipitated proteins [54-58]. The high protein contamination from these methods prevents the use of EV proteins as biomarkers in addition to RNA. The result from our plasma isolation experiment by ultrathin nanomembranes showing capture of EVs with minimal contamination suggests promising potential of TFAC for isolation of EVs with high purity (**Figure 2.12**).

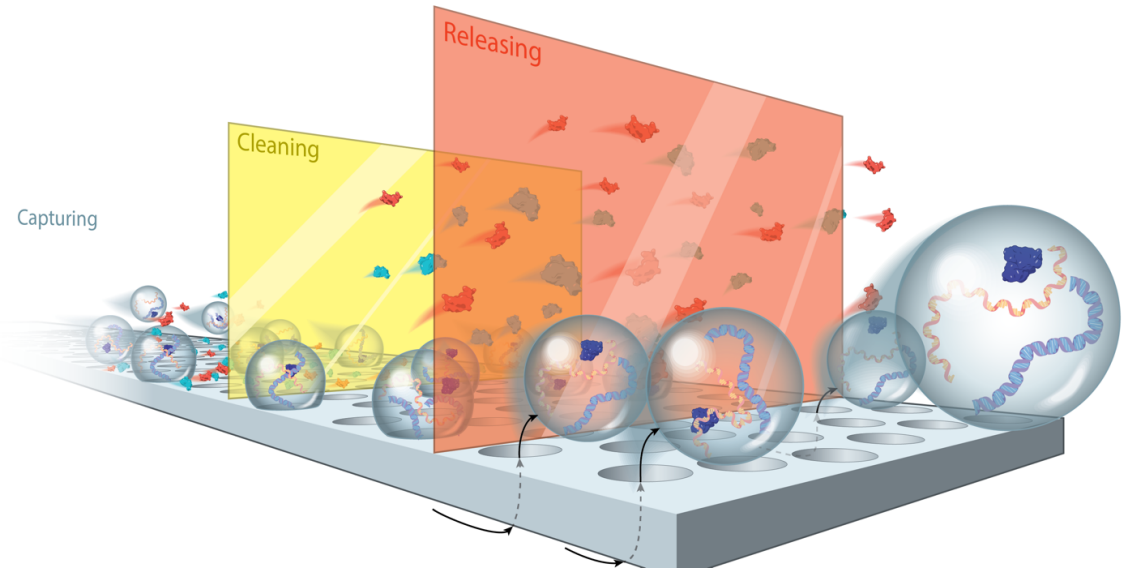


**Figure 2.12 - Tangential Flow for Analyte Capture (TFAC) Illustration Showing Capturing, Cleaning and Releasing Steps.**

Additionally, the pore size of the ultrathin NPN membranes can be tuned to capture different subpopulations of EVs that vary in size [59, 60]. This includes microvesicles, exosomes and apoptotic bodies which are diagnostically informative [61]. In all cases, TFAC method eliminates the necessity of preprocessing biofluids which can be both time consuming, result in sample loss, and often requires specialized equipment reducing the utility of these particles in point of care diagnostic devices [62, 63].

Another potential application of TFAC would be a membrane-based '*in situ'* analysis to detect EVs carrying cancer biomarkers among a larger population using the same membrane for capture, labeling, and imaging by fluorescence microscopy. TFAC using NPN membranes showed that captured particles were associated with membrane surface, rather than trapped in a bulk-matrix which means that the captured particles can be analyzed directly on the membrane. Furthermore, TFAC captured extracellular vesicles from whole plasma with minimal contamination (**Figure 2.2**) as opposed to rapidly formed cake on the membrane by NFF which increases the sensitivity and specify of EVs biomarker detection. Also, the excellent optical properties of ultrathin inorganic membranes like NPN, would also be key to enabling this application [64]. In comparison, track-etch membranes lack this optical transparency and as the current study indicates, trap EVs below the membrane surface, together precluding the ability to detect specific diagnostic markers directly in and on the EVs captured on the membranes [65].

The abundant presence of EVs and lipoproteins with similar physical characteristics such as size and density in blood makes it one of the most difficult body fluids to isolate EVs from [66]. Co-purification of EVs and lipoproteins has been observed using other size based separation

methods such as size exclusion chromatography and density gradient ultracentrifugation [44, 45]. Therefore, contamination of EVs with blood lipoproteins may occur using TFAC. However, affinity-based separation can be performed downstream to decrease the blood lipoproteins contaminants level when EV samples with high purity is desired [67, 68]. On the other hand, lipoproteins are not likely to be present in cell-conditioned media, especially when cells are cultured with serum-free media.

## 2.6 Future Directions

### 2.6.1 NPN Membranes

TFAC is a novel technique for separation of nanoparticles such as EVs based on size using ultrathin nanomembranes. Here, we showed the feasibility of this technique for purification of EVs. The TFAC system can be further optimized for higher yield and purity. In order to do so, following ideas can be explored;

#### 2.6.1.1 Minimizing the non-specific adsorption

The yield can be improved by minimizing the non-specific adsorption due to their interaction with the surface of membrane and device channels. The surface of the channels and the membrane can be coated prior to purification step by 1% pluronic (PEO-PPO-PEO-block copolymer) solution. The system can be rinsed and washed with PBS after 1 hour of incubation with pluronic solution. This can help to maximize the EV retrieval and increase the purification yield.

#### 2.6.1.2 EV sample recirculation

No loss of nanoparticles was observed in the pore channels of NPN membranes and the membrane stayed intact after the releasing step. Therefore, the purification yield can be further improved by collecting the sample from the outlet and recirculating them again in the system. After releasing the captured nanoparticles, the collected sample from the device outlet can be pumped to the device again for capturing the nanoparticles that were not purified in the

first step. Therefore, recirculation can be explored to increase the yield, especially since both the device and the membrane stay intact.

#### 2.6.1.3 Modifying the operating condition and the device design

The flow rates applied for the purification need to be further optimized for the best yield and purity. Different flow rate combinations for pushing tangentially and pulling across the membrane can be tested and the number of particles purified can be then measured by NTA. Furthermore, the geometry of the channels is an important factor in the resistance and the transmembrane pressure, similar to the flow rates. Decreasing the height of the channels can help to increase the sample volume that is experiencing the transmembrane pressure required for nanoparticles to interact with the pores and get captured.

### 2.6.2 Nanopocket Membranes

#### 2.6.2.1 Size based separation of subpopulation of EVs

Separation of subpopulations of EVs based on size has received a lot of attention recently. Different sizes of EVs have recently purified by different steps of differential ultracentrifugation. The authors categorized the EVs in three subpopulations; **large EVs** which were pelleted by low centrifugation speed (2,000 × g), **medium EVs** pelleted by medium centrifugation speed (10,000 × g), and **small EVs** which were recovered after high centrifugation speed (100,000 × g). However, the NTA analysis of separated EVs showed an overlap in the size of different subpopulations of EVs.

In our lab, we have developed a new approach for fabrication of nanomembranes with well-controlled pore sizes using nanosphere lithography (NSL) [69]. NSL uses close-packing of

nanoparticles to pattern pores in an ultrathin membranes **(Figure 2.13**). We have shown fabrication of ultrathin nanomembranes with pores in the same size range as EVs which can be used for separation of nanoparticles and EVs. In short, self-assembly of polystyrene nanoparticles was achieved at a water/hexane interface. By extracting it as a constant speed, the self-assembled monolayer of polystyrene nanoparticles was then deposited on a substrate. Using $O_2$ plasma treatment, the size of nanoparticles was reduced. A mask was created by a thin Al deposition before the nanoparticles are removed via sonication. The generated voids in the Al mask was used to etch the pores and the membranes were then released from the silicon wafer substrate [69].

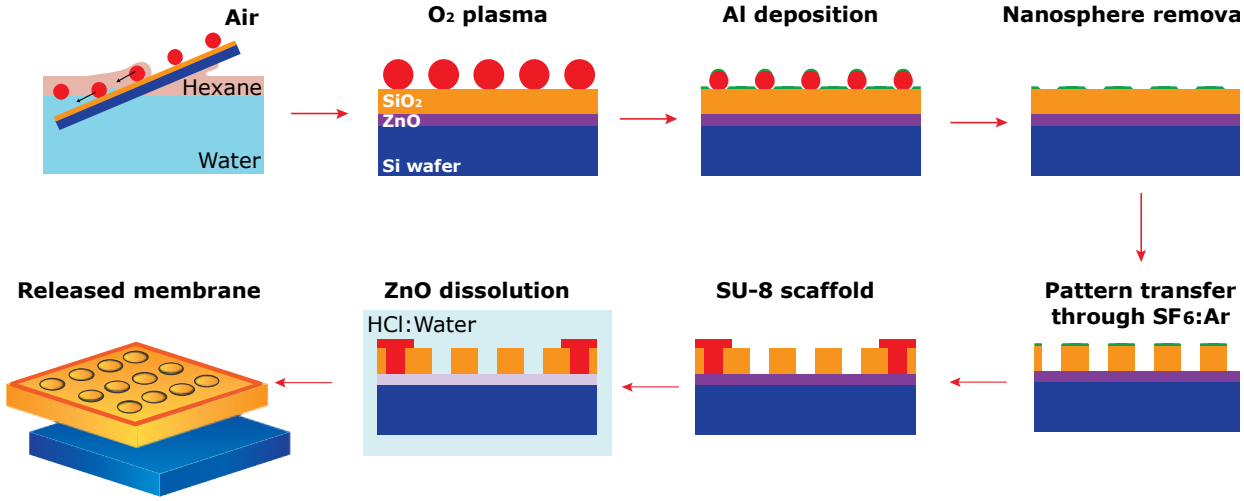


**Figure 2.13 - Nanosphere Lithography (NSL) Process for Fabrication of Ultrathin Nanomembranes [69].**

The NSL technique can be extended to fabricate a novel nanomembrane, termed as, nanopocket membranes. Nanopocket membranes are a novel type of membranes with pores fabricated as a bowl with a hole at the bottom (**Figure 2.14**). Parylene film is a great candidate due to its conformal deposition properties, low cost, the biocompatibility. The nanopocket membrane purification can be performed in a TFF mode with a slight transmembrane pressure

to capture target nanoparticles in the nanopockets. After capturing the nanoparticles, they can be released and collected simply by reversing the transmembrane pressure.

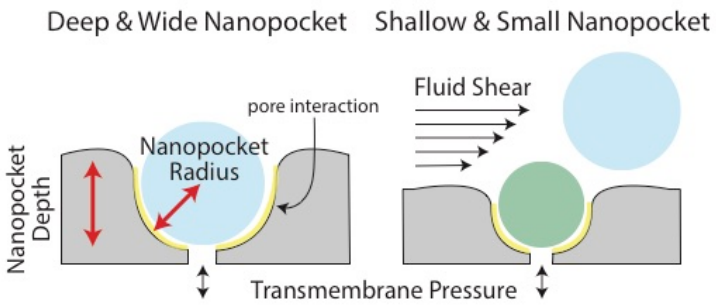


**Figure 2.14 – Cross-section Schematic of a Nanopocket Membrane.**

The ideal operating condition in TFF can be defined by critical flux, such that below this value, the process can be operated without membrane fouling. Below the critical flux value, the shear force is enough to keep the surface of the membrane clean and prevents the cake formation or the protein build up. This leads to continuous filtration with a transmembrane pressure rise under the constant flux conditions. We have recently studied the critical flux behavior of ultrathin (NTN) and conventional thick polymeric (nPCTE) nanomembranes and found that ultrathin nature of NPN membranes could enable a higher critical flux that nPCTE under the same protein concentration and flow conditions [70]. This result suggests that protein rich biofluids can be processed in TFF mode under the low transmembrane pressure of NPN membranes without fouling. The critical flux behavior of nanopocket membranes can be determined using a flux stepping technique and different concentrations of BSA solutions mimicking the protein concentration level of biological fluids. This can help to eliminate concerns regarding membrane fouling and damaging the filtered species in TFF mode in concentrated biofluids.

Furthermore, As a proof of concept, fluorescent nanoparticles with different sizes can be used to optimize the operation condition of the system like the applied flow rates for the highest purification yield and capturing efficiency. The concentration of fluorescent nanoparticles captured and released under different operation conditions can be determined by NTA. Nanopockets dimensions such as radius and depth can be tailored by adjusting the beads size and etching parameters, respectfully (**Figure 2.14**). Different nanopocket dimensions can be fabricated and used in TFAC system to separate subpopulations of EVs based on size. Purified EV samples can first be used to study feasibility of separation of subpopulations of EVs and the yield can be examined by NTA. The optimized operating condition for purification of EVs from different biofluids can be defined based on the results from fluorescent nanoparticles experiments for the highest yield, critical flux behavior of nanopocket membranes and separation of subpopulations of EVs from purified samples.

#### 2.6.2.2 Affinity based separation of subpopulation of EVs

In addition to the size based, surface marker based separation of EVs have also received a lot of attention recently to identify the phenotype subsets of EVs. A recent study reported a microfluid based technique for single EV analysis to identify heterogenous biomarker profiles of EVs. The EVs were first immobilized inside a microfluidic chamber and then on-chip immuno-staining and imaging were performed [71].

As another future direction for TFAC system using nanopocket membranes, nanopocket membranes can be coated by specific ligands that selectively bind to EVs expressing the target protein marker. This can help to capture a specific subset of EVs which is beneficial for identifying their phenotype as well as utilizing them as therapeutic and diagnostic tools.

## 2.7 Conclusion

In this work, we have developed a method called tangential flow for analyte capture (TFAC) to capture and release of particles. We contend that ultrathin membranes are ideally suited for TFAC for two reasons: 1) operating pressures are orders-of-magnitude lower for ultrathin membranes than for membranes with conventional thicknesses (1-10 μm) and 2) captured particles are associated with a surface, rather than trapped in a bulk-matrix and 3) higher efficiency of capture and release of particles. Experiments performed in normal flow filtration with human plasma demonstrated formation of a protein cake on the surface of ultrathin membranes. However, testing human plasma in TFAC mode resulted in capturing extracellular vesicles with minimal contamination. Captured vesicles were further labeled *in situ*, providing a convenient platform for downstream detection and analysis. Together, these findings suggest promising potential of TFAC for both isolation of EVs and biomarker detection on captured EVs.

## 2.8 Acknowledgements and Funding:

I would like to acknowledge Kilean Lucas, Ph. D. candidate at University of Rochester for the simulation work on the transmembrane pressure comparison between PCTE and NPN membranes and the scanning electron microscopy images EVs captured in plasma experiments. I would like to also acknowledge Brad Kwarta for the EV capture and release illustration. Research reported in this chapter was supported in part by the National Science Foundation (IIP 1660177) to J.L.M and T.R.G., Department of Defense (CA170373) to J.L.M., and the National Institutes of Health (R35GM119623) to T.R.G.

## 2.9 References


[1] R. van Reis, A. Zydney, Membrane separations in biotechnology, Curr Opin Biotech 12(2) (2001) 208-211.

[2] C. Christy, G. Adams, R. Kuriyel, G. Bolton, A. Seilly, High-performance tangential flow filtration: a highly selective membrane separation process, Desalination 144(1-3) (2002) 133-136.

[3] M. Segura, A. Kamen, A. Garnier, Overview of Current Scalable Methods for Purification of Viral Vectors, in: O.-W. Merten, M. Al-Rubeai (Eds.), Viral Vectors for Gene Therapy: Methods and Protocols, Humana Press2011, pp. 89-116.

[4] R.T. Kurnik, A.W. Yu, G.S. Blank, A.R. Burton, D. Smith, A.M. Athalye, R. van Reis, Buffer exchange using size exclusion chromatography, countercurrent dialysis, and tangential flow filtration: Models, development, and industrial application, Biotechnol Bioeng 45(2) (1995) 149-57.

[5] S. Sweeny, G. Woehrle, J. Hutchinson, Rapid Purification and Size Separation of Gold Nanoparticles via Diafiltration, Journal of American Chemical Society 128 (2006) 3190-3197.

[6] R. van Reis, S. Gadam, L.N. Frautschy, S. Orlando, E.M. Goodrich, S. Saksena, R. Kuriyel, C.M. Simpson, S. Pearl, A.L. Zydney, High performance tangential flow filtration, Biotechnol Bioeng 56(1) (1997) 71-82.

[7] J. Fritsch, C.I. Moraru, Development and optimization of a carbon dioxide-aided cold microfiltration process for the physical removal of microorganisms and somatic cells from skim milk, J Dairy Sci 91(10) (2008) 3744-3760.

[8] T. Okada, M. Nonaka-Sarukawa, R. Uchibori, K. Kinoshita, H. Hayashita-Kinoh, Y. Nitahara-Kasahara, S. Takeda, K. Ozawa, Scalable purification of adeno-associated virus serotype 1 (AAV1) and AAV8 vectors, using dual ion-exchange adsorptive membranes, Hum Gene Ther 20(9) (2009) 1013-21.

[9] K.K. Langfield, H.J. Walker, L.C. Gregory, M.J. Federspiel, Manufacture of Measles Viruses, in: O.-W. Merten, M. Al-Rubeai (Eds.), Viral Vectors for Gene Therapy: Methods and Protocols, Humana Press2011, pp. 345-366.

[10] M. Lock, M.R. Alvira, J.M. Wilson, Analysis of particle content of recombinant adeno-associated virus serotype 8 vectors by ion-exchange chromatography, Hum Gene Ther Methods 23(1) (2012) 56-64.

[11] G. Belfort, R.H. Davis, A.L. Zydney, The behavior of suspensions and macromolecular solutions in crossflow microfiltration, J Memb Sci 96 (1994) 1-58.

[12] R. Ghosh, Rapid antibody screening by membrane chromotagraphic immunoassay technique, J Chromatogr B 844 (2006) 163-167.

[13] R.W. Field, D. Wu, J.A. Howell, B.B. Gupta, Critical Flux Concept for Microfiltration Fouling, J Membrane Sci 100(3) (1995) 259-272.

[14] T.R. Gaborski, J.L. Snyder, C.C. Striemer, D.Z. Fang, M. Hoffman, P.M. Fauchet, J.L. McGrath, High-performance separation of nanoparticles with ultrathin porous nanocrystalline silicon membranes, ACS nano 4(11) (2010) 6973-6981.

[15] J.L. Snyder, A. Clark, Jr., D.Z. Fang, T.R. Gaborski, C.C. Striemer, P.M. Fauchet, J.L. McGrath, An experimental and theoretical analysis of molecular separations by diffusion through ultrathin nanoporous membranes, J Memb Sci 369(1-2) (2011) 119-129.

[16] D.G. Johnson, T.S. Khire, Y.L. Lyubarskaya, K.J. Smith, J.P. Desormeaux, J.G. Taylor, T.R. Gaborski, A.A. Shestopalov, C.C. Striemer, J.L. McGrath, Ultrathin silicon membranes for wearable dialysis, Advances in chronic kidney disease 20(6) (2013) 508-15.

[17] K.J.P. Smith, M. May, R.E. Baltus, J.L. McGrath, A predictive model of separations in dead-end filtration with ultrathin membranes, Separation and Purification Technology 189 (2017) 40-47.

[18] M. Mireles, T.R. Gaborski, Fabrication techniques enabling ultrathin nanostructured membranes for separations, Electrophoresis 38(19) (2017) 2374-2388.

[19] J.P. DesOrmeaux, J.D. Winans, S.E. Wayson, T.R. Gaborski, T.S. Khire, C.C. Striemer, J.L. McGrath, Nanoporous silicon nitride membranes fabricated from porous nanocrystalline silicon templates, Nanoscale 6(18) (2014) 10798-805.

[20] S.G. Harris, M.L. Shuler, Growth of endothelial cells on microfabricated silicon nitride membranes for an in vitro model of the blood-brain barrier, Biotechnology and Bioprocess Engineering 8(4) (2003) 246-251.

[21] A.R. Mazzocchi, A.J. Man, J.P.S. DesOrmeaux, T.R. Gaborski, Porous Membranes Promote Endothelial Differentiation of Adipose-Derived Stem Cells and Perivascular Interactions, Cell Mol Bioeng 7(3) (2014) 369-378.
[22] R.R. Nair, H.A. Wu, P.N. Jayaram, I.V. Grigorieva, A.K. Geim, Unimpeded permeation of water through helium-leak-tight graphene-based membranes, Science 335(6067) (2012) 442-4.
[23] C.C. Striemer, T.R. Gaborski, J.L. McGrath, P.M. Fauchet, Charge- and size-based separation of macromolecules using ultrathin silicon membranes, Nature 445(7129) (2007) 749-753.
[24] S.P. Surwade, S.N. Smirnov, I.V. Vlassiouk, R.R. Unocic, G.M. Veith, S. Dai, S.M. Mahurin, Water desalination using nanoporous single-layer graphene, Nat Nanotechnol 10(5) (2015) 459-64.
[25] J. Winans, K. Smith, T. Gaborski, J. Roussie, J. McGrath, Membrane capacity and fouling mechanisms for ultrathin nanomembranes in dead-end filtration, J Memb Sci 499 (2016) 282-289.
[26] K.J. Smith, J. Winans, J. McGrath, Ultrathin Membrane Fouling Mechanism Transitions in Dead-End Filtration of Protein, ASME 2016 14th International Conference on Nanochannels, Microchannels, and Minichannels collocated with the ASME 2016 Heat Transfer Summer Conference and the ASME 2016 Fluids Engineering Division Summer Meeting, American Society of Mechanical Engineers, 2016, pp. V001T15A001-V001T15A001.
[27] J.P.S. DesOrmeaux, J.D. Winans, S.E. Wayson, T.R. Gaborski, T.S. Khire, C.C. Striemer, J.L. McGrath, Nanoporous silicon nitride membranes fabricated from porous nanocrystalline silicon templates, Nanoscale 6(18) (2014) 10798-10805.
[28] A. Gallo, M. Tandon, I. Alevizos, G.G. Illei, The majority of microRNAs detectable in serum and saliva is concentrated in exosomes, PLoS One 7(3) (2012) e30679.
[29] M.R. Fernando, C. Jiang, G.D. Krzyzanowski, W.L. Ryan, New evidence that a large proportion of human blood plasma cell-free DNA is localized in exosomes, PLoS One 12(8) (2017) e0183915.
[30] M. Li, E. Zeringer, T. Barta, J. Schageman, A. Cheng, A.V. Vlassov, Analysis of the RNA content of the exosomes derived from blood serum and urine and its potential as biomarkers, Philos Trans R Soc Lond B Biol Sci 369(1652) (2014).
[31] D. Armstrong, D.E. Wildman, Extracellular Vesicles and the Promise of Continuous Liquid Biopsies, J Pathol Transl Med 52(1) (2018) 1-8.
[32] R.E. Lane, D. Korbie, M.M. Hill, M. Trau, Extracellular vesicles as circulating cancer biomarkers: opportunities and challenges, Clin Transl Med 7(1) (2018) 14.
[33] R.S. Conlan, S. Pisano, M.I. Oliveira, M. Ferrari, I.M. Pinto, Exosomes as reconfigurable therapeutic systems, Trends in molecular medicine 23(7) (2017) 636-650.
[34] P. Li, M. Kaslan, S.H. Lee, J. Yao, Z. Gao, Progress in Exosome Isolation Techniques, Theranostics 7(3) (2017) 789-804.
[35] D. Kang, S. Oh, S.M. Ahn, B.H. Lee, M.H. Moon, Proteomic analysis of exosomes from human neural stem cells by flow field-flow fractionation and nanoflow liquid chromatography-tandem mass spectrometry, J Proteome Res 7(8) (2008) 3475-80.
[36] S. Busatto, G. Vilanilam, T. Ticer, W.L. Lin, D.W. Dickson, S. Shapiro, P. Bergese, J. Wolfram, Tangential Flow Filtration for Highly Efficient Concentration of Extracellular Vesicles from Large Volumes of Fluid, Cells 7(12) (2018).
[37] R.P. McNamara, C.P. Caro-Vegas, L.M. Costantini, J.T. Landis, J.D. Griffith, B.A. Damania, D.P. Dittmer, Large-scale, cross-flow based isolation of highly pure and endocytosis-competent extracellular vesicles, J Extracell Vesicles 7(1) (2018) 1541396.
[38] C. Théry, K.W. Witwer, E. Aikawa, M.J. Alcaraz, J.D. Anderson, R. Andriantsitohaina, A. Antoniou, T. Arab, F. Archer, G.K. Atkin-Smith, D.C. Ayre, J.-M. Bach, D. Bachurski, H. Baharvand, L. Balaj, S. Baldacchino, N.N. Bauer, A.A. Baxter, M. Bebawy, C. Beckham, A. Bedina Zavec, A. Benmoussa, A.C. Berardi, P. Bergese, E. Bielska, C. Blenkiron, S. Bobis-Wozowicz, E. Boilard, W. Boireau, A. Bongiovanni, F.E. Borràs, S. Bosch, C.M. Boulanger, X. Breakefield, A.M. Breglio, M.Á. Brennan, D.R. Brigstock, A. Brisson, M.L.D. Broekman, J.F. Bromberg, P. Bryl-Górecka, S. Buch, A.H. Buck, D. Burger, S. Busatto, D. Buschmann, B. Bussolati, E.I. Buzás, J.B. Byrd, G. Camussi, D.R.F. Carter, S. Caruso, L.W. Chamley, Y.-T. Chang, C. Chen, S. Chen, L. Cheng, A.R. Chin, A. Clayton, S.P. Clerici, A. Cocks, E. Cocucci, R.J. Coffey, A. Cordeiro-da-Silva, Y. Couch, F.A.W. Coumans, B. Coyle, R. Crescitelli, M.F. Criado, C. D'Souza-Schorey, S. Das, A. Datta Chaudhuri, P. de Candia, E.F. De Santana, O. De Wever, H.A. del Portillo, T. Demaret, S. Deville, A. Devitt, B. Dhondt, D. Di

Vizio, L.C. Dieterich, V. Dolo, A.P. Dominguez Rubio, M. Dominici, M.R. Dourado, T.A.P. Driedonks, F.V. Duarte, H.M. Duncan, R.M. Eichenberger, K. Ekström, S. El Andaloussi, C. Elie-Caille, U. Erdbrügger, J.M. Falcón-Pérez, F. Fatima, J.E. Fish, M. Flores-Bellver, A. Försönits, A. Frelet-Barrand, F. Fricke, G. Fuhrmann, S. Gabrielsson, A. Gámez-Valero, C. Gardiner, K. Gärtner, R. Gaudin, Y.S. Gho, B. Giebel, C. Gilbert, M. Gimona, I. Giusti, D.C.I. Goberdhan, A. Görgens, S.M. Gorski, D.W. Greening, J.C. Gross, A. Gualerzi, G.N. Gupta, D. Gustafson, A. Handberg, R.A. Haraszti, P. Harrison, H. Hegyesi, A. Hendrix, A.F. Hill, F.H. Hochberg, K.F. Hoffmann, B. Holder, H. Holthofer, B. Hosseinkhani, G. Hu, Y. Huang, V. Huber, S. Hunt, A.G.-E. Ibrahim, T. Ikezu, J.M. Inal, M. Isin, A. Ivanova, H.K. Jackson, S. Jacobsen, S.M. Jay, M. Jayachandran, G. Jenster, L. Jiang, S.M. Johnson, J.C. Jones, A. Jong, T. Jovanovic-Talisman, S. Jung, R. Kalluri, S.-i. Kano, S. Kaur, Y. Kawamura, E.T. Keller, D. Khamari, E. Khomyakova, A. Khvorova, P. Kierulf, K.P. Kim, T. Kislinger, M. Klingeborn, D.J. Klinke, M. Kornek, M.M. Kosanović, Á.F. Kovács, E.-M. Krämer-Albers, S. Krasemann, M. Krause, I.V. Kurochkin, G.D. Kusuma, S. Kuypers, S. Laitinen, S.M. Langevin, L.R. Languino, J. Lannigan, C. Lässer, L.C. Laurent, G. Lavieu, E. Lázaro-Ibáñez, S. Le Lay, M.-S. Lee, Y.X.F. Lee, D.S. Lemos, M. Lenassi, A. Leszczynska, I.T.S. Li, K. Liao, S.F. Libregts, E. Ligeti, R. Lim, S.K. Lim, A. Linē, K. Linnemannstöns, A. Llorente, C.A. Lombard, M.J. Lorenowicz, Á.M. Lörincz, J. Lötvall, J. Lovett, M.C. Lowry, X. Loyer, Q. Lu, B. Lukomska, T.R. Lunavat, S.L.N. Maas, H. Malhi, A. Marcilla, J. Mariani, J. Mariscal, E.S. Martens-Uzunova, L. Martin-Jaular, M.C. Martinez, V.R. Martins, M. Mathieu, S. Mathivanan, M. Maugeri, L.K. McGinnis, M.J. McVey, D.G. Meckes, K.L. Meehan, I. Mertens, V.R. Minciacchi, A. Möller, M. Møller Jørgensen, A. Morales-Kastresana, J. Morhayim, F. Mullier, M. Muraca, L. Musante, V. Mussack, D.C. Muth, K.H. Myburgh, T. Najrana, M. Nawaz, I. Nazarenko, P. Nejsum, C. Neri, T. Neri, R. Nieuwland, L. Nimrichter, J.P. Nolan, E.N.M. Nolte-'t Hoen, N. Noren Hooten, L. O'Driscoll, T. O'Grady, A. O'Loghlen, T. Ochiya, M. Olivier, A. Ortiz, L.A. Ortiz, X. Osteikoetxea, O. Østergaard, M. Ostrowski, J. Park, D.M. Pegtel, H. Peinado, F. Perut, M.W. Pfaffl, D.G. Phinney, B.C.H. Pieters, R.C. Pink, D.S. Pisetsky, E. Pogge von Strandmann, I. Polakovicova, I.K.H. Poon, B.H. Powell, I. Prada, L. Pulliam, P. Quesenberry, A. Radeghieri, R.L. Raffai, S. Raimondo, J. Rak, M.I. Ramirez, G. Raposo, M.S. Rayyan, N. Regev-Rudzki, F.L. Ricklefs, P.D. Robbins, D.D. Roberts, S.C. Rodrigues, E. Rohde, S. Rome, K.M.A. Rouschop, A. Rughetti, A.E. Russell, P. Saá, S. Sahoo, E. Salas-Huenuleo, C. Sánchez, J.A. Saugstad, M.J. Saul, R.M. Schiffelers, R. Schneider, T.H. Schøyen, A. Scott, E. Shahaj, S. Sharma, O. Shatnyeva, F. Shekari, G.V. Shelke, A.K. Shetty, K. Shiba, P.R.M. Siljander, A.M. Silva, A. Skowronek, O.L. Snyder, R.P. Soares, B.W. Sódar, C. Soekmadji, J. Sotillo, P.D. Stahl, W. Stoorvogel, S.L. Stott, E.F. Strasser, S. Swift, H. Tahara, M. Tewari, K. Timms, S. Tiwari, R. Tixeira, M. Tkach, W.S. Toh, R. Tomasini, A.C. Torrecilhas, J.P. Tosar, V. Toxavidis, L. Urbanelli, P. Vader, B.W.M. van Balkom, S.G. van der Grein, J. Van Deun, M.J.C. van Herwijnen, K. Van Keuren-Jensen, G. van Niel, M.E. van Royen, A.J. van Wijnen, M.H. Vasconcelos, I.J. Vechetti, T.D. Veit, L.J. Vella, É. Velot, F.J. Verweij, B. Vestad, J.L. Viñas, T. Visnovitz, K.V. Vukman, J. Wahlgren, D.C. Watson, M.H.M. Wauben, A. Weaver, J.P. Webber, V. Weber, A.M. Wehman, D.J. Weiss, J.A. Welsh, S. Wendt, A.M. Wheelock, Z. Wiener, L. Witte, J. Wolfram, A. Xagorari, P. Xander, J. Xu, X. Yan, M. Yáñez-Mó, H. Yin, Y. Yuana, V. Zappulli, J. Zarubova, V. Žėkas, J.-y. Zhang, Z. Zhao, L. Zheng, A.R. Zheutlin, A.M. Zickler, P. Zimmermann, A.M. Zivkovic, D. Zocco, E.K. Zuba-Surma, Minimal information for studies of extracellular vesicles 2018 (MISEV2018): a position statement of the International Society for Extracellular Vesicles and update of the MISEV2014 guidelines, Journal of Extracellular Vesicles 7(1) (2018) 1535750.

[39] P.K. Yuen, V.N. Goral, Low-cost rapid prototyping of flexible microfluidic devices using a desktop digital craft cutter, Lab on a Chip 10(3) (2010) 384-387.

[40] T. Burgin, D. Johnson, H. Chung, A. Clark, J. McGrath, Analytical and Finite Element Modeling of Nanomembranes for Miniaturized, Continuous Hemodialysis, Membranes 6(1) (2015) 6.

[41] H.H. Chung, C.K. Chan, T.S. Khire, G.A. Marsh, A. Clark, R.E. Waugh, J.L. McGrath, Highly permeable silicon membranes for shear free chemotaxis and rapid cell labeling, Lab Chip 14 (2014) 2456-68.

[42] A. Mossu, M. Rosito, T. Khire, H. Li Chung, H. Nishihara, I. Gruber, E. Luke, L. Dehouck, F. Sallusto, F. Gosselet, J.L. McGrath, B. Engelhardt, A silicon nanomembrane platform for the visualization of immune cell trafficking across the human blood-brain barrier under flow, J Cereb Blood Flow Metab (2018) 271678X18820584.

[43] A.T. Salminen, J. Zhang, G.R. Madejski, T.S. Khire, R.E. Waugh, J.L. McGrath, T.R. Gaborski, Ultrathin Dual-Scale Nano- and Microporous Membranes for Vascular Transmigration Models, Small (2019) e1804111.

[44] B. Simonsen Jens, What Are We Looking At? Extracellular Vesicles, Lipoproteins, or Both?, Circulation Research 121(8) (2017) 920-922.
[45] B.W. Sódar, Á. Kittel, K. Pálóczi, K.V. Vukman, X. Osteikoetxea, K. Szabó-Taylor, A. Németh, B. Sperlágh, T. Baranyai, Z. Giricz, Z. Wiener, L. Turiák, L. Drahos, É. Pállinger, K. Vékey, P. Ferdinandy, A. Falus, E.I. Buzás, Low-density lipoprotein mimics blood plasma-derived exosomes and microvesicles during isolation and detection, Scientific reports 6 (2016) 24316-24316.
[46] C.T. Burkhart, K.L. Maki, M.J. Schertzer, Effects of Interface Velocity, Diffusion Rate, and Radial Velocity on Colloidal Deposition Patterns Left by Evaporating Droplets, Journal of Heat Transfer 139(11) (2017) 111505.
[47] Y. Li, Q. Yang, M. Li, Y. Song, Rate-dependent interface capture beyond the coffee-ring effect, Scientific reports 6 (2016) 24628.
[48] Z. Dagan, S. Weinbaum, R. Pfeffer, Theory and experiment on the three-dimensional motion of a freely suspended spherical particle at the entrance to a pore at low Reynolds number, Chemical Engineering Science 38(4) (1983) 583-596.
[49] J.S. Brzozowski, H. Jankowski, D.R. Bond, S.B. McCague, B.R. Munro, M.J. Predebon, C.J. Scarlett, K.A. Skelding, J. Weidenhofer, Lipidomic profiling of extracellular vesicles derived from prostate and prostate cancer cell lines, Lipids in Health and Disease 17(1) (2018) 211.
[50] K.C. Keri, K.R. Regner, A.T. Dall, F. Park, Urinary exosomal expression of activator of G protein signaling 3 in polycystic kidney disease, BMC Res Notes 11(1) (2018) 359-359.
[51] Y. Kitamura, M. Kojima, T. Kurosawa, R. Sasaki, S. Ichihara, Y. Hiraku, H. Tomimoto, M. Murata, S. Oikawa, Proteomic Profiling of Exosomal Proteins for Blood-based Biomarkers in Parkinson's Disease, Neuroscience 392 (2018) 121-128.
[52] V. Rollet-Cohen, M. Bourderioux, J. Lipecka, C. Chhuon, V.A. Jung, M. Mesbahi, T. Nguyen-Khoa, S. Guérin-Pfyffer, A. Schmitt, A. Edelman, I. Sermet-Gaudelus, I.C. Guerrera, Comparative proteomics of respiratory exosomes in cystic fibrosis, primary ciliary dyskinesia and asthma, Journal of Proteomics 185 (2018) 1-7.
[53] T. Skotland, K. Sandvig, A. Llorente, Lipids in exosomes: Current knowledge and the way forward, Progress in Lipid Research 66 (2017) 30-41.
[54] T. Baranyai, K. Herczeg, Z. Onódi, I. Voszka, K. Módos, N. Marton, G. Nagy, I. Mäger, M.J. Wood, S. El Andaloussi, Z. Pálinkás, V. Kumar, P. Nagy, Á. Kittel, E.I. Buzás, P. Ferdinandy, Z. Giricz, Isolation of Exosomes from Blood Plasma: Qualitative and Quantitative Comparison of Ultracentrifugation and Size Exclusion Chromatography Methods, PLOS ONE 10(12) (2015) e0145686.
[55] A.N. Böing, E. van der Pol, A.E. Grootemaat, F.A.W. Coumans, A. Sturk, R. Nieuwland, Single-step isolation of extracellular vesicles by size-exclusion chromatography, Journal of Extracellular Vesicles 3 (2014) 10.3402/jev.v3.23430.
[56] D. Enderle, A. Spiel, C.M. Coticchia, E. Berghoff, R. Mueller, M. Schlumpberger, M. Sprenger-Haussels, J.M. Shaffer, E. Lader, J. Skog, M. Noerholm, Characterization of RNA from Exosomes and Other Extracellular Vesicles Isolated by a Novel Spin Column-Based Method, PLOS ONE 10(8) (2015) e0136133.
[57] F. Wu, T.J. Antes, Abstract 3030: An exosome isolation system for serum-based cancer biomarker discovery, Cancer Research 70(8 Supplement) (2010) 3030.
[58] C. Lee, S. Carney Rp Fau - Hazari, Z.J. Hazari S Fau - Smith, A. Smith Zj Fau - Knudson, C.S. Knudson A Fau - Robertson, K.S. Robertson Cs Fau - Lam, S. Lam Ks Fau - Wachsmann-Hogiu, S. Wachsmann-Hogiu, 3D plasmonic nanobowl platform for the study of exosomes in solution, (2040-3372 (Electronic)).
[59] D.Z. Fang, C.C. Striemer, T.R. Gaborski, J.L. McGrath, P.M. Fauchet, Methods for controlling the pore properties of ultra-thin nanocrystalline silicon membranes, J Phys Condens Matter 22(45) (2010) 454134.
[60] S. Jamaly, C. Ramberg, R. Olsen, N. Latysheva, P. Webster, T. Sovershaev, S.K. Brækkan, J.-B. Hansen, Impact of preanalytical conditions on plasma concentration and size distribution of extracellular vesicles using Nanoparticle Tracking Analysis, Scientific Reports 8(1) (2018) 17216.
[61] A. Clayton, D. Buschmann, J.B. Byrd, D.R.F. Carter, L. Cheng, C. Compton, G. Daaboul, A. Devitt, J.M. Falcon-Perez, C. Gardiner, D. Gustafson, P. Harrison, C. Helmbrecht, A. Hendrix, A. Hill, A. Hoffman, J.C. Jones, R. Kalluri, J.Y. Kang, B. Kirchner, C. Lässer, C. Lawson, M. Lenassi, C. Levin, A. Llorente, E.S. Martens-Uzunova, A. Möller, L. Musante, T. Ochiya, R.C. Pink, H. Tahara, M.H.M. Wauben, J.P. Webber, J.A. Welsh, K.W. Witwer, H. Yin, R. Nieuwland, Summary of the ISEV workshop on extracellular vesicles as disease

biomarkers, held in Birmingham, UK, during December 2017, Journal of extracellular vesicles 7(1) (2018) 1473707-1473707.

[62] S. Das, A.B. Abdel-Mageed, C. Adamidi, P.D. Adelson, K.M. Akat, E. Alsop, K.M. Ansel, J. Arango, N. Aronin, S.K. Avsaroglu, A. Azizian, L. Balaj, I.Z. Ben-Dov, K. Bertram, M. Bitzer, R. Blelloch, K.A. Bogardus, X.O. Breakefield, G.A. Calin, B.S. Carter, A. Charest, C.C. Chen, T. Chitnis, R.J. Coffey, A. Courtright-Lim, S. Das, A. Datta, P. DeHoff, T.G. Diacovo, D.J. Erle, A. Etheridge, M. Ferrer, J.L. Franklin, J.E. Freedman, D.J. Galas, T. Galeev, R. Gandhi, A. Garcia, M.B. Gerstein, V. Ghai, I.C. Ghiran, M.D. Giraldez, A. Goga, T. Gogakos, B. Goilav, S.J. Gould, P. Guo, M. Gupta, F. Hochberg, B. Huang, M. Huentelman, C. Hunter, E. Hutchins, A.R. Jackson, M.Y.S. Kalani, P. Kanlikilicer, R.A. Karaszti, K. Van Keuren-Jensen, A. Khvorova, Y. Kim, H. Kim, T.K. Kim, R. Kitchen, R.P. Kraig, A.M. Krichevsky, R.Y. Kwong, L.C. Laurent, M. Lee, N. L'Etoile, S.E. Levy, F. Li, J. Li, X. Li, G. Lopez-Berestein, R. Lucero, B. Mateescu, A.C. Matin, K.E.A. Max, M.T. McManus, T.R. Mempel, C. Meyer, A. Milosavljevic, D. Mondal, K.J. Mukamal, O.D. Murillo, T. Muthukumar, D.A. Nickerson, C.J. O'Donnell, D.J. Patel, T. Patel, J.G. Patton, A. Paul, E.R. Peskind, M.A. Phelps, C. Putterman, P.J. Quesenberry, J.F. Quinn, R.L. Raffai, S. Ranabothu, S.J. Rao, C. Rodriguez-Aguayo, A. Rosenzweig, M.E. Roth, J. Rozowsky, M.S. Sabatine, N.A. Sakhanenko, J.A. Saugstad, T.D. Schmittgen, N. Shah, R. Shah, K. Shedden, J. Shi, A.K. Sood, A. Sopeyin, R.M. Spengler, R. Spetzler, S. Srinivasan, S.L. Subramanian, M. Suthanthiran, K. Tanriverdi, Y. Teng, M. Tewari, W. Thistlethwaite, T. Tuschl, K.K. Urbanowicz, K.C. Vickers, O. Voinnet, K. Wang, A.M. Weaver, Z. Wei, H.L. Weiner, Z.R. Weiss, Z. Williams, D.T.W. Wong, P.G. Woodruff, X. Xiao, I.K. Yan, A. Yeri, B. Zhang, H.-G. Zhang, K.M. Ansel, M. Bitzer, X.O. Breakefield, A. Charest, D.J. Galas, M.B. Gerstein, M. Gupta, A. Milosavljevic, M.T. McManus, T. Patel, R.L. Raffai, J. Rozowsky, M.E. Roth, J.A. Saugstad, K. Van Keuren-Jensen, A.M. Weaver, L.C. Laurent, The Extracellular RNA Communication Consortium: Establishing Foundational Knowledge and Technologies for Extracellular RNA Research, Cell 177(2) (2019) 231-242.

[63] C. Soekmadji, A.F. Hill, M.H. Wauben, E.I. Buzás, D. Di Vizio, C. Gardiner, J. Lötvall, S. Sahoo, K.W. Witwer, Towards mechanisms and standardization in extracellular vesicle and extracellular RNA studies: results of a worldwide survey, Journal of extracellular vesicles 7(1) (2018) 1535745-1535745.

[64] R.N. Carter, S.M. Casillo, A.R. Mazzocchi, J.S. DesOrmeaux, J.A. Roussie, T.R. Gaborski, Ultrathin transparent membranes for cellular barrier and co-culture models, Biofabrication 9(1) (2017) 015019.

[65] P. Martínez-Pérez, J. García-Rupérez, Commercial polycarbonate track-etched membranes as substrates for low-cost optical sensors, Beilstein J Nanotechnol 10 (2019) 677-683.

[66] M. Wu, C. Chen, Z. Wang, H. Bachman, Y. Ouyang, P.-H. Huang, Y. Sadovsky, T.J. Huang, Separating extracellular vesicles and lipoproteins via acoustofluidics, Lab on a Chip 19(7) (2019) 1174-1182.

[67] M. Mørk, A. Handberg, S. Pedersen, M.M. Jørgensen, R. Bæk, M.K. Nielsen, S.R. Kristensen, Prospects and limitations of antibody-mediated clearing of lipoproteins from blood plasma prior to nanoparticle tracking analysis of extracellular vesicles, Journal of extracellular vesicles 6(1) (2017) 1308779-1308779.

[68] T. Wang, I.V. Turko, Proteomic Toolbox To Standardize the Separation of Extracellular Vesicles and Lipoprotein Particles, Journal of Proteome Research 17(9) (2018) 3104-3113.

# Chapter 3

## 3 Systematic Evaluation of PKH Labeling of Extracellular Vesicles Size by Nanoparticle Tracking Analysis

## 3.1 Abstract

Extracellular vesicles (EVs) are membrane vesicles secreted by cells and can modulate biological activities by transferring their content following uptake into recipient cells. Labeling of EVs is a commonly used technique for understanding their cellular targeting and biodistribution. A reliable fluorescent technique needs to preserve the size of EVs since changes in size may alter their uptake and biodistribution. Lipophilic fluorescent dye molecules such as the PKH family have been widely used for EV Labeling. Here, the effect of PKH Labeling on the size of EVs was systematically evaluated using nanoparticle tracking analysis (NTA), which is a widely used technique for determining the size and concentration of nanoparticles. NTA analysis showed a size increase in all the PKH Labeling conditions tested. As opposed to lipophilic dye molecules, no significant shift in the size of Labeled EVs was detected with luminal binding dye molecules such as CFSE. This finding suggests that PKH Labeling may not be a reliable technique for the tracking of EVs.

## 3.2 Introduction

EVs are small membrane bound vesicles (50-1000 nm in diameter) secreted by all cell types examined and can be found in almost all biofluids including blood, breast milk, urine and saliva as well as in cell culture media [1,2]. EVs mediate cell-cell communication by exchanging proteins, DNA, RNA and lipids between donor and recipient cells and activating signaling pathways in target cells via receptor ligand interaction [3,4]. They have been shown to play a role in regulating both physiological and pathological processes including immune regulation and cancer [5].

Studies that examine EVs uptake into target cells and *in vivo* biodistribution have utilized a range of Labeling and tracking approaches to follow EVs fate [6]. The most common technique for studying EVs biodistribution and target cell interaction involves Labeling of EVs with fluorescent dye molecules. Many strategies have been developed for Labeling EVs such as staining their membranes using fluorescent lipid membrane dye molecules such as PKH26 [7,8], PKH67 [9,10], DiI [11], and DiD [12]. The PKH family has been widely used in the lipophilic class as they have a highly fluorescent polar head group and long aliphatic hydrocarbon tails which readily intercalate into any lipid structure leading to long-term dye retention and stable fluorescence [12,13]. Using fluorescent Labeling, EVs secreted by cells into the extracellular environment have been found to be internalized through different routes and mechanisms including fusion with the plasma membrane and a range of endocytic pathways such as receptor-mediated endocytosis, phagocytosis, lipid raft-dependent endocytosis and micropinocytosis [14–16]. Furthermore, the internalization of EVs has been shown with a wide

range of recipient cells such as dendritic cells [9], macrophages [17], dermal fibroblast [18], endothelial and myocardial cells [10].

Previous studies have shown that the fate of nanoparticles can be affected by the size, shape, surface chemistry and hydrophobicity of nanoparticles [19–22]. In particular, the size-dependent uptake of nanoparticles composed of inorganic materials including those made of polystyrene [23] and silica [24] has been conclusively studied. Lower cellular uptake of nanoparticles has been consistently observed with increasing nanoparticle size, possibly due to the increased energy required to take up the larger nanoparticles [24–27]. Additionally, size impacts the biodistribution of nanoparticles *in vivo*. For instance, more rapid accumulation of larger nanoparticles was observed to take place in liver and spleen [28]. Large nanoparticles also tend to exhibit shorter circulation half-life, which may be due to the activation of the complement system and quick removal of large nanoparticles from blood [29]. Therefore, size of nanoparticles plays an important role in uptake, biodistribution and circulation half-life of nanoparticles.

Since previous studies have shown that cells preferentially uptake smaller EVs [30], altering the size of EVs may also affect their uptake into target cells. Therefore, a reliable fluorescent dye must preserve native properties of EVs, such as size, after Labeling. Despite the importance of preserving the size of EVs for uptake and biodistribution studies, the effect of the widely used PKH dye on the size of EVs has never been systematically characterized. The objective of this study was to systematically evaluate the effect of PKH Labeling on the size of EVs using nanoparticle tracking analysis (NTA). NTA is a technique for measuring the size and

concentration of nanoparticles in real time based on tracking the light scattered from suspended nanoparticles undergoing Brownian motion [25,31,32].

In the present work, the ratio of PKH dye molecules to EVs was systematically varied and the particles' size distribution were measured using NTA. In all the Labeling conditions tested by NTA, EVs size mode increased after Labeling. The observed size shift may trigger abnormalities in their tissue distribution and cellular uptake in both *in vivo* and *in vitro* studies. In contrast to PKH Labeling, CFSE-Labeled EVs showed similar size distribution as unLabeled EVs indicating that CFSE preserves the size of EVs.

## 3.3 Materials and Methods

### EVs Labeling with lipophilic dye (PKH)

Lyophilized urinary CD63, CD9, CD81 positive EVs (HansaBioMed, Estonia) were diluted in ultra-pure water to a protein concentration of 100 μg/mL, following manufacturer instructions. Prior to staining, 1.2 μL of 1 mM PKH26 stock (Red Fluorescent Cell linker for General Cell Membrane, Sigma-Aldrich) was added to 300 μL of diluent C and incubated at 37° C for 15 minutes. Then, 1 μL of EVs stock was added to PKH26 in diluent C, resulting in a sample with final concentrations of 0.3 μg/mL of EVs and 4 μM of PKH26. Other concentrations of EVs (4.5, 1.5 and 0.03 μg/mL) and PKH (20 and 0.16 μM) were made following the same overall procedure in diluent C.

### EVs Labeling with luminal binding dye (CFSE)

5-(and-6)-Carboxyfluorescein Diacetate Succinimidyl Ester (CFSE) stock was made following the manufacturer instructions (CellTrace™ CFSE Cell Proliferation Kit, Thermo Scientific Fisher) by adding 18 μL of dimethyl sulfoxide (DMSO, Sigma-Aldrich) to the CFSE dye resulting in a 5 mM stock. In order to stain EVs with CFSE, 1 μL of CFSE stock was added to 300 μL of PBS prior to staining and then 1 μL of EVs from 0.1 μg/mL EVs stock was added and incubated for 2 hours at 37° C, as was previously described [33]. In order to remove unbound dye molecules, the samples were ultracentrifuged (Optima MAX-XP, Beckman Coulter) at 100000 x g for 60 minutes at 4 °C (TLA 110 rotor with cleaning factor of 81).

## Nanoparticle tracking analysis (NTA)

For each run, 300 µL of the prepared samples were injected into the sample chamber of a NS300 instrument (NanoSight, Aumesbery, UK) with a 532 nm green laser. Seven measurements of each sample were performed for 30 seconds each. For the “Blur”, “Minimum expected particle size”, and “Minimal track lengths” the auto adjustment settings provided by software developer were used. The camera level (9-12) and detection threshold (2-6) were adjusted manually for each experiment as recommended by the manufacturer. For data capturing and analysis, the NTA analytical software (NanoSight NTA 3.2) was used. Briefly, from the recorded video, the mean square displacement of each detected particle was determined. Then, using the Stokes-Einstein equation, the diffusion coefficient and sphere-equivalent hydrodynamic radius were determined by the software.

## Fluorescent imaging and analysis

Fluorescent images were taken using a Keyence BZ-X700 microscope (Keyence Corp. of America, MA, USA) with the same exposure time for all samples. The line scan analysis was conducted using the NIH ImageJ software.

## 3.4 Results

### 3.4.1 Size Characterization of PKH Labeling of EVs

In order to investigate the effect of PKH Labeling on the size of EVs, the particles' size distribution was assessed by NTA (**Figure 3.1**). A heterogenous population of nanoparticles with a typical size range of small EVs (80 – 300 nm) was found in the EVs only control. Moreover, the PKH only control (without EVs) contained PKH nanoparticles, possibly micelles and aggregation, with a polydisperse particles' distribution in the size range of 80 – 400 nm (**Figure 3.1-A and B**), which is in agreement with previously reported results [33,34]. Furthermore, after Labeling EVs with PKH, larger particles than those found in either the EVs or PKH only controls were detected by NTA (**Figure 3.1-A and B**), suggesting a size shift towards larger particles after PKH Labeling. In order to confirm that PKH is the reason for the observed size shift after Labeling EVs, the interaction of 100 nm polystyrene (PS) nanoparticles with PKH was studied as a control experiment. In contrast to EVs, PKH should not interact with PS nanoparticles and as expected, no size shift towards larger particles was observed by NTA when 100 nm PS nanoparticles were added to PKH (**Figure 3.1-C**). Therefore, Labeling EVs with PKH caused a size shift towards larger sizes.

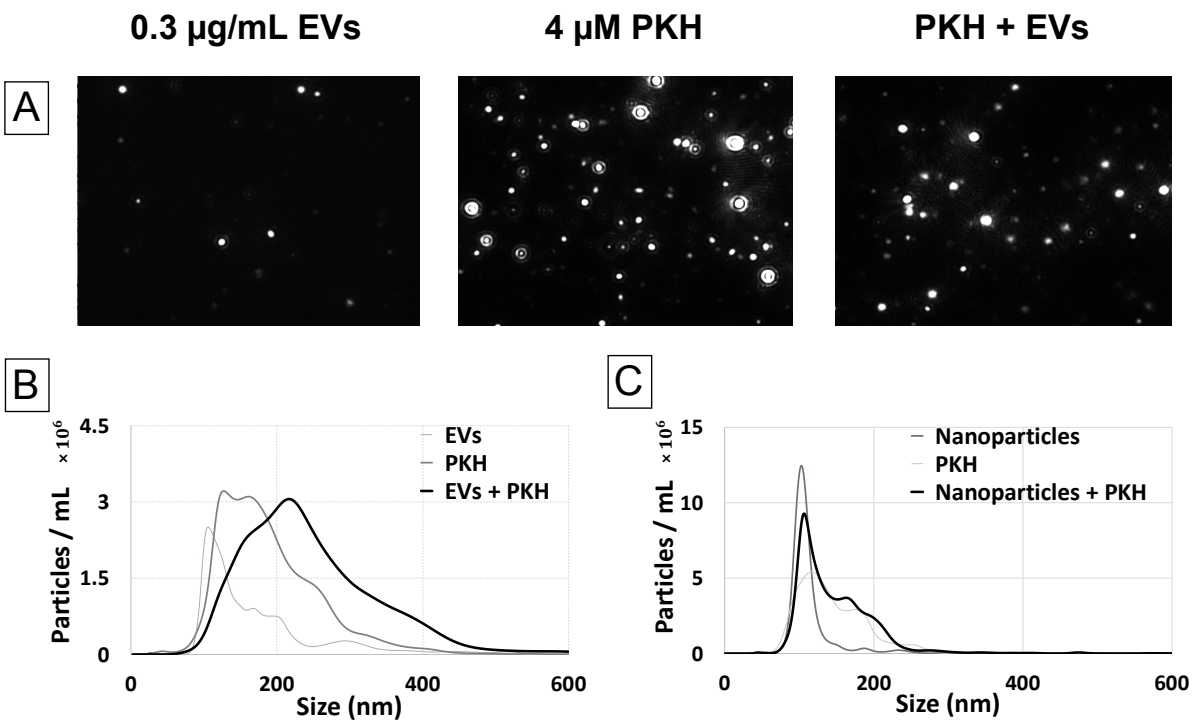


**Figure 3.1 - Size Characterization of PKH Labeling of EVs by Nanoparticle Tracking Analysis (NTA).**

**(A)** NTA video frames of 0.3 µg/mL EVs only as control (EVs), 4 µM PKH only as control (PKH), and PKH-Labeled EVs (PKH+EVs) in diluent C. **(B)** Size distribution of EVs only control (EVs), PKH only control (PKH), and PKH-Labeled EVs (PKH+EVs) samples (n=7) in diluent C. **(C)** Size distribution of PS nanoparticles only control, PKH only control, and PS nanoparticles in PKH (n=7) in diluent C.

### 3.4.2 Determination of the Fluorescent Detection Range of PKH-labeled EVs

The fluorescent detection range of PKH-Labeled EVs samples was determined. PKH to EVs ratios were adjusted by changing the concentration of PKH while holding the EVs concentration constant (**Figure 3.2**). The fluorescent level of these samples along with that of the PKH and EVs only, as well as background only control groups were visualized using fluorescent microscopy and quantified by sampling the cross-sectional fluorescent intensity of the captured images (line scan).

Initially, the same concentrations of PKH and EVs were used as in **Figure 3.1**. Weakly fluorescent features consistent with the presence of PKH nanoparticles in the PKH only control were observed by fluorescent imaging (**Figure 3.2-A**). In comparison to the PKH only control, several brighter features were observed in PKH Labeled EVs which are likely the larger particles formed after PKH Labeling of EVs (**Figure 3.2-B**). The line scan taken from the PKH-Labeled EVs showed higher fluorescent intensity compared to the background signal (**Figure 3.2-E**). Line scan analysis of the PKH-Labeled EVs revealed a reduction in the baseline signal when compared to the PKH only control; possibly as the result of floating PKH dye molecules interacting with EVs (**Figure 3.2-E**). Furthermore, intensity spikes found in the PKH-Labeled EVs further support the presence of larger Labeled EVs (**Figure 3.2-E**). In contrast, a 25-fold reduction of the PKH concentration (0.16 μM) led to a decrease in the fluorescent intensity that reached background level. This PKH reduction also caused the fluorescently bright features, observed at higher concentrations of PKH, to fall below the detectable limit (**Figure 3.2-[C-E]**).

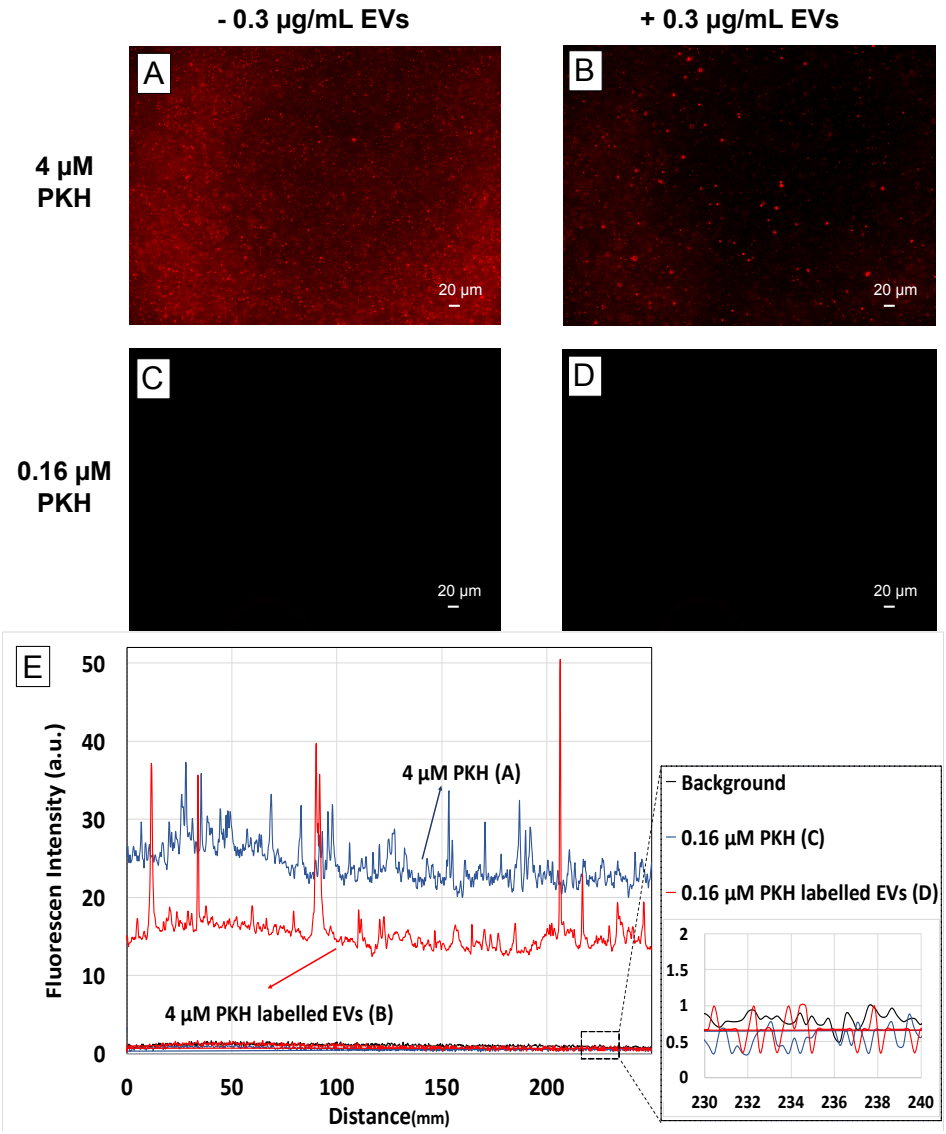


**Figure 3.2 - Determination of the Fluorescent Detection Range.**

Fluorescent images of **(A)** 4 µM PKH only control, **(B)** 4 µM PKH-Labeled EVs (1.5 µg/mL), **(C)** 0.16 µM PKH only control, **(D)** 0.16 µM PKH-Labeled EVs (0.3 µg/mL) in diluent C. **(E)** Representative line scan analysis of fluorescent images (A-D). Inset shows the line scan analysis of background, 0.16 µM PKH only control and 0.16 µM PKH-Labeled EVs (0.3 µg/mL) in diluent C.

### 3.4.3 Effect of PKH Concentration on the Size Distribution of PKH-labeled EVs

Possible mechanisms causing the observed size increase are the aggregation/fusion of PKH nanoparticles with EVs or the intercalation of PKH molecules into EVs membranes, both of which would result in the formation of larger species. This suggests the possibility of minimizing the size increase by reducing the PKH concentration, while maintaining detectable fluorescent signal from PKH Labeled EVs. Therefore, after determining the fluorescent detection range of PKH-Labeled EVs, the effect of PKH concentration on the particles' size distribution was explored by NTA (**Figure 3.3**). The concentration of PKH was systematically varied while holding EVs concentration constant. Representative examples of the particles' size distribution measured by NTA for different concentrations of PKH can be seen in (**Figure 3.3- [A-D]**). For all concentrations of PKH, NTA analysis of particles' size distributions showed that Labeling with PKH caused the formation of larger species relative to EVs and PKH only controls. Quantitative determination of NTA results was done by comparing the modes of the nanoparticle sizes (**Figure 3.3-E**). Consistent with size distribution results, a shift in the modes towards larger particles was observed in all PKH-Labeled EVs (PKH+EVs) compared to the EVs only control. Furthermore, no size shift was observed when the suspension buffer (diluent C) was added to EVs in the absence of PKH confirming that PKH is the cause for the size shift observed (**Figure 3.3-D**). Therefore, Labeling EVs with different concentrations of PKH, even for the PKH concentration below the fluorescent detection limit, showed a size distribution shift indicative of the generation of larger species. This finding suggests that minimizing the formation of larger species by reducing the concentration of PKH used for Labeling EVs while maintaining the fluorescent detectability may not be feasible.

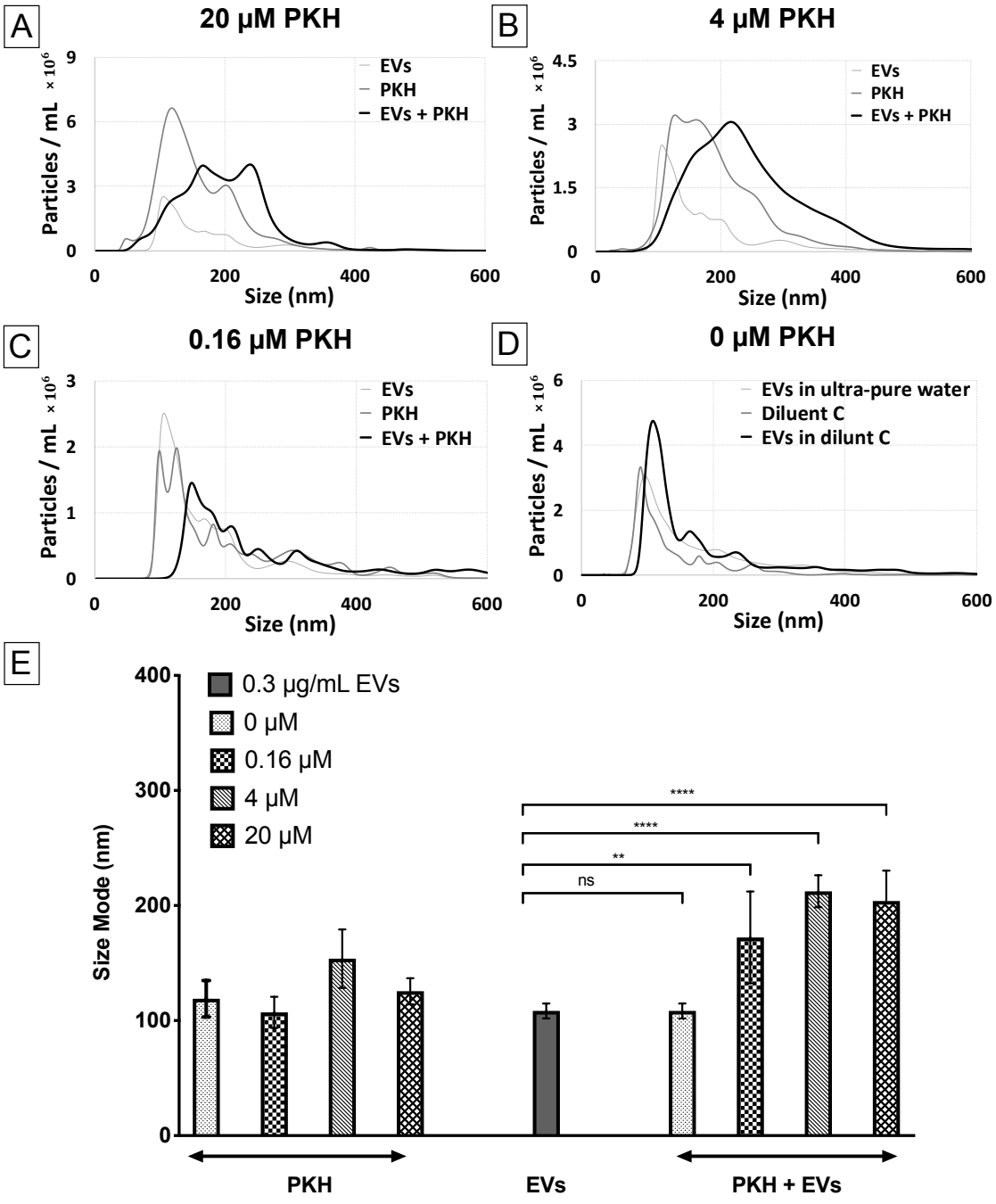


**Figure 3.3 - Effect of PKH Concentration on the Size Distribution of Particles in PKH-Labeled EVs by Nanoparticle Tracking Analysis (NTA).**

**(A-D)** Size distribution of PKH-Labeled EVs with different PKH concentrations (20, 4, 0.16 and 0 µM respectively) with 0.3 µg/mL of EVs (n=7) in diluent C. **(E)** Particle size modes for EVs only control, PKH only controls, and PKH-Labeled EVs (Error bars represent the 95% confidence interval of the mean) in diluent C.

### 3.4.4 Effect of EVs Concentration on the Size Distribution of PKH-labeled EVs

Further confirmation of PKH induced larger species was done by varying the concentration of EVs while holding the PKH concentration constant (**Figure 3.4**). The PKH concentration (0.16 μM) used was the level shown to generate fluorescently detectable PKH-Labeled EVs (**Figure 3.2-B**). Representative examples of the particles' size distribution measured by NTA for different concentration of EVs Labeled with PKH dye molecules can be seen in **Figure 3.4-[A-D]**. Additionally, quantitative determination of NTA results was conducted by comparing the size modes of the nanoparticles (**Figure 3.4-E**). As expected, generation of larger species was observed by size distribution as well as the shift in the size mode regardless of the EVs concentration tested.

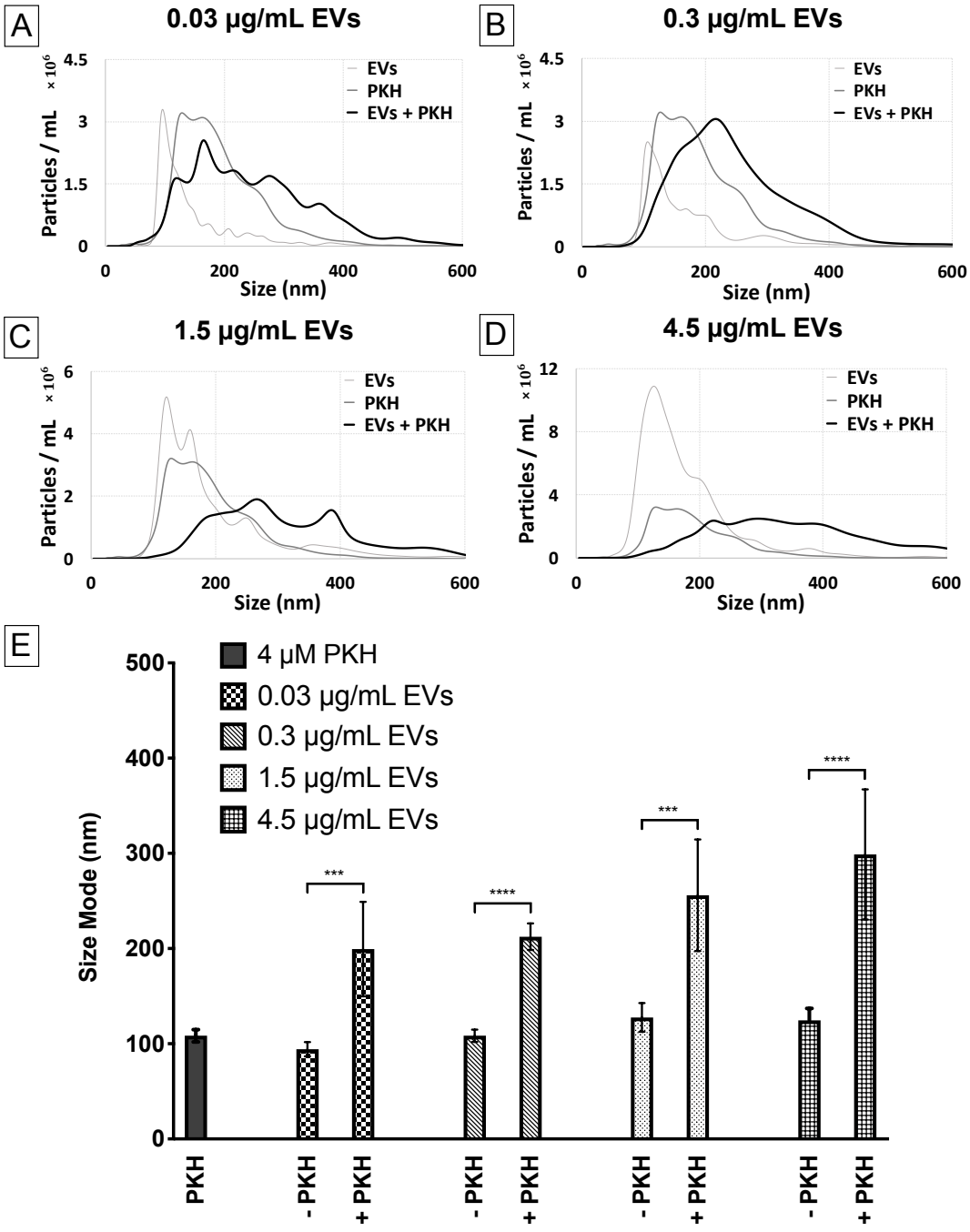


**Figure 3.4 - Effect of EVs Concentration on the Size Distribution of Particles in PKH-Labeled EVs Evaluated by Nanoparticle Tracking Analysis (NTA).**

**(A-D)** Size distribution of PKH-Labeled EVs with different EVs concentrations (0.03, 0.3, 1.5, 4.5 µg/mL respectively) with 4 µM of PKH (n=7) in diluent C. **(E)** Particle Size modes of EVs only control, PKH only controls, and PKH-Labeled EVs (Error bars represent 95% confidence interval of the mean) in diluent C.

### 3.4.5 Size Characterization of CFSE labeling of EVs

As opposed to lipophilic dye molecules which may cause a size shift towards larger particles, potentially through PKH nanoparticles fusion/aggregation or PKH dye molecules intercalation with EVs, it is anticipated that direct luminal Labeling of EVs with fluorescent compounds will not change the size of EVs. In order to study this hypothesis, EVs were Labeled with the CFSE luminal binding dye using a previously established protocol (**Figure 3.5**) [33]. Compared to the EVs only control and CFSE dye control (**Figure 3.5-A**), several brighter features were found in their fluorescent images (CFSE dye + EVs) which are likely the CFSE-Labeled EVs (**Figure 3.5-B**). Additionally, the line scan obtained from the CFSE-Labeled EVs showed intensity spikes indicating the presence of CFSE-Labeled EVs (**Figure 3.5-C**). In contrast to PKH dye, NTA analysis showed that CFSE did not form nanoparticles in the CFSE only control (**Figure 3.5-A and D**), which was in agreement with the previously reported findings [33]. Size distribution and quantitative determination of the particle size modes measured by NTA showed no significant change in CFSE-Labeled EVs compared to unlabeled EVs (**Figure 3.5-D and E**). This result suggests that luminal Labeling by luminal binding dye (CFSE) preserve the size of EVs after Labeling which makes this type of dye more reliable when compared to PKH.

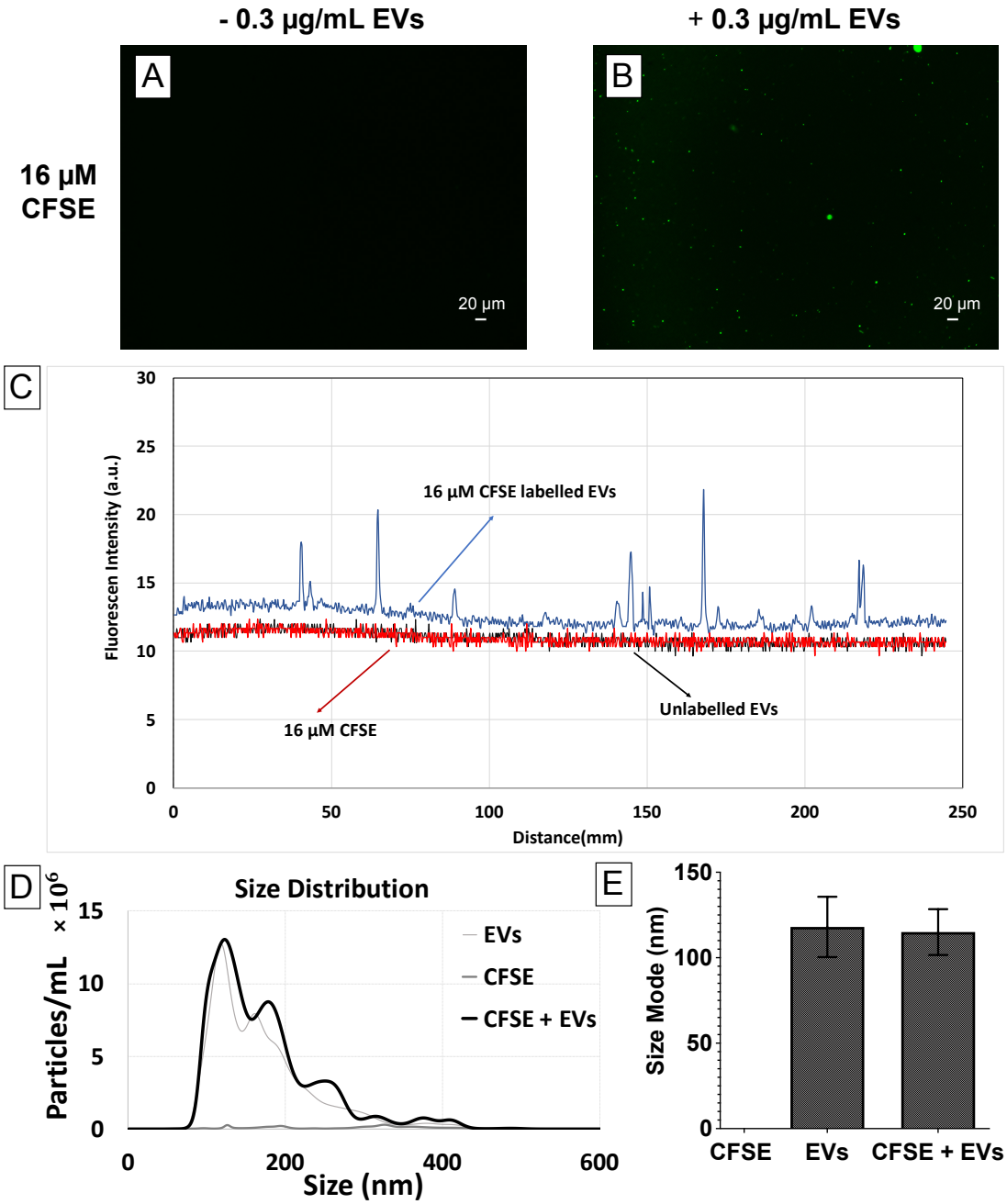


**Figure 3.5 - Size Characterization of CFSE Labeling of EVs by Nanoparticle Tracking Analysis (NTA).**

Fluorescent images of **(A)** 16 4 µM CFSE only control, **(B)** 4 µM CFSE-Labeled EVs (0.3 µg/mL) in PBS. **(C)** Representative line scan analysis of fluorescent images (A and B). **(D)** Size distribution of EVs only control, CFSE only control, and CFSE-Labeled EVs (n=7) in PBS. **(E)** Size mode of EVs only control, CFSE only control, and CFSE-Labeled EVs (Error bars represent 95% confidence interval of the mean) in PBS.

## 3.5 Discussion

All cell types are capable of shedding membrane-enclosed vesicles called EVs that play a key role in intercellular communication. EVs have been found in diverse bodily fluids including blood, urine, saliva, amniotic fluids, ascites, cerebrospinal fluid and breast milk [2,35]. The use of extracellular vesicles for diagnostic and therapeutic applications has seen a major interest increase in recent years because of their capability to exchange components such as nucleic acids, lipids and proteins between cells [36]. Endocytosis and plasma fusion are considered as the main pathways for EVs internalization resulting in transferring EVs cargo to the recipient cell [15].

To investigate the fate of EVs, many imaging tools and Labeling methods have been developed. Electron and optical microscopy are the most commonly used techniques for visualizing EVs [37]. However, due to the small size of EVs, their tracking can be challenging and they need to be fluorescently Labeled in their native state. Lipophilic Labeling with dye molecules such as the PKH family have been widely used to label a range of cell types such as mesenchymal stem cells [38,39] and tumor cells [40] in proliferation and migration studies [39,41]. Since EVs have a lipid bilayer structure similar to that of the cells plasma membrane, the PKH family has been adapted for EV Labeling due to the hydrophobic interactions between the EV lipids and the long alkane tails of PKH. Internalization of PKH-Labeled EVs by dendric cells [9], macrophages [17], endothelial cells [8] and fibroblasts [8] has been reported.

Using polymeric, organic and inorganic nanoparticles, it has been shown that size, shape, surface chemistry and hydrophobicity of nanoparticles are important factors in their uptake and

biodistribution [19–22]. The effect of nanoparticle size alone on their uptake has been investigated using different types of nanoparticles and cells such as mesoporous silica nanoparticles on HeLa cells by [28], fluorescent latex beads on B16 cells [42], as well as polystyrene nanoparticles on Caco-2 and MDCK cells [23]. In addition to cellular uptake efficiency, It has been shown that nanoparticles smaller than 200 nm can be taken up by clathrin-coated pits, while larger particles tend to be internalized by caveolae-mediated processes [42]. In addition to uptake studies, the biodistribution of intravenously injected polystyrene nanoparticles has been reported in different organs of rats [23]. The authors found 200 nm nanoparticles showed higher accumulation in both liver and spleen compared to 100 nm nanoparticles. All taken together, these evidences suggest a size shift from 100 nm to 200 nm decreases the cellular uptake efficiency and kinetics and affects their biodistribution. Although studies have recognized the importance of size of nanoparticles in uptake and biodistribution, the research has yet to systematically investigate the effect of fluorescent Labeling on the size of EVs. Importantly, fluorescent Labeling must preserve the size of EVs since any size change may alter the uptake and distribution of EVs.

The size and concentration of nanoparticles including EVs have been determined using different techniques with their own advantages and limitations such as electron microscopy (SEM and TEM), atomic force microscopy (AFM), dynamic electron microscopy (DLS) and nanoparticle tracking analysis (NTA). NTA is a widely used technique in the field and is of particular interest in this study since it is quick to perform and it provides a detailed analysis of the measuring sample leading to statistically significant nanoparticles' size distribution. Furthermore, NTA does not require processing procedures such as drying and coating which can affect the

nanoparticles properties [43–46]. Hence, the present study set out with the aim of assessing the impact of PKH Labeling on the size of EVs using NTA. The concentration of both PKH dye and EVs were systematically varied and the particles' size distribution was determined by NTA. In all conditions tested, NTA analysis revealed a size mode shift from ~100 nm for unlabeled EVs to ~200 nm for PKH Labeled EVs.

In agreement with our findings, one study used the lipophilic tracer dialkylcarbocyanine (DiI) to enhance clustering and aggregation of EVs which was confirmed by electron microscopy and flow cytometry [47]. Furthermore, It has been shown that another lipophilic dye, styryl dye (also referred to as FM™ dye), results in larger EVs after Labeling which was characterized by flow cytometry [48]. Additionally, different approaches for Labeling EVs has been evaluted by nanoscale flow cytometry [33]. The study's main focus was to identify the method that generates fewer background contaminants during the Labeling process and not the effect of Labeling on EVs size. Their NTA data also showed a size shift towards larger particles after PKH Labeling of EVs, however this was not mentioned by the authors in the study [33]. Additionally the biodistribution of EVs using DiR (a similar lipophilic dye as PKH) has been examined and it was found that lipophilic Labeling of EVs increased the localization of EVs in liver and spleen [28]. This change in the biodistribution may be due to the increase in size of EVs after Labeling by lipophilic dye molecules. These previously reported results further support our findings regarding the size change of EVs after Labeling with lipophilic dye molecules such as the one belonging to the PKH family. In summary, the size shift towards larger particles caused by PKH Labeling of EVs is likely to change the cellular uptake level and internalization mechanism as well as the biodistribution of EVs, reducing its validity as an EVs tracer.

In addition to the concern regarding the size change of EVs after Labeling, recent studies have highlighted the generation of artifacts such as formation of numerous nanoparticles which consist exclusively of micelles/aggregates of PKH, without EV content [33,34,49]. It was further shown that in terms of size, surface area and fluorescent intensity, the PKH nanoparticles cannot be distinguished from PKH Labeled EVs and were taken up by astrocytes. Therefore, this capacity for cell uptake of PKH nanoparticles may lead to false positive signals in EV tracking studies [34]. However, cyanine-based membrane probes called MemBright have been recently developed which do not form nanoparticles which is essential for tracking EVs, in contrast to the commonly used PKH family [50,51]. Another lipophilic dye, CellMask orange, has been also used for labeling EVs without affecting the size of EVs, characterized by NTA [52].

One alternative to lipophilic dye molecules that stain the membrane of EVs, is luminal Labeling such as CFDA-SE. CFDA-SE dye molecules are membrane permeable chemical compounds that covalently bind to primary amine inside EVs and fluoresce after ester hydrolysis of the dye in the lumen of the EVs which forms active CFSE molecules [53–56]. Therefore, we hypothesized that luminal binding dye molecules do not affect the size of EVs. In order to study this hypothesis, the luminal binding dye CFSE was used to label EVs and the size of EVs was determined before and after Labeling with NTA. NTA results showed that as opposed to PKH Labeling of EVs which increased the size of EVs, CFSE dye Labeling maintained the normal size of EVs which precludes any size related cellular uptake and biodistribution aberrancies. Consistent with our finding, other studies have found luminal binding fluorescent compounds did not form nanoparticles and did not increase EVs size after Labeling using flow cytometry [33,48].

Here, NTA was employed to systematically explore the effect of PKH Labeling on the size of EVs by changing the PKH to EVs ratio. In all conditions tested, a size mode shift towards larger particles was observed after PKH Labeling of EVs which may cause aberrancies in cellular uptake, biodistribution and half-life circulation. This observed size shift combined with other previously reported artifacts such as formation of PKH nanoparticles suggest that the PKH family dye is not reliable for Labeling EVs. In contrast to the lipophilic class such as PKH, luminal binding dye molecules like CFSE did not cause a size shift in Labeled EVs, suggesting that CFSE may be a better Labeling option for EVs by preserving the size of EVs after Labeling. However, It is important to note that the effect of CFSE Labeling of EVs on their biological behavior such as their uptake and biodistribution needs to be further explored. Furthermore, CFSE is not the only alternative for lipophilic dye molecules such as PKH and suitability of other fluorescent Labeling methods needs to be investigated in future studies using different techniques such as NTA, flow cytometry and electron microscopy.

One alternative to lipophilic dye molecules that stain the membrane of EVs, is luminal Labeling such as CFDA-SE. CFDA-SE dye molecules are membrane permeable chemical compounds that covalently bind to primary amine inside EVs and fluoresce after ester hydrolysis of the dye in the lumen of the EVs which forms active CFSE molecules [53–56]. Therefore, we hypothesized that luminal binding dye molecules do not affect the size of EVs. In order to study this hypothesis, the luminal binding dye CFSE was used to label EVs and the size of EVs was determined before and after Labeling with NTA. NTA results showed that as opposed to PKH Labeling of EVs which increased the size of EVs, CFSE dye Labeling maintained the normal size of EVs which precludes any size related cellular uptake and biodistribution aberrancies.

Consistent with our finding, other studies have found luminal binding fluorescent compounds did not form nanoparticles and did not increase EVs size after Labeling using flow cytometry [33,48] .

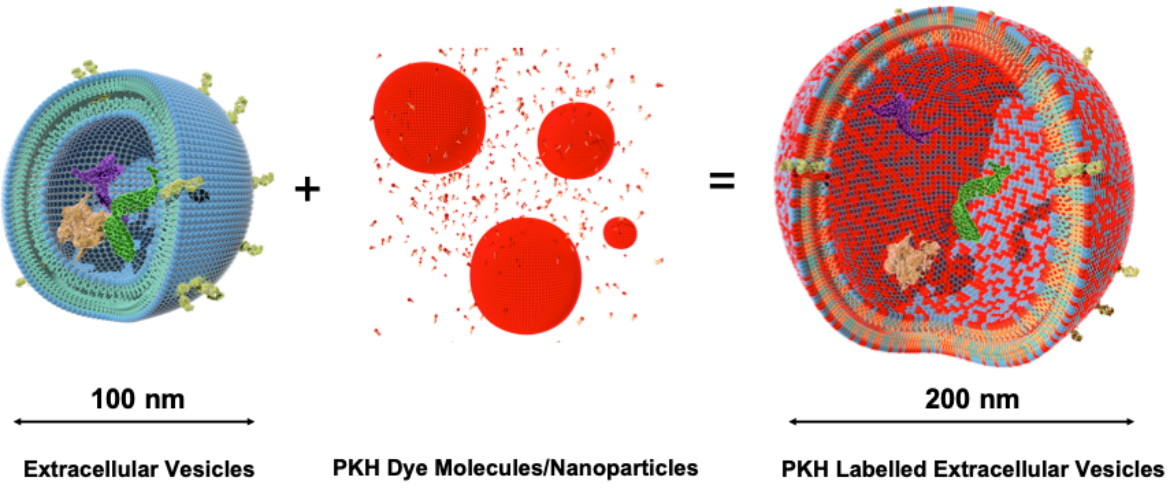


**Figure 3.6 – PKH Labeling of Extracellular Vesicles Results in a Size Shift Towards Larger Particles**

Here, NTA was employed to systematically explore the effect of PKH Labeling on the size of EVs by changing the PKH to EVs ratio. In all conditions tested, a size mode shift towards larger particles was observed after PKH Labeling of EVs which may cause aberrancies in cellular uptake, biodistribution and half-life circulation. This observed size shift combined with other previously reported artifacts such as formation of PKH nanoparticles suggest that the PKH family dye is not reliable for Labeling EVs (**Figure 3.6**) . In contrast to the lipophilic class such as PKH, luminal binding dye molecules like CFSE did not cause a size shift in Labeled EVs, suggesting that CFSE may be a better Labeling option for EVs by preserving the size of EVs after

Labeling. However, It is important to note that the effect of CFSE Labeling of EVs on their biological behavior such as their uptake and biodistribution needs to be further explored.

It is important to note that CFSE is not the only alternative for lipophilic dye molecules such as PKH. The suitability of other fluorescent Labeling methods needs to be investigated in future studies using different techniques such as NTA, flow cytometry, and electron microscopy, and atomic force microscopy.

## 3.6 Future Directions

Many new dyes have been recently developed to fluorescently label EVs. However, there is no ideal generic fluorescent dye in the field that can label all and only EVs. The ideal generic fluorescent dye stills needs to developed and should fulfill the following requirements;

**A. Labeling of all EVs:** Labeling only a subpopulation of EVs can lead to inaccurate conclusions in uptake, biodistribution and characterization of EVs. Therefore, an ideal fluorescent dye must label all EVs.

**B. Specificity to EVs:** Labeling non-EV contaminants in the samples can lead to false positive signals in EV studies. Therefore, a fluorescent dye with specificity to EVs is required for reliable characterizations and conclusions.

**C. Minimal Background Signal:** Presence of excess dye and dye nanoparticles are important challenges in studying EVs which can result in inaccurate conclusions by contributing to the detected signal. An ideal dye must not fluoresce in the absence of EVs.

**D. High Signal-to-Noise:** Brightness and stability of the dyes is an important factor in their detection, especially in flow cytometry analysis where a high signal to noise ratio is necessary with sufficient sensitivity to detect all EVs.

**E. Preserving the native biological behavior of EVs:** Affecting the natural biological behavior of EVs can be problematic specially in uptake and biodistribution studies. An ideal dye must not modify the natural biological behavior of EVs.

**F. Preserving the physical properties of EVs:** An ideal fluorescent dye must preserve the physical properties of EVs such as size which can affect their behavior in uptake and biodistribution studies.

### 3.6.1 Confirming the Size Shift of EVs After PKH Labeling by Tangential Techniques

Here we explored the effect of PKH labeling on the size of EVs using NTA. To further confirm and understand the mechanism of the observed size shift, other techniques such as electron microscopy (EM) and atomic force microscopy (AFM) can provide valuable information. In order to do so, the size of EVs can be characterized by imaging before and after labeling using EM or AFM as a tangential technique with different principles than NTA .In addition to PKH labeling, the effect of fluorescent dyes on the size of EVs after labeling by other available and commonly used fluorescent dyes still needs to be systematically evaluated using NTA, AFM and EM.

### 3.6.2 Studying the Biological Significance of the Observed Size Shift by PKH labeling

Furthermore, we believe that the size shift can affect the uptake and biodistribution of EVs based on previous studies using different types of nanoparticles. However, the biological significance of the observed size shift on the uptake or biodistribution of EVs can be further explored to support this conclusion. This can be done by experimentally addressing the effect of the increase in EV size on uptake level and mechanism or their biodistribution.

## 3.7 Conclusion

Lipophilic Labeling of EVs has been shown to have multiple drawbacks. First, non-specific labeling of non-EV biofluid components such as microvesicles, lipoprotein particles, and proteins [49]. Second, the *in vivo* biodistribution of EVs has been shown to be altered by lipophilic Labeling [23]. Third, the formation of PKH nanoparticles was observed which can potentially cause false positive results in EV cell uptake and biodistribution studies. Fourth, a size shift in the size of EVs was shown after labeling, most likely due to PKH nanoparticle fusion/aggregation and PKH dye intercalation with EVs. These larger species formed after PKH labeling of EVs may cause aberrancies in cellular uptake, biodistribution and half-life circulation. Here, the relative ratio of PKH to EVs was systematically studied in order to minimize the EV size shift towards larger particles by PKH Labeling while maintaining the fluorescent detection of Labeled EVs. In all conditions tested, formation of larger species after Labeling was detected, even in the conditions where the PKH level is below the fluorescent detection level. In contrast to lipophilic dyes such as PKH, protein binding dyes like CFSE did not cause a size shift in Labeled EVs, suggesting that CFSE may be a better Labeling option for EVs.

## 3.8 Acknowledgements and Funding:

I would like to acknowledge Shannon M. Gulvin and Jonathan Flax, M.D., for their contributions in designing and performing experiments as well as writing and editing the manuscript. I would also like to acknowledge Brad Kwarta for the illustrations. Research reported in this chapter

was supported by the National Institutes of Health (R35GM119623) and National Science Foundation (IIP 1660177) to T.R.G.

## 3.9 References


[1] S.C. Tao, S.C. Guo, C.Q. Zhang, Modularized Extracellular Vesicles: The Dawn of Prospective Personalized and Precision Medicine, Adv. Sci. 5 (2018). doi:10.1002/advs.201700449.

[2] G. Van Niel, G. D'Angelo, G. Raposo, Shedding light on the cell biology of extracellular vesicles, Nat. Rev. Mol. Cell Biol. 19 (2018) 213–228. doi:10.1038/nrm.2017.125.

[3] M. Yáñez-Mó, P.R.M. Siljander, Z. Andreu, A.B. Zavec, F.E. Borràs, E.I. Buzas, K. Buzas, E. Casal, F. Cappello, J. Carvalho, E. Colás, A. Cordeiro-Da Silva, S. Fais, J.M. Falcon-Perez, I.M. Ghobrial, B. Giebel, M. Gimona, M. Graner, I. Gursel, M. Gursel, N.H.H. Heegaard, A. Hendrix, P. Kierulf, K. Kokubun, M. Kosanovic, V. Kralj-Iglic, E.M. Krämer-Albers, S. Laitinen, C. Lässer, T. Lener, E. Ligeti, A. Line, G. Lipps, A. Llorente, J. Lötvall, M. Manček-Keber, A. Marcilla, M. Mittelbrunn, I. Nazarenko, E.N.M. Nolte-'t Hoen, T.A. Nyman, L. O'Driscoll, M. Olivan, C. Oliveira, É. Pállinger, H.A. Del Portillo, J. Reventós, M. Rigau, E. Rohde, M. Sammar, F. Sánchez-Madrid, N. Santarém, K. Schallmoser, M.S. Ostenfeld, W. Stoorvogel, R. Stukelj, S.G. Van Der Grein, M. Helena Vasconcelos, M.H.M. Wauben, O. De Wever, Biological properties of extracellular vesicles and their physiological functions, J. Extracell. Vesicles. 4 (2015) 1–60. doi:10.3402/jev.v4.27066.

[4] A. Lo Cicero, P.D. Stahl, G. Raposo, Extracellular vesicles shuffling intercellular messages: For good or for bad, Curr. Opin. Cell Biol. 35 (2015) 69–77. doi:10.1016/j.ceb.2015.04.013.

[5] L. Console, M. Scalise, C. Indiveri, Exosomes in inflammation and role as biomarkers, Clin. Chim. Acta. 488 (2019) 165–171. doi:10.1016/j.cca.2018.11.009.

[6] T. Tian, Y. Wang, H. Wang, Z. Zhu, Z. Xiao, Visualizing of the cellular uptake and intracellular trafficking of exosomes by live-cell microscopy, J. Cell. Biochem. 111 (2010) 488–496. doi:10.1002/jcb.22733.

[7] A. Riches, E. Campbell, E. Borger, S. Powis, Regulation of exosome release from mammary epithelial and breast cancer cells-A new regulatory pathway, Eur. J. Cancer. 50 (2014) 1025–1034. doi:10.1016/j.ejca.2013.12.019.

[8] A. Shabbir, A. Cox, L. Rodriguez-Menocal, M. Salgado, E. Van Badiavas, Mesenchymal Stem Cell Exosomes Induce Proliferation and Migration of Normal and Chronic Wound Fibroblasts, and Enhance Angiogenesis In Vitro, Stem Cells Dev. 24 (2015) 1635–1647. doi:10.1089/scd.2014.0316.

[9] A.E. Morelli, A.T. Larregina, W.J. Shufesky, M.L.G. Sullivan, D.B. Stolz, G.D. Papworth, A.F. Zahorchak, A.J. Logar, Z. Wang, S.C. Watkins, L.D. Falo, A.W. Thomson, Endocytosis, intracellular sorting, and processing of exosomes by dendritic cells, Blood. 104 (2004) 3257–3266. doi:10.1182/blood-2004-03-0824.

[10] G. Di Noto G., M. Chiarini, L.L. Paolini, E.L. Mazzoldi, V. Giustini, A. Radeghieri, L. Caimi, D. Ricotta, Immunoglobulin free light chains and GAGs mediate multiple myeloma extracellular vesicles uptake and secondary NfκB nuclear translocation, Front. Immunol. 5 (2014). doi:10.3389/fimmu.2014.00517.

[11] D.G. Meckes, K.H.Y. Shair, A.R. Marquitz, C.-P. Kung, R.H. Edwards, N. Raab-Traub, Human tumor virus utilizes exosomes for intercellular communication, Proc. Natl. Acad. Sci. 107 (2010) 20370–20375. doi:10.1073/pnas.1014194107.

[12] C.P. Lai, E.Y. Kim, C.E. Badr, R. Weissleder, T.R. Mempel, B.A. Tannous, X.O. Breakefield, Visualization and tracking of tumour extracellular vesicle delivery and RNA translation using multiplexed reporters, Nat. Commun. 6 (2015) 1–12. doi:10.1038/ncomms8029.

[13] P.K. Wallace, J.D. Tario, J.L. Fisher, S.S. Wallace, M.S. Ernstoff, K.A. Muirhead, Tracking antigen-driven responses by flow cytometry: Monitoring proliferation by dye dilution, Cytom. Part A. 73 (2008) 1019–1034. doi:10.1002/cyto.a.20619.

[14] K.J. Svensson, H.C. Christianson, A. Wittrup, E. Bourseau-Guilmain, E. Lindqvist, L.M. Svensson, M. Mörgelin, M. Belting, Exosome uptake depends on ERK1/2-heat shock protein 27 signaling and lipid raft-mediated endocytosis negatively regulated by caveolin-1, J. Biol. Chem. 288 (2013) 17713–17724. doi:10.1074/jbc.M112.445403.

[15] L.A. Mulcahy, R.C. Pink, D.R.F. Carter, Routes and mechanisms of extracellular vesicle uptake, J. Extracell. Vesicles. 3 (2014) 1–14. doi:10.3402/jev.v3.24641.

[16] D. Feng, W.L. Zhao, Y.Y. Ye, X.C. Bai, R.Q. Liu, L.F. Chang, Q. Zhou, S.F. Sui, Cellular internalization of exosomes occurs through phagocytosis, Traffic. 11 (2010) 675–687. doi:10.1111/j.1600-0854.2010.01041.x.

[17] C. Lässer, V. Seyed Alikhani, K. Ekström, M. Eldh, P. Torregrosa Paredes, A. Bossios, M. Sjöstrand, S. Gabrielsson, J. Lötvall, H. Valadi, Human saliva, plasma and breast milk exosomes contain RNA: Uptake by macrophages, J. Transl. Med. 9 (2011) 1–8. doi:10.1186/1479-5876-9-9.

[18] N. Bakhtyar, M.G. Jeschke, E. Herer, M. Sheikholeslam, S. Amini-nik, Exosomes from acellular Wharton ' s jelly of the human umbilical cord promotes skin wound healing, (2018) 1–14. doi:10.1186/s13287-018-0921-2.

[19] E. Blanco, H. Shen, M. Ferrari, Principles of nanoparticle design for overcoming biological barriers to drug delivery, Nat. Biotechnol. 33 (2015) 941–951. doi:10.1038/nbt.3330.

[20] J.K. Patra, G. Das, L.F. Fraceto, E.V.R. Campos, M.D.P. Rodriguez-Torres, L.S. Acosta-Torres, L.A. Diaz-Torres, R. Grillo, M.K. Swamy, S. Sharma, S. Habtemariam, H.S. Shin, Nano based drug delivery systems: Recent developments and future prospects 10 Technology 1007 Nanotechnology 03 Chemical Sciences 0306 Physical Chemistry (incl. Structural) 03 Chemical Sciences 0303 Macromolecular and Materials Chemistry 11 Medical and He, J. Nanobiotechnology. 16 (2018) 1–33. doi:10.1186/s12951-018-0392-8.

[21] H. Cabral, Y. Matsumoto, K. Mizuno, Q. Chen, M. Murakami, M. Kimura, Y. Terada, M.R. Kano, K. Miyazono, M. Uesaka, N. Nishiyama, K. Kataoka, Accumulation of sub-100 nm polymeric micelles in poorly permeable tumours depends on size, Nat. Nanotechnol. 6 (2011) 815–823. doi:10.1038/nnano.2011.166.

[22] A. Salvati, A.S. Pitek, M.P. Monopoli, K. Prapainop, F.B. Bombelli, D.R. Hristov, P.M. Kelly, C. Åberg, E. Mahon, K.A. Dawson, Transferrin-functionalized nanoparticles lose their targeting capabilities when a biomolecule corona adsorbs on the surface, Nat. Nanotechnol. 8 (2013) 137–143. doi:10.1038/nnano.2012.237.

[23] S.A. Kulkarni, S.S. Feng, Effects of particle size and surface modification on cellular uptake and biodistribution of polymeric nanoparticles for drug delivery, Pharm. Res. 30 (2013) 2512–2522. doi:10.1007/s11095-012-0958-3.

[24] F. Lu, S.H. Wu, Y. Hung, C.Y. Mou, Size effect on cell uptake in well-suspended, uniform mesoporous silica nanoparticles, Small. 5 (2009) 1408–1413. doi:10.1002/smll.200900005.

[25] C.Y. Soo, Y. Song, Y. Zheng, E.C. Campbell, A.C. Riches, F. Gunn-Moore, S.J. Powis, Nanoparticle tracking analysis monitors microvesicle and exosome secretion from immune cells, Immunology. 136 (2012) 192–197. doi:10.1111/j.1365-2567.2012.03569.x.

[26] S. Salatin, S. Maleki Dizaj, A. Yari Khosroushahi, Effect of the surface modification, size, and shape on cellular uptake of nanoparticles, Cell Biol. Int. 39 (2015) 881–890. doi:10.1002/cbin.10459.

[27] L. Shang, K. Nienhaus, G.U. Nienhaus, Engineered nanoparticles interacting with cells: Size matters, J. Nanobiotechnology. 12 (2014) 1–11. doi:10.1186/1477-3155-12-5.

[28] P. Gangadaran, X.J. Li, H.W. Lee, J.M. Oh, S. Kalimuthu, R.L. Rajendran, S.H. Son, S.H. Baek, T.D. Singh, L. Zhu, S.Y. Jeong, S.-W. Lee, J. Lee, B.-C. Ahn, A new bioluminescent reporter system to study the biodistribution of systematically injected tumor-derived bioluminescent extracellular vesicles in mice, Oncotarget. 8 (2017) 109894–109914. doi:10.18632/oncotarget.22493.

[29] A.L.B. de Barros, A. Tsourkas, B. Saboury, V.N. Cardoso, A. Alavi, Emerging role of radiolabeled nanoparticles as an effective diagnostic technique, EJNMMI Res. 2 (2012) 1–15. doi:10.1186/2191-219X-2-39.

[30] F. Caponnetto, I. Manini, M. Skrap, T. Palmai-Pallag, C. Di Loreto, A.P. Beltrami, D. Cesselli, E. Ferrari, Size-dependent cellular uptake of exosomes, Nanomedicine Nanotechnology, Biol. Med. 13 (2017) 1011–1020. doi:10.1016/j.nano.2016.12.009.

[31] E. van der Pol, F.A.W. Coumans, A.E. Grootemaat, C. Gardiner, I.L. Sargent, P. Harrison, A. Sturk, T.G. van Leeuwen, R. Nieuwland, Particle size distribution of exosomes and microvesicles determined by transmission electron microscopy, flow cytometry, nanoparticle tracking analysis, and resistive pulse sensing, J. Thromb. Haemost. 12 (2014) 1182–1192. doi:10.1111/jth.12602.

[32] R.A. Dragovic, C. Gardiner, A.S. Brooks, D.S. Tannetta, D.J.P. Ferguson, P. Hole, B. Carr, C.W.G. Redman, A.L. Harris, P.J. Dobson, P. Harrison, I.L. Sargent, Sizing and phenotyping of cellular vesicles using Nanoparticle Tracking Analysis, Nanomedicine Nanotechnology, Biol. Med. 7 (2011) 780–788. doi:10.1016/j.nano.2011.04.003.

[33] A. Morales-Kastresana, B. Telford, T.A. Musich, K. McKinnon, C. Clayborne, Z. Braig, A. Rosner, T. Demberg, D.C. Watson, T.S. Karpova, G.J. Freeman, R.H. Dekruyff, G.N. Pavlakis, M. Terabe, M. Robert-Guroff, J.A. Berzofsky, J.C. Jones, Labeling extracellular vesicles for nanoscale flow cytometry, Sci. Rep. 7 (2017) 1–10. doi:10.1038/s41598-017-01731-2.

[34] P. Pužar Dominkuš, M. Stenovec, S. Sitar, E. Lasič, R. Zorec, A. Plemenitaš, E. Žagar, M. Kreft, M. Lenassi, PKH26 labeling of extracellular vesicles: Characterization and cellular internalization of contaminating PKH26 nanoparticles, Biochim. Biophys. Acta - Biomembr. 1860 (2018) 1350–1361. doi:10.1016/j.bbamem.2018.03.013.
[35] M. Colombo, G. Raposo, C. Théry, Biogenesis, Secretion, and Intercellular Interactions of Exosomes and Other Extracellular Vesicles, Annu. Rev. Cell Dev. Biol. 30 (2014) 255–289. doi:10.1146/annurev-cellbio-101512-122326.
[36] H. Kalra, G.P.C. Drummen, S. Mathivanan, Focus on extracellular vesicles: Introducing the next small big thing, Int. J. Mol. Sci. 17 (2016). doi:10.3390/ijms17020170.
[37] S.T.Y. Chuo, J.C.Y. Chien, C.P.K. Lai, Imaging extracellular vesicles: Current and emerging methods, J. Biomed. Sci. 25 (2018) 1–10. doi:10.1186/s12929-018-0494-5.
[38] Z. Shao-Fang, Z. Hong-Tian, Z. Zhi-Nian, H. Yuan-Li, PKH26 as a fluorescent label for live human umbilical mesenchymal stem cells, Vitr. Cell. Dev. Biol. - Anim. 47 (2011) 516–520. doi:10.1007/s11626-011-9424-5.
[39] A. Kelp, T. Abruzzese, S. Wohrle, V. Frajs, W.K. Aicher, Labeling Mesenchymal Stromal Cells with PKH26 or VybrantDil Significantly Diminishes their Migration, but does not affect their Viability, Attachment, Proliferation and Differentiation Capacities, J. Tissue Sci. Eng. 08 (2017). doi:10.4172/2157-7552.1000199.
[40] I. Bonaccorsi, B. Morandi, O. Antsiferova, G. Costa, D. Oliveri, R. Conte, G. Pezzino, G. Vermiglio, G.P. Anastasi, G. Navarra, C. Münz, E. Di Carlo, M.C. Mingari, G. Ferlazzo, Membrane Transfer from Tumor Cells Overcomes Deficient Phagocytic Ability of Plasmacytoid Dendritic Cells for the Acquisition and Presentation of Tumor Antigens, J. Immunol. 192 (2014) 824–832. doi:10.4049/jimmunol.1301039.
[41] S. Khurana, A. Mukhopadhyay, Characterization of the Potential Subpopulation of Bone Marrow Cells Involved in the Repair of Injured Liver Tissue, Stem Cells. 25 (2007) 1439–1447. doi:10.1634/stemcells.2006-0656.
[42] J. Rejman, V. Oberle, I.S. Zuhorn, D. HoekstOEKSTRA, Size-dependent internalization of particles via the pathways of clathrin- and caveolae-mediated endocytosis, Biochem. J. 377 (2004) 159–169. doi:10.1042/bj20031253.
[43] Z. Nizamudeen, R. Markus, R. Lodge, C. Parmenter, M. Platt, L. Chakrabarti, V. Sottile, Rapid and accurate analysis of stem cell-derived extracellular vesicles with super resolution microscopy and live imaging, Biochim. Biophys. Acta - Mol. Cell Res. 1865 (2018) 1891–1900. doi:10.1016/j.bbamcr.2018.09.008.
[44] V. Kestens, V. Bozatzidis, P.J. De Temmerman, Y. Ramaye, G. Roebben, Validation of a particle tracking analysis method for the size determination of nano- and microparticles, J. Nanoparticle Res. 19 (2017). doi:10.1007/s11051-017-3966-8.
[45] K.P.M. McComiskey, L. Tajber, Comparison of particle size methodology and assessment of nanoparticle tracking analysis (NTA) as a tool for live monitoring of crystallisation pathways, Eur. J. Pharm. Biopharm. 130 (2018) 314–326. doi:10.1016/j.ejpb.2018.07.012.
[46] M. Majka, M. Durak-Kozica, A. Kamińska, A. Opalińska, M. Szczęch, E. Stępień, The effects of subdiffusion on the NTA size measurements of extracellular vesicles in biological samples, (2017). http://arxiv.org/abs/1701.09001.
[47] Y. Wu, W. Deng, D.J. Klinke, Exosomes: Improved methods to characterize their morphology, RNA content, and surface protein biomarkers, Analyst. 140 (2015) 6631–6642. doi:10.1039/c5an00688k.
[48] V. Pospichalova, J. Svoboda, Z. Dave, A. Kotrbova, K. Kaiser, D. Klemova, L. Ilkovics, A. Hampl, I. Crha, E. Jandakova, L. Minar, V. Weinberger, V. Bryja, Simplified protocol for flow cytometry analysis of fluorescently labeled exosomes and microvesicles using dedicated flow cytometer, J. Extracell. Vesicles. 4 (2015) 1–15. doi:10.3402/jev.v4.25530.
[49] K. Takov, D.M. Yellon, S.M. Davidson, Confounding factors in vesicle uptake studies using fluorescent lipophilic membrane dyes, J. Extracell. Vesicles. 6 (2017) 1388731. doi:10.1080/20013078.2017.1388731.
[50] M. Collot, P. Ashokkumar, H. Anton, E. Boutant, O. Faklaris, T. Galli, Y. Mély, L. Danglot, A.S. Klymchenko, MemBright: A Family of Fluorescent Membrane Probes for Advanced Cellular Imaging and Neuroscience, Cell Chem. Biol. 26 (2019) 600-614.e7. doi:10.1016/j.chembiol.2019.01.009.
[51] V. Hyenne, S. Ghoroghi, M. Collot, J. Bons, G. Follain, S. Harlepp, B. Mary, J. Bauer, L. Mercier, I. Busnelli, O. Lefebvre, N. Fekonja, M.J. Garcia-Leon, P. Machado, F. Delalande, A.A. López, S.G. Silva, F.J. Verweij, G. van Niel, F. Djouad, H. Peinado, C. Carapito, A.S. Klymchenko, J.G. Goetz, Studying the Fate of Tumor

Extracellular Vesicles at High Spatiotemporal Resolution Using the Zebrafish Embryo, Dev. Cell. 48 (2019) 554-572.e7. doi:10.1016/j.devcel.2019.01.014.
[52] B. Giebel, C. Helmbrecht, Chapter 1: Methods to Analyze EVs, 2017. doi:10.1016/j.semcdb.2017.05.016.
[53] A. Cvjetkovic, J. Lo, C. La, The influence of rotor type and centrifugation time on the yield and purity of extracellular vesicles, 1 (2014) 1–11.
[54] N. Hoshyar, S. Gray, H. Han, G. Bao, The effect of nanoparticle size on in vivo pharmacokinetics and cellular interaction, Nanomedicine. 11 (2016) 673–692. doi:10.2217/nnm.16.5.
[55] B.J.C. Quah, C.R. Parish, The Use of Carboxyfluorescein Diacetate Succinimidyl Ester (CFSE) to Monitor Lymphocyte Proliferation, J. Vis. Exp. (2010) 4–7. doi:10.3791/2259.
[56] J. Lannigan, U. Erdbruegger, Imaging flow cytometry for the characterization of extracellular vesicles, Methods. 112 (2017) 55–67. doi:10.1016/j.ymeth.2016.09.018.

# Chapter 4

## 4 Quantification and Characterization of Extracellular Vesicles by Virus Counter® 3100

## 4.1 Abstract

Robust and well-established techniques for the quantification and characterization of extracellular vesicles (EVs) are a crucial need for their utilization as they emerge as a potential diagnostic and therapeutic. Current bulk analysis techniques such as proteomics and western blot suffer from low-resolution in the detection of small changes in target marker expression levels, exemplified by the heterogeneity of EVs. Microscopy-based techniques can provide valuable information from individual EVs; however, they are time consuming and statistically less powerful than other techniques. Flow cytometry has been successfully employed for the quantification and characterization of individual EVs within larger populations. However, traditional flow cytometry is not highly suited for the examination of smaller, sub-micron particles. Here we demonstrate accurate and precise quantification of nanoparticles such as EVs using the Virus Counter 3100 platform (VC3100), a fluorescence-based technique with similar principles as flow cytometry with critical enhancements to enable the effective detection of smaller particles. This approach can detect nanoparticles precisely with no evidence of inaccurate concentration measurement from masking effects associated with traditional nanoparticle tracking analysis (NTA). Fluorescently labeled EVs from different sources were successfully quantified using the VC3100 without a post-labeling washing step. Moreover, protein profiling and characterization of individual EVs was achieved and shown to determine the expression level of target protein markers.

## 4.2 Introduction

Several studies have reported an elevated EV release when cells are subjected to stress, activation, stimulation, as well as disease states such as cardiovascular disease, cancer, sepsis, and auto-immune diseases compared to the healthy cells [1–3]. EVs in biological fluids have been proposed as novel biomarkers for noninvasive detection and monitoring of diseases [2,4,5]. Therefore, precise quantification and biomarker profiling of EVs are essential to enable their potential as diagnostic and therapeutic tools.

EVs are highly heterogeneous with respect to size, cells of origin, composition, and surface protein expression [6–8]. Due to their small size and heterogeneity, quantitative and qualitative analysis of EVs remains challenging using bulk analysis techniques such as proteomics, lipidomics, and Western blot. For example, bulk analysis techniques are incapable of detecting small changes to target markers for example. Moreover, the detected differences in the target expression may be related to the number of EVs tested [6,9–12]. A preferred alternative would be the quantification and characterization of EVs on a single particle basis. Visualization based techniques such as electron microscopy (EM) and atomic force microscopy (AFM) have been used to characterize EVs [13–15]. However, these techniques are time-consuming and are not sufficiently statistically powerful [6,7,12]. Nanoparticle tracking analysis (NTA) is the most widely used technique for determining the size and concentration of EVs [16–18]. Nevertheless, NTA as a scattering based technique is less accurate and precise with heterogeneous sample populations such as EVs and is incapable of discriminating contaminants such as protein aggregates from true individual EVs [12,19–21]. In recent years, high-resolution flow cytometry

has been developed to detect nano-sized particles [10,11,22]. However, the scattering-based analysis by flow cytometry can lead to incorrect measurements due to the confounding issues of coincidence and swarm detection caused by the simultaneous presence of multiple EVs within the analysis window [10,21]. Additionally, the small size of EVs and their low refractive indices make their detection from the high background instrument noise challenging [12,20,23]. Fluorescent-based detection of EVs using flow cytometry has been employed to better resolve EVs from the background noise and is independent of size and refractive index [5,24]. However, the unincorporated fluorescent dyes post labeling can contribute to the background noise and consequently adversely affect the signal to noise ratios [22,24,25]. Therefore, a sensitive, reliable, and high throughput technique is needed to precisely quantify and characterize EVs.

The Virus Counter 3100 platform (VC3100) is a powerful, automated, and fluorescence-based technique originally developed explicitly for the quantification and characterization of viruses [26,27]. As viruses and extracellular vesicles share many common features, we were interested in determining if the VC3100 could be adapted to the study of EVs [28]. Here, we demonstrate that the VC3100 can be used for accurate quantification and biomarker profiling of EVs, where an assay does not require washing to remove unbound fluorescent reagents. We compare the performance of the VC3100 and NTA and find that the VC3100 is not prone to small particle masking by larger particles that we observe with NTA analysis. We further studied the effect of coincidence and swarm detection on the measured concentration to verify the analysis of individual nanoparticles. We also showed that EVs from different sources can be reliably analyzed using this dedicated flow cytometry approach.

## 4.3 Materials and Methods

### Virus Counter 3100

VC3100 was purpose-built for the detection of viruses. It uses the principle of hydrodynamic focusing to align particles in a narrow core for interrogation by laser light. The emitted light from fluorescent particles passing the laser spot is captured in photomultiplier tubes and time stamped (**Figure 4.1**). Unique design features that support nanoparticle detection include a sample flow rate that is orders of magnitude lower than what is used in conventional flow cytometry; a core stream that is half to a third of conventional instruments; and a laser that is an order of magnitude higher in power than conventional cytometry, all combined with other unique design features. The detection limits of the VC3100 are $5\times10^5$ - $1\times10^9$particles/mL.

### Virus Counter 3100 measurement of nanoparticles

For each test, 300 µL of the prepared nanoparticles samples (ThermoFisher) were run through the flow cell of the VC3100 instrument equipped with a 532 nm laser line. Three independent replicates of each sample were tested (n=3) for 60 seconds each.

### Nanoparticle tracking analysis measurement of nanoparticles

For each analysis run, 300 µL of the prepared samples were injected into the sample chamber of an NS300 instrument (NanoSight, Amesbury, UK) equipped with a 532 nm laser line. Three measurements of each sample were performed for 30 seconds each. Three independent replicates of each sample were tested (n=3). For the "Blur," "Minimum expected particle size," and "Minimal track lengths," the stock auto adjustment settings provided with the instrument

software were employed. The camera level (13) and detection threshold (5) were kept constant between measurements. For data capturing and analysis, the NTA analytical software (NanoSight NTA 3.2) was used.

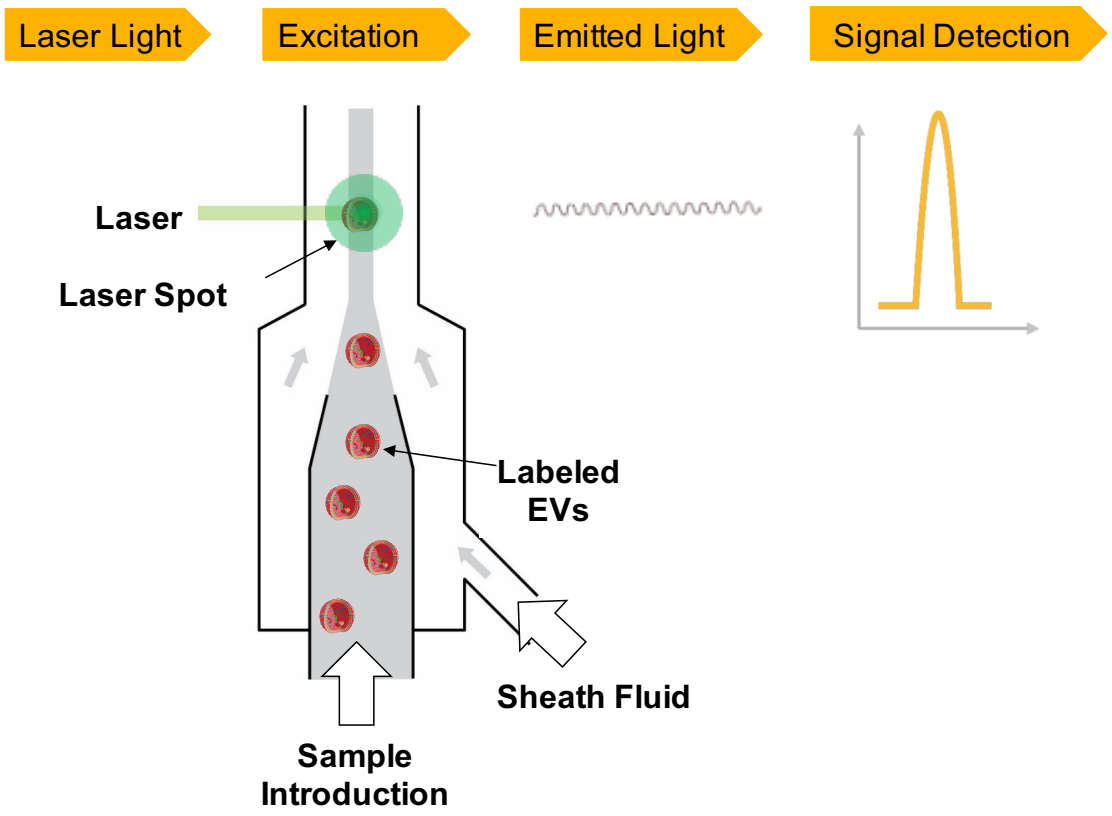


**Figure 4.1 - Schematic Showing the Working Principle of the Virus Counter 3100.**

## Serial dilution experiments

3-fold serially diluted samples of 50, 100, and 200 nm polystyrene nanoparticles were prepared in the concentration range of $5\times10^{7}$ - $5\times10^{9}$ for NTA and $5\times10^{5}$ - $5\times10^{9}$ for VC3100. For each sample, 3 independent replicates with a total volume of 300 µL were tested.

## Mixture of Nanoparticles experiments

Stocks samples with the same concentrations of 50, 100, 200 nm polystyrene nanoparticles (ThermoFisher) were made. Different ratios of mixtures of nanoparticles were subsequently added together in PBS with the final concentration of 300 µL. For example, 50 µL of 50, 100, and 200 nm nanoparticles (same concentrations) were added to 150 µL PBS.

## Extracellular Vesicles Samples

Lyophilized exosome standards from biofluids (plasma, serum, urine, and saliva) of healthy donors and exosomes derived from conditioned cell culture medium (HEK293 and mouse cell line B16F10), were used from HansaBioMed, Estonia. 1 mL of deionized water was added to 100 µg lyophilized standard to a final protein concentration of 0.1 µg/µL. The exosome samples were then resuspended by repeated pipetting. The reconstituted standards were mixed by vortex for 60 seconds. Following a brief centrifugation step, the samples were then aliquoted into polypropylene vials and stored at -20° C for up to 6 months.

## CellMask Orange Labeling

CellMask orange (CMO) plasma membrane stain (5 mg/mL) was purchased from ThermoFisher. The CMO stock was diluted 1000 times to a final concentration of 5 µg/mL. 10 µL of EVs from stock ($2.5\times10^{11}$) were added to 10 µL of 1000X diluted CMO (5 µg/mL) and were incubated for 30 minutes. 10 µL of the labeled EVs were then added to 290 µL of PBS and analyzed on the VC3100.

## Detergent Treatment Experiment

5 µL of CMO dye (1000X or 5 µg/mL) was added to 10 µL of EVs ($5\times10^9$) from different sources of EVs. After 30 minutes of incubation at room temperature, 85 µL of PBS was added. 45 µL of CMO labeled EVs were treated with 5 µL of 10% Triton-X100 or PBS as the untreated control for on ice. After an hour of incubation on ice, 5 µL of the untreated and detergent treated samples were added to 195 µL of PBS and then measured by the VC3100.

## Immunofluorescent labeling of EVs

PE-conjugated CD9 (Clone MEM-61), PE-conjugated CD63 (Clone H5C6), PE-conjugated CD81 (Clone JS-81), and PE-conjugated mouse IgG1, *k* (Clone MG1) were all purchased (Novus Biologicals, Littleton, Co). 5 µL of 50 µg/mL PE-conjugated antibodies against CD9, CD63, CD81 and the isotype control were added to 10 µL of EVs ($2\times10^{10}$). The mixture was incubated for 2 hours at 37 °C and was diluted 100 times prior to the analysis on the VC3100.

## Statistical Analysis

GraphPad Prism version 8.0 (GraphPad software) was used for all statistical analyses. Paired two-tailed Student's t-tests were performed to determine the significance of the differences in the measured concentrations. Differences with P values below 0.05 were considered statistically significant.

## 4.4 Results

### 4.4.1 Performance of VC3100 in the Detection of Polystyrene Nanoparticles

A guideline was recently published as a framework for standardized reporting of extracellular vesicles flow cytometry experiments [29]. As recommended by the guideline, serial dilution of the samples is a requisite assay controls to establish individual nanoparticles detection on an instrument. Serial dilutions of 200, 100 and 50 nm polystyrene (PS) nanoparticles were measured in the VC3100. The serial dilution plots of PS nanoparticles could be defined by three regions (**Figure 4.2**); **a) The linear region;** The nanoparticles samples maintained a linear count consistent with the dilution factor indicating the detection of single PS nanoparticles by the VC3100 in this region. **b) The coincidence region;** The nanoparticles counts were no longer linear in relation to the dilution factor anymore and reached a plateau. In this region, two or more nanoparticle were present in front of the laser and were counted as one event leading to an underestimation of the sample's concentrations. **c) The swarm region;** The samples concentrations were high enough such that a large number of particles entered the laser spot simultaneously. As a result, the baseline values failed to restore to the PBS to control levels. This resulted in consistently elevated baseline values. At high sample concentrations, the core stream was saturated with nanoparticles, leading to a reduction in the measured concentration by the VC3100. These results demonstrate that the VC3100 is capable of individual nanoparticles detection from both the ability to demonstrate a linear correlation with dilution but also in fact that the signal is saturable.

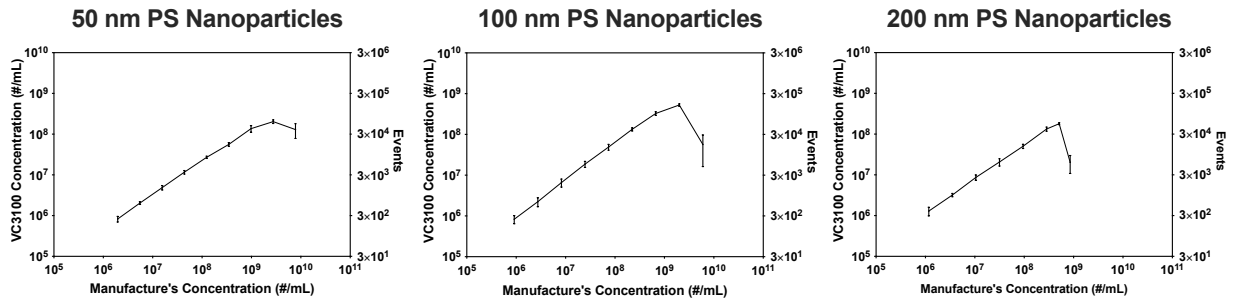


**Figure 4.2 - Serial Dilution of 50, 100, 200 nm Polystyrene (PS) Nanoparticle to Evaluate the Performance of VC3100 in the Linear and Saturable Enumeration of Individual Nanoparticles.**

### 4.4.2 Performance Evaluation of NTA and VC3100 for Accurate Quantification of Nanoparticles in Polydisperse Samples

Nanoparticle Tracking Analysis (NTA) is the most widely used technique in the extracellular vesicles (EVs) field for enumeration and sizing of nanoparticles in suspension. We evaluated and compared the performance of NTA and VC3100 for precise measurements of nanoparticles. Since NTA is a scattering based technique, refractive index (RI) of the nanoparticles plays an important role in the brightness of measured nanoparticles. Nanoparticles with higher RI (1.59) such as polystyrene (PS) nanoparticles lead to a stronger scattering signal. Therefore, It is essential to use suitable reference materials with similar refractive index as EVs to compare the performance of different techniques. We used silica nanoparticles with the RI of 1.46 as the reference nanoparticles provide the most appropriate surrogate of EVs (RI of 1.4) [30–32]. The size distribution of the nanoparticles was first characterized by scanning electron microscopy (SEM) and NTA (**Figure 4.3**). The nanoparticle samples (200, 100, and 50 nm) are not perfectly monodispersed, and variations in their size were observed using both SEM and NTA.

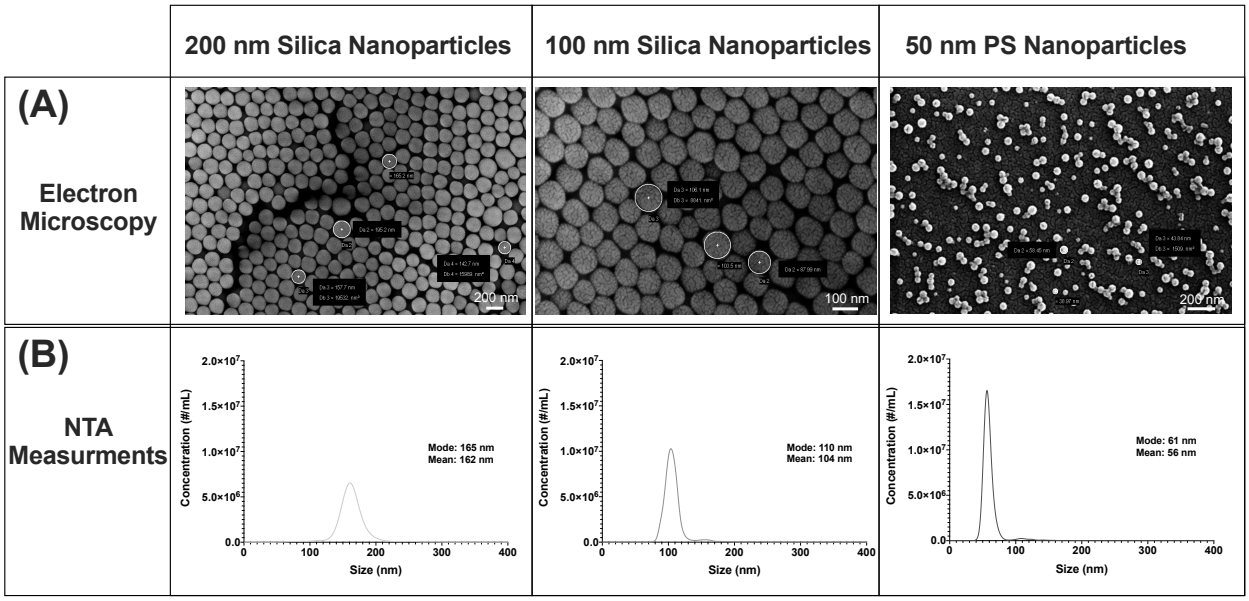


**Figure 4.3 - Size Characterization of 200 and 100 nm Silica Nanoparticles and 50 nm Polystyrene (PS) Nanoparticles.**

**(A)** Scanning electron microscopy images and **(B)** Size distribution using nanoparticle tracking analysis (NTA).

In addition to the refractive index, the brightness of the scattering particles in NTA depends on nanoparticles' size. The scattering intensity of nanoparticles is proportional to the sixth power of their diameter [18,33]. Therefore, for nanoparticles with equal refractive indices, smaller particles scatter less light and are harder to detect compared to larger ones (**Figure 4.4-A**). NTA is designed to give the operator the power to obtain accurate measurements by several adjustment steps such as camera level during the video recording and tracking analysis. The effect of camera level on the concentration of 200, 100, and 50 nm nanoparticles was evaluated by systematically changing the camera level while keeping the other parameters constant.

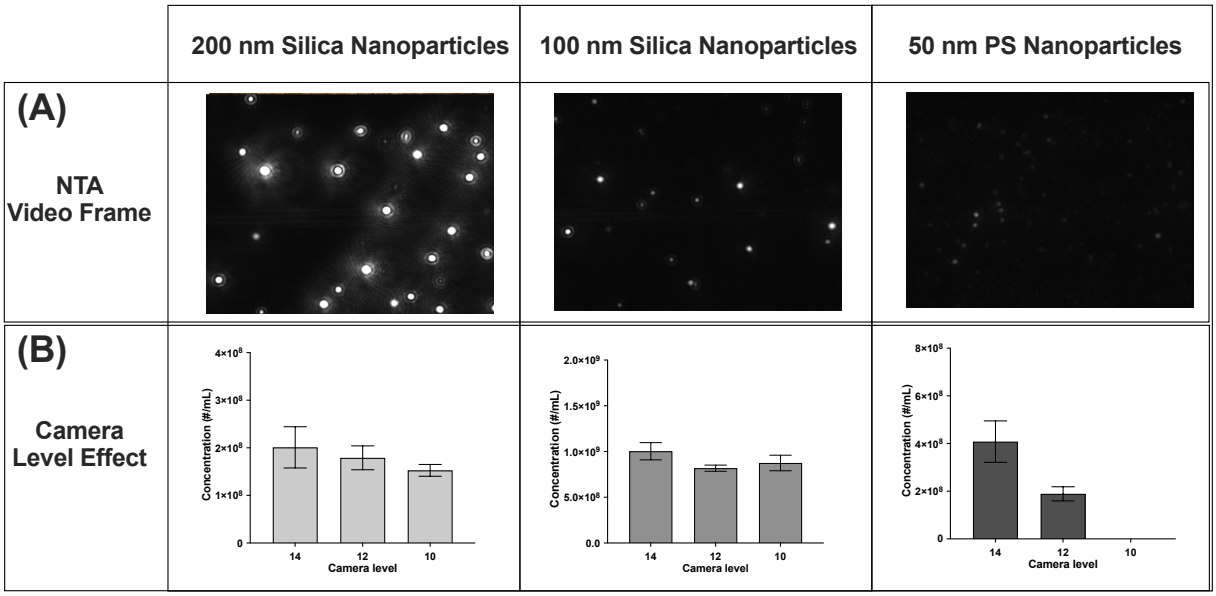


**Figure 4.4 - Effect of Camera Level on Detection of 200 and 100 nm Silica Nanoparticles and 50 nm Polystyrene (PS) Nanoparticles.**

(**A**) Nanoparticle tracking analysis (NTA) video frame and (**B**) Quantitative analysis of the camera level effect on the detection of nanoparticles.

Adjustments to the camera level did not have any significant effect on the detected concentration of 200 and 100 nm particles (**Figure 4.4-B**). However, adjustments to the camera level revealed a concerning effect on 50 nm PS nanoparticles concentration measurements. NTA was not able to detect 50 nm PS nanoparticles when the camera level was decreased to 10. The 200 and 100 nm nanoparticles scatter sufficient light such that changes to the camera level does not significantly affect the measured concentration. However, 50 nm nanoparticles scatter much less light compared to larger particles so the adjusted camera level plays an essential role in the measured concentration. This result illustrates the importance of the camera level in the detection of smaller EVs. It is important to note that NTA (CL 10) is not able to detect 50 nm PS nanoparticles with higher RI, which are even brighter than EVs.

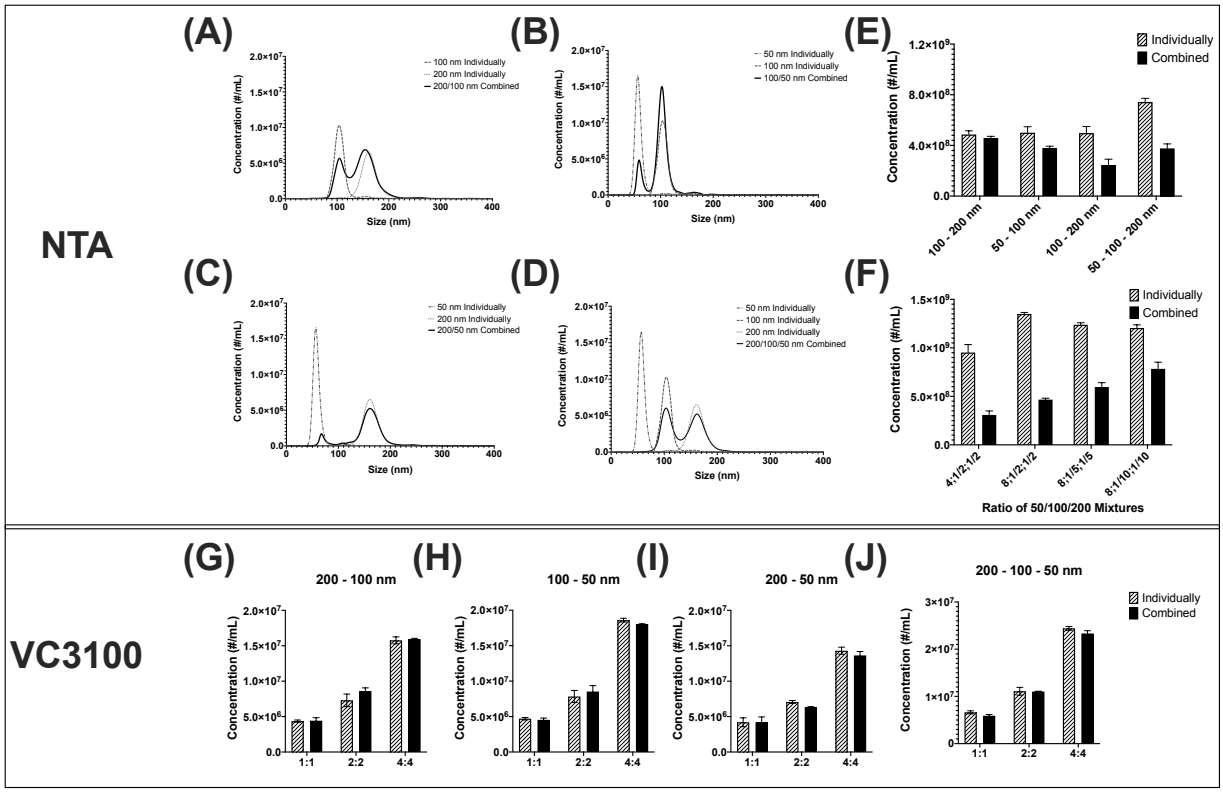


**Figure 4.5 - Performance Comparison of NTA and VC3100 for Accurate Quantification of Nanoparticles in Polydisperse Samples.**

NTA plots of mixtures with 1 to 1 ratio of **(A)** 200 and 100 nm nanoparticles, **(B)** 100 and 50 nm nanoparticles, **(C)** 200 and 50 nm nanoparticles, and **(D)** 200, 100, and 50 nm nanoparticles. **(E)** Quantitative analysis of different mixtures of nanoparticles with 1 to 1 ratio. **(F)** Quantitative analysis of mixtures of 200, 100, and 50 nanoparticles with different ratios. Quantitative analysis of mixtures of nanoparticles with different ratios using the VC3100 **(G)** 200 and 100 nm nanoparticles, **(H)** 100 and 50 nm nanoparticles, **(I)** 200 and 50 nm nanoparticles, and **(J)** 200, 100, and 50 nm nanoparticles.

The performance of NTA for measuring the concentration of polydisperse samples was evaluated. Mixtures of 200/100, 100/50, and 200/50 nm at a 1:1 ratio were first measured using the same instrument settings. In all 3 samples, the NTA failed to measure the concentration of smaller nanoparticles in the mixture accurately (**Figure 4.5**). This is due to a phenomenon that is referred to as the "masking effect". The intense light scattering of larger nanoparticles makes the smaller nanoparticles more challenging to detect and prevents some of them from being tracked by the software (**Figure 4.5-[A-C]**) [16,32,34]. This masking effect

was significant in the mixtures with 50 nm nanoparticles (**Figure 4.5-A, B, and C**). Quantitative analysis of the concentrations individually and combined illustrated inaccuracy in the resulting concentration measurements (**Figure 4.5-E**). In fact, the 50 nm nanoparticles were barely detected in the 200/50 nm mixture. In the next iteration, a mixture of 50/100/200 nm nanoparticles with a 1:1:1 ratio was measured using the same instrument settings. The masking effect was observed again and 50 nm nanoparticles were barely detectable in the mixture of 3 different size nanoparticles by NTA (**Figure 4.5-D**).

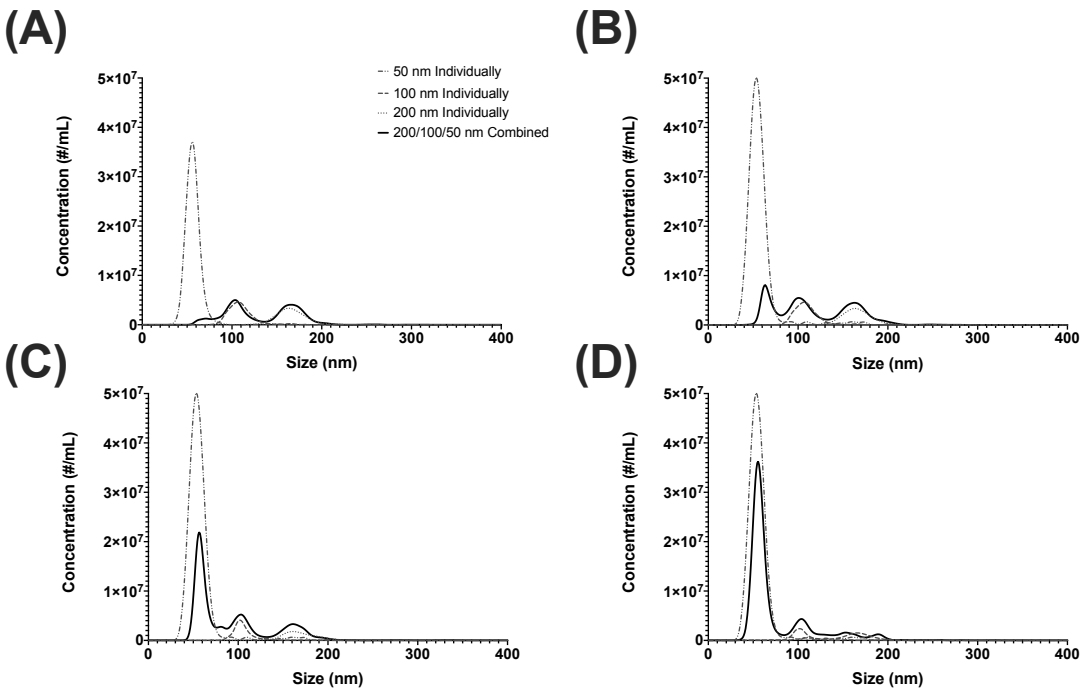


**Figure 4.6 - Masking Effect in Different Ratios of 200,100, 50 nm Nanoparticles Mixtures.**

Mixture of 50; 100; 200 nm nanoparticles with **(A)** 4;1/2;1/2, **(B)** 8;1/2;1/2, **(C)** 8;1/5;1/5, and **(D)** 8;1/10;1/10 ratios.

We hypothesized that if the reason for masking was the presence of larger nanoparticles, by increasing the ratio of 50 nm nanoparticles to 100 and 200 nm particles then the masking effect should be less significant. To test this hypothesis, the ratio of nanoparticles in the mixture was systematically changed, and the samples were measured by NTA. The concentration of 50 nm nanoparticles was increased while the concentrations of 100 and 200 nm nanoparticles were systematically decreased. By increasing the ratio of 50 nm to 100 and 200 nm nanoparticles, signals from 50 nm nanoparticles increased and at high ratios approached the expected concentration values (**Figure 4.6**). However, even as the number of 50 nm nanoparticles approached 80 times the levels of 100 and 200 nm particles, they were still not fully represented by NTA (**Figure 4.5-F**).

Similar to NTA, the performance of the VC3100 for the concentration measurements of polydisperse samples was also evaluated. Initially, mixtures of 2 different size nanoparticles with different ratios were first tested. In all samples tested, the concentrations in polydisperse samples demonstrated an accurate enumeration of particles within different mixed ratios (**Figure 4.5-[G-I]**). Subsequently, samples with 50, 100, and 200 nm nanoparticles in 4 separate ratios were tested on the VC3100. The concentration analysis of samples individually and combined showed no evidence of underestimation of the concentration (**Figure 4.5-J**). In aggregate, and in contrast to NTA, measurements using the VC3100 did not appear to be affected by the masking effect. These data support the VC3100 as a powerful platform for more accurate quantification of nanoparticles in polydisperse samples.

### 4.4.3 Quantification of Extracellular Vesicles by VC3100

In this study, commercially available purified EV samples derived from urine of healthy donors were purchased and tested. As the VC3100 is a fluorescence-based technique, quantification can only be achieved by labeling EVs with a fluorescent dye compatible with the system. Urinary EVs were labeled by CellMask Orange (CMO), a lipophilic dye that labels the lipid membrane of EVs and were analyzed on the VC3100 in a no-wash assay. In this assay, with proper controls, CMO labeled urinary EVs were successfully quantified by the VC3100 without conducting a washing step. To confirm the detection of individual vesicles, the EV samples were serially diluted and their concentrations were measured using the VC3100. Similar to PS nanoparticles, a linear count consistent with the dilution was observed, indicating the successful enumeration of individual EVs (**Figure 4.7-A**). For concentrations near the upper detection limit of the VC3100, the sample counts were lower than predicted due to the coincidence. Finally, in the swarm region, the measured concentration of EVs dropped when the core stream was saturated with EVs as expected (**Figure 4.7-A**).

Next, the utility of the VC3100 for measuring EVs from different sources was evaluated. Purified EVs derived from urine, serum, saliva, plasma, HEK293 conditioned medium, and B16F10 mouse cell line. EVs from different sources of EVs were successfully quantified by the VC3100 (**Figure 4.7-*B***). As suggested by "MIFlowCyt-EVs; a framework for standardized reporting of extracellular vesicle flow cytometry experiment," published in 2020 [29], different assay controls were examined to support the hypothesis of single vesicle detection. Isolated EV samples from different sources can be contaminated with non-EV complexes and have the potential to be

labeled and counted as positive EV events. Therefore, Triton X-100 was used to lyse their phospholipid membranes to determine whether the measured events were membrane-enclosed vesicles or other non-EV complexes. Here, CMO labeled EVs were lysed with 1% Triton X-100 and were measured by the VC3100. For all sources of EVs tested, the number of detected events dropped to the lower detection limit of the VC3100, supporting the hypothesis that intact membrane-enclosed vesicles were being enumerated prior to the treatment (**Figure 4.7 and Figure 4.8**).

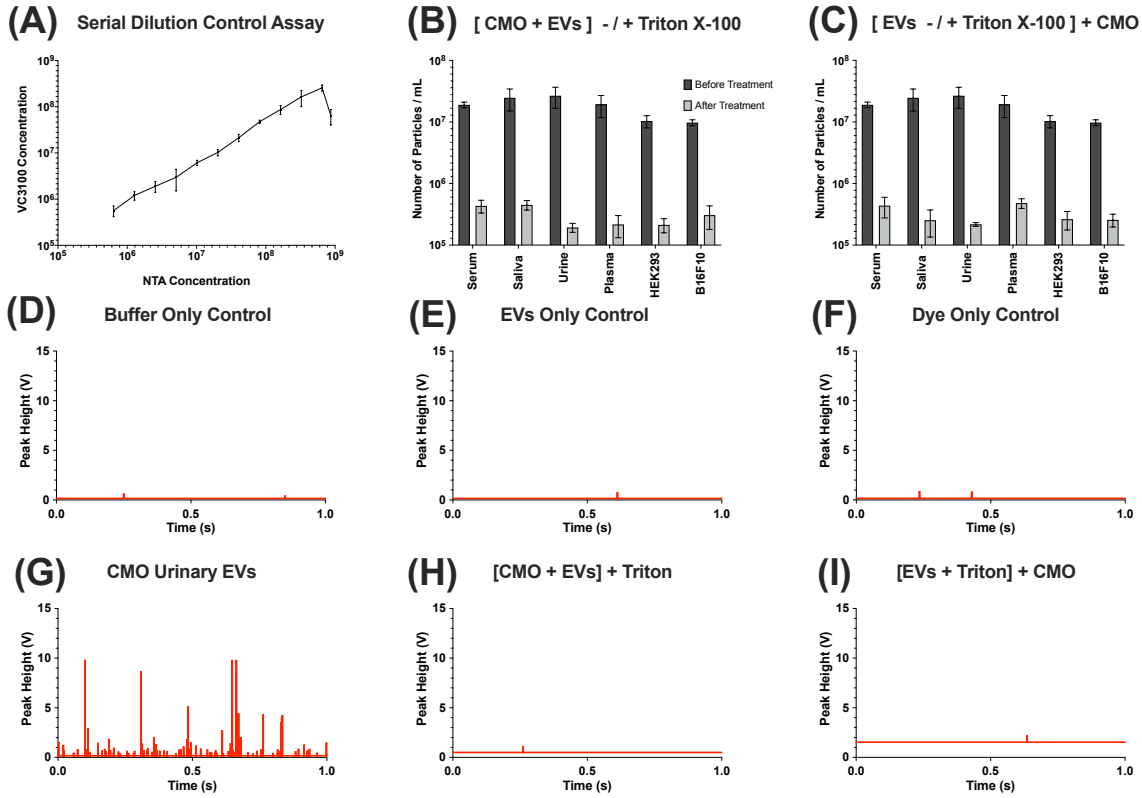


**Figure 4.7 - Quantification of Extracellular Vesicles from Different Sources by the VC3100.**

**(A)** Serial dilution of urinary EVs labeled with CMO. **(B)** Detection of CMO labeled EVs from different sources before and after treatment with 1% Triton X-100. **(C)** CMO labeling of treated EVs with 1% Triton X-100. Peak histogram of **(D)** Buffer only control, **(E)** EVs only control, **(F)** CMO only control, (G) CMO labeled EVs from urine, **(H)** Triton X-100 treating of CMO labeled EVs, and **(I)** CMO labeling of Triton X-100 treated EVs.

To evaluate the possibility of confounding membrane fragments with intact EVs, unlabeled EVs were also treated by Triton-X100 and then labeled with CMO (**Figure 4.7-C**). Similarly, the number of detected events decreased to the same level as controls, which demonstrated that the VC3100 could only detect intact CMO labeled EVs. The peak histograms from 1 second of the measurements are illustrated for; the buffer only (**Figure 4.7-D**), EVs only (**Figure 4.7-E**), CMO dye only (**Figure 4.7-F**), CMO urinary EV sample (**Figure 4.7-G**), Triton X-100 treated CMO labeled EVs (**Figure 4.7-H**), and CMO labeled Triton X-100 EVs (**Figure 4.7-I**).

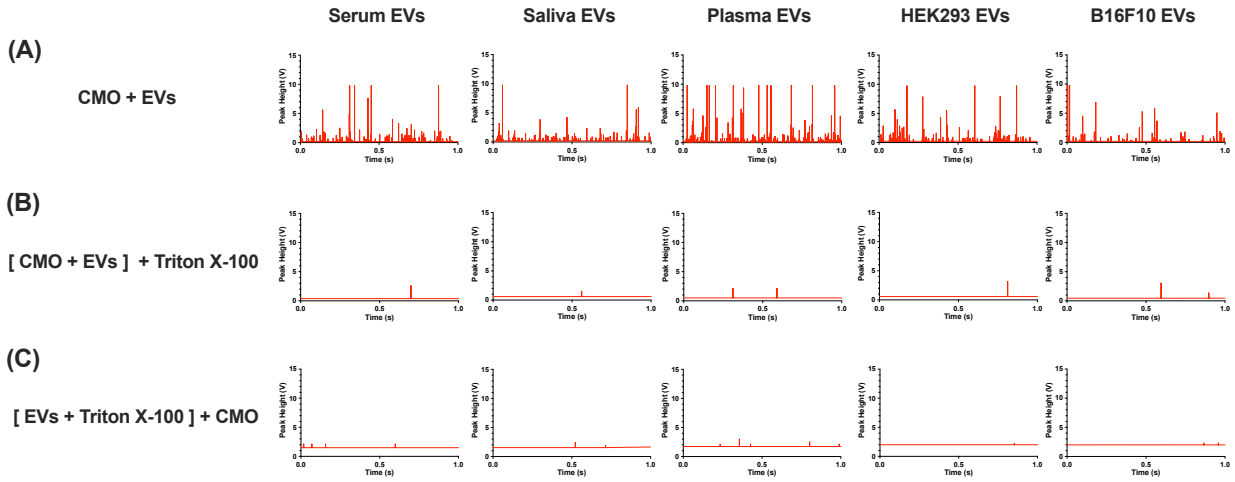


**Figure 4.8 - Triton X-100 Treatment of EVs from Different Sources.**

Peak histogram of **(A)** CMO labeled EVs from different sources, **(B)** Triton X-100 treating of CMO labeled EVs from different sources, and **(C)** CMO labeling of Triton X-100 treated EVs from different sources.

### 4.4.4 Protein Profiling of Individual EVs by VC3100

In addition to quantification of EVs by CMO labeling, they can be further characterized using fluorochrome-conjugated antibodies. This allows identifying marker expression level and analyzing different subsets of EVs. Purified urinary EVs were labeled using phycoerythrin (PE) conjugated monoclonal antibodies against three different tetraspanins; CD9, CD63, and CD81 as common exosome markers. As previously proposed, control experiments such as buffer only, unlabeled EVs, and PE conjugated antibodies only (**Figure 4.9**) were tested to confirm that the detected events are individual EVs and not false positive signals.

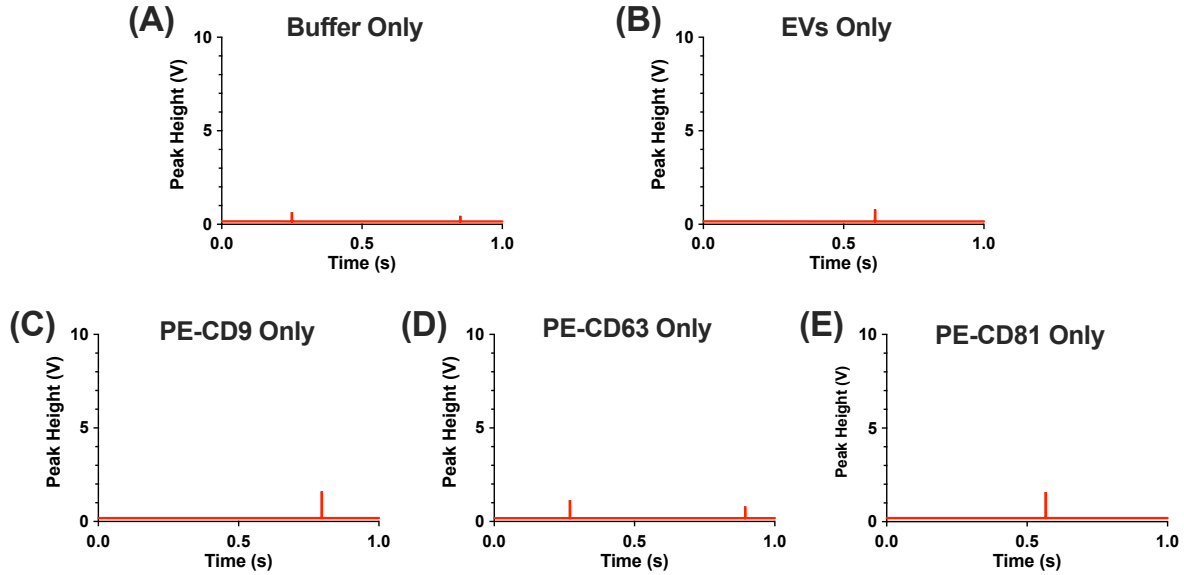


**Figure 4.9 - Control Samples for Protein Profiling of Extracellular Vesicles.**

Peak histograms of **(A)** Buffer only control, **(B)** EVs only control, **(C)** PE-CD9 antibody only control, **(D)** PE-CD63 antibody only control, and **(E)** PE-CD81 antibody only control.

Subpopulations of EVs were effectively identified by the VC3100 without a post labeling washing step. The peak histograms of isotype control only and PE conjugated labeled urinary EVs are illustrated in **Figure 4.10-[A-D].** The number of positive events were well above the

tested controls such as isotype control antibody labeling. The total number of urinary EVs was quantified by CMO labeling and the expression levels of different tetraspanins were identified; 27.4 % were found to express the CD63 surface protein, 5.3 % positive for CD81 and 4.3 % for CD9 (**Figure 4.10-E**). To further confirm the detection of individual PE conjugated antibody labeled EVs, a dilution series of urinary EVs in two-fold steps was evaluated. The number of positive events detected of PE-CD63 labeled urinary EVs, decreased proportionally with the dilution factor, and resulted in the same calculated concentration at each dilution (**Figure 4.10-F**). Therefore, the VC3100 can be successfully used for protein profiling of heterogenous EV samples with no washing step to remove the unbound dyes.

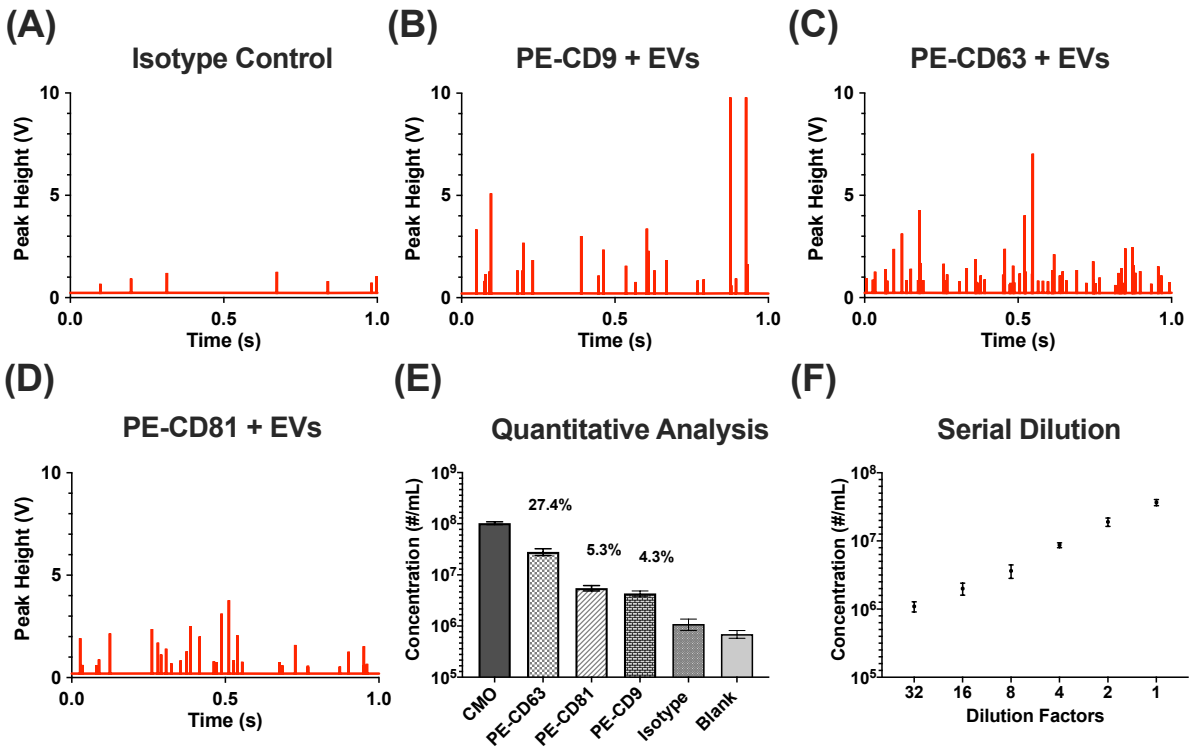


**Figure 4.10 - Protein Profiling of EVs by VC3100.**

Peak histogram of **(A)** Isotype control sample, **(B)** PE-CD9 positive urinary EVs, **(C)** PE-CD63 positive urinary EVs, and **(D)** PE-CD81 positive urinary EVs. **(E)** Quantitative analysis of tetraspanins positive urinary EVs. **(F)** Serial dilution of PE-CD63 positive urinary EVs.

## 4.5 Discussion

Flow cytometry based approaches hydrodynamically focus the sample flow in the center of sheath fluid to focus particles to pass the laser spot one by one. However, at high concentrations, two or more nanoparticles can pass the laser spot spontaneously, especially when the samples concentrations are unknown. As a result, the signals is detected as single event and separate events are no longer distinguishable. This phenomena is known as coincidence or swarm which leads to inaccurate concentration measurements and is one of the main challenges in flow cytometry approaches for quantifying and analyzing nanoparticles [5,24,25]. In order to study this phenomena, serial dilution has been proposed as the appropriate control assay [29]. We evaluated the possibility of random coincidence and swarm detection in the Virus Counter 3100 using 200, 100, and 50 nm PS nanoparticles. We found that event counts were proportional to the dilution factors in the linear region ($5\times10^5$ - $5\times10^8$ particles/mL) suggesting the detection of individual nanoparticles. However, as the samples concentrations approached the upper detection limit of the VC3100, random coincidence was observed due to the presence of two or more nanoparticles in front of the laser leading to underestimation of the concentration measurements. For even higher concentrations of nanoparticles, the core stream was saturated with nanoparticles and elevated baseline values were observed. This led to a drop in the concentration of the samples and caused inaccurate measurements (**Figure 4.2**). Therefore, serial dilution is an important and necessary control assay for confirming the detection of individual nanoparticles in flow cytometry based approaches.

Nanoparticle tracking analysis (NTA) has been extensively used in the EV field for determining the size and concentration of nanoparticles. NTA uses laser light scattering microscopy with a charge-coupled device (CCD) camera. In short, after introducing the sample into the system, the movement of particles is recorded from scattered light. The scattering centers of the particles are tracked simultaneously but individually by the software. Based on the Brownian motion of the particles, the diffusion coefficient of each tracked particle is calculated. Using the Stokes-Einstein equation, the software calculates and reports the size of tracked particles, assuming they are spherical. The concentration of nanoparticles in the sample is reported based on the number of tracked particles in the recorded video [16,32,34].

We compared the performance of NTA with VC3100 using reference nanoparticles. Polystyrene (PS) nanoparticles are commonly used as the reference material for EVs in comparison studies as well as calibration in flow cytometry. However, because EVs have a refractive index (RI) of 1.4, it has been suggested that silica nanoparticles, with RI of 1.46, maybe better suited as the appropriate reference materials as an alternative to PS nanoparticles (RI 1.59).[41–43] Therefore, 200 and 100 nm silica nanoparticles were used as the reference nanoparticles. It's important to mention that 50 nm polystyrene nanoparticles were used due to the challenges in manufacturing silica nanoparticles smaller than 100 nm.

Different parameters need to be adjusted to optimize detection of nanoparticles using NTA. These parameters can be divided into video recording and tracking analysis categories. Camera level (CL) is one of the video recording parameters that can be adjusted by the operator. This defines the sensitivity of the camera. Detection threshold (DT) is adjusted after the recording and before analysis. This establishes the minimum intensity required to establish the detected

event as a particle. In other words, the DT separates the signal from the noise.[29,44] The effect of the camera level on the detection of nanoparticles was systematically evaluate. The adjustment of the camera level did not have any significant effect on the detection of 200 and 100 nanoparticles. However, 50 nm nanoparticles were not detected by NTA when the camera level was decreased to 10 (**Figure 4.4**). This can lead to variations in measurements between samples to samples and also shows that NTA is an operator dependent technique.

We evaluated the performance of NTA for accurate measurements of nanoparticles in polydisperse samples using mixtures of 200, 100 and 50 nm nanoparticles. We found that NTA measurements are affected by the masking effect caused by the presence of larger nanoparticles in polydisperse samples leading to inaccurate measurements. In all samples tested, 50 nm nanoparticles were not accurately detected by NTA due to the masking effect caused by the presence of larger nanoparticles in polydisperse samples (**Figure 4.2 and Figure 4.6**). The observed inaccurate measurements by NTA is concerning when precise quantification of heterogenous EV samples is needed. As opposed to NTA, VC3100 showed precise and accurate measurements of nanoparticles with no evidence of the masking effect suggesting that the VC3100 is a reliable technique for quantification of nanoparticles in heterogenous samples such as EVs (**Figure 4.2**).

As the VC3100 is a fluorescence-based technique, quantification can only be achieved by labeling EVs with a fluorescent dye compatible with the system. Fluorescent dyes can be categorized into three types; lipid membrane dyes, luminal dyes and protein labeling dyes. Lipid membrane dyes such as the PKH family have been extensively used as a generic marker in the field for uptake, biodistribution and characterization studies [15,35,36]. However, in recent

years, a couple of studies have shown artifacts such as formation of PKH nanoparticles which are indistinguishable in terms of size and fluorescent intensity from PKH labeled EVs which can lead to false positive signals [22,35]. In addition, it has been recently shown that PKH labeling can affect the physical properties of EVs and results in an increase in the size of labeled EVs which may affect the uptake, biodistribution and characterization results [37]. CellMask Orange is a lipophilic dye that has been used for labeling EVs and fluoresces when inserted into a lipid-membranes. Cornell-Morris *et al.* showed that CellMask Orange (CMO) dye can be used for analysis of EVs by NTA using the instrument's fluorescence mode [38]. The authors further found that CMO does not affect the size of EVs compared to unlabeled EVs by NTA and unlike the PKH family, does not form micelles.

In recent years, several studies have utilized high sensitivity fluorescent based flow cytometry for analyzing EVs. However, one of the biggest challenges in fluorescence mode is the contribution of light from unbound dye molecules to the background signal which can decrease the signal to noise ratio [22,24,25]. Therefore, flow cytometry analysis of EVs typically requires a post labeling washing step to remove the unbound dye molecules for accurate analysis. Different techniques such as ultracentrifugation [35], density gradient [5,24], size exclusion chromatography [22], and filtration [39–41] can be used for removing the excess dye from fluorescently labeled EV samples. However, the washing steps are time consuming and expensive and can cause sample loss and aggregation of EVs.[21]

CMO labeled EVs derived from different sources such as plasma, urine, saliva, serum, HEK293 conditioned media and B16F10 mouse cell line were successfully quantified by the VC3100 with no washing assay. In order to confirm the detection of individual EVs, different control assays

were performed such as serial dilution of CMO labeled EVs. Control samples such as buffer only, CMO dye only, and unlabeled EVs only showed a concentration below the lower limit of the VC3100. Detergent treatment control is another important assay to confirm the detection of membrane enclosed vesicles. CMO labeled EVs were treated by 1% Triton-X100 and measured by the VC3100. The number of detected events for EV samples from all sources tested significantly dropped after the treatment, confirming that the lipid membrane particles were detected before the treatment (**Figure 4.7 and Figure 4.8**).

Specific subtypes of EVs may play important roles in distinct functions. For instance, surface proteins of EVs such as tetraspanins (CD9, CD63, and CD81) are involved in uptake of EVs by the recipient cell, protection of them from phagocytosis, and their circulation clearance. However, since EVs are highly heterogenous in size and surface proteins, changes in the expression level of a specific marker could be easily masked in bulk analysis.[7,9] Therefore, a fast, specific, reliable technique is required for protein profiling of EVs in diagnostic and therapeutic applications.

The fluorescent intensity due to surface marker labeling depends on *(i)* the expression level of the target proteins, *(ii)* the efficiency of the labeling process, *(iii)* the light source excitation strength and the fluorescent dye quantum yield.[42–45] Successful protein profiling of urinary EVs labeled with PE-conjugated tetraspanins (CD9, CD63, and CD81) was further observed by the VC3100 with necessary control assays such as the isotype control (**Figure 4.9 and Figure 4.10**). This result suggests that the VC3100 can be used for accurate and standardized quantification and phenotype analysis of EVs as an important factor for biomarker profiling and

therapeutic applications. In summary, this study has determined the VC3100 as a highly reliable and sensitive technique for the robust quantification and characterization of EVs (**Figure 4.11**).

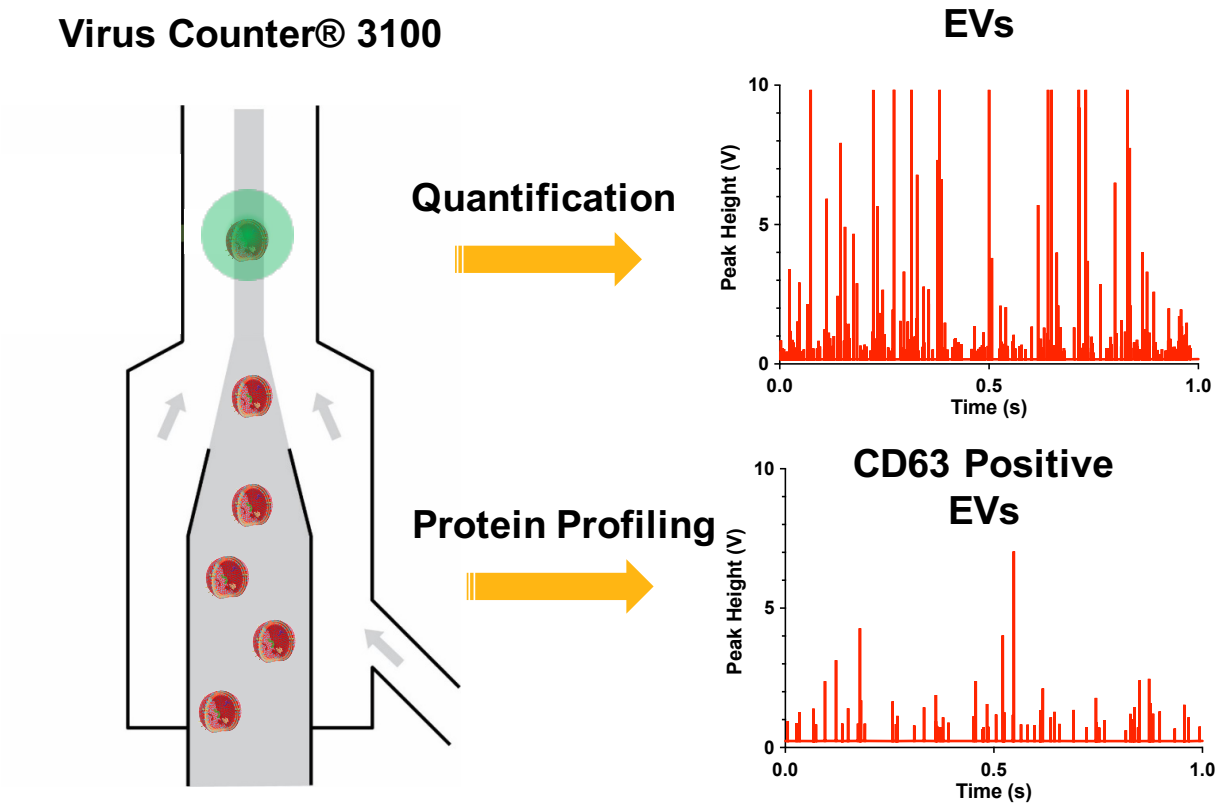


**Figure 4.11 – Virus Counter 3100 for Quantification and Characterization of EVs**

## 4.6 Future Directions

### 4.6.1 Multiparametric Analysis

VC3100 is capable of detecting nanoparticles on two fluorescent channels, therefore, as a future direction, multiparametric analysis can be performed to investigate the co-expression of CD9, CD63, and CD81. This can help to better understand the phenotype of EVs and can provide valuable information for biomarker profiling regarding the heterogeneity of EVs.

### 4.6.2 Sizing by VC3100

Particle size and distribution of nanoparticles such as EVs are one of the important physical properties that are involved in uptake and biodistribution studies. Conventional transmission electron microscopy (TEM) have been widely used for studying the size and morphology of EVs. However, the sample preparation steps before imaging such as dehydration, chemical fixation and staining can affect the size and morphology of EVs. Cryo-electron microscopy is more reliable than conventional EM and does not require the mentioned sample preparation steps, hence preserves the physical properties of EVs. However, imaging techniques such as EM and AFM are not statistically powerful [14].

Single EV analysis techniques such as flow cytometry and NTA have been used for determining size. However, EVs are below the detection range of these techniques due to their small size and low refractive index. It is not clear if all sizes of EVs can be successfully detected by flow cytometry. The smallest size nanoparticles detected varies from system to system or it hasn't been reported in many of flow cytometry based studies. Van der pol et al. investigated the

minimum detectable vesicle size of widely used techniques in the field [32]. The authors reported that the minimum detectable vesicle sizes were 270-600 nm for conventional flow cytometry and 150-190 for dedicated flow cytometry for detection of sub-micrometer particles. In this aim, we also showed that masking effect is a major challenge in quantification of nanoparticles in heterogenous samples such as EVs by NTA. Since NTA cannot detect all of EVs, therefore the size distribution results are misinterpreted and inaccurate.

In the last aim, we found that nanoparticles can be quantified accurately and precisely by the Virus Counter 3100. Another potential of the VC3100 that needs to be explored in detail, is the capability of this technique for identifying the size of nanoparticles. This can be achieved by analyzing the raw data from the detected events. Particularly, peak characteristics, such as peak height and width, can be correlated to nanoparticles' physical properties, such as size. Proof of concept experiments showed promising results in order to identify the size of nanoparticles by the VC3100, which are fully explained here;

#### 4.6.2.1 Peak Height

Peak height represents the intensity of a signal from a detected event and the peak height's unit is voltage. We first studied and compared the peak height values in monodisperse samples of 50, 100, and 200 nm nanoparticles. The Peak height frequency plots of these nanoparticles can be seen in **Figure 4.12** with a bin width set to 0.5 V. In monodisperse samples of these nanoparticles, the peak height values were different, suggesting that peak height can be used to distinguish between particles in a mixture sample.

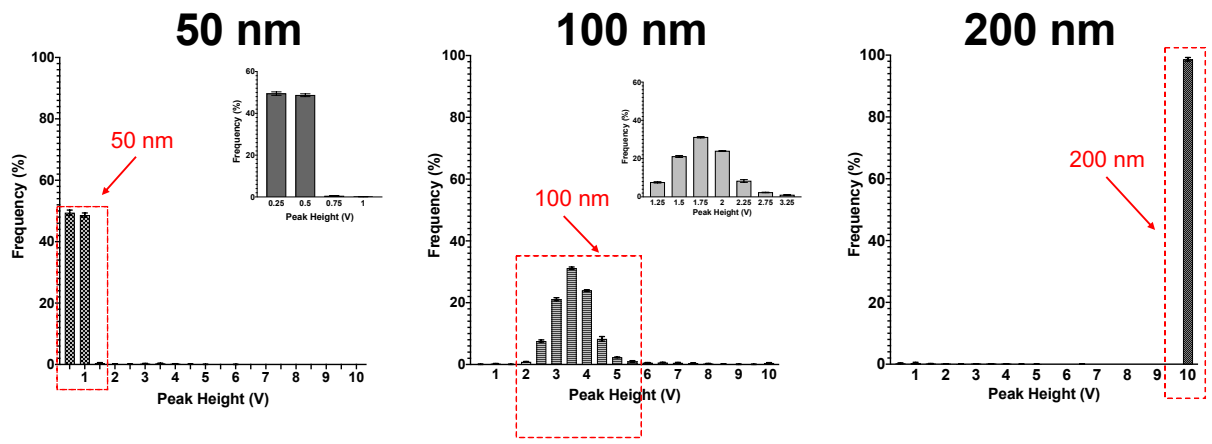


**Figure 4.12 - Peak Height Values in Monodisperse Samples of 50, 100, and 200 nm Nanoparticles.**

In order to test this hypothesis, mixtures of two nanoparticles with one to one ratios were made and the peak height values were studied. As shown in **Figure 4.13**, in all these mixtures tested, two distinguished peaks can be observed and correlated to different size nanoparticles. Quantitative analysis of the samples also showed no significant difference between individual and combined samples.

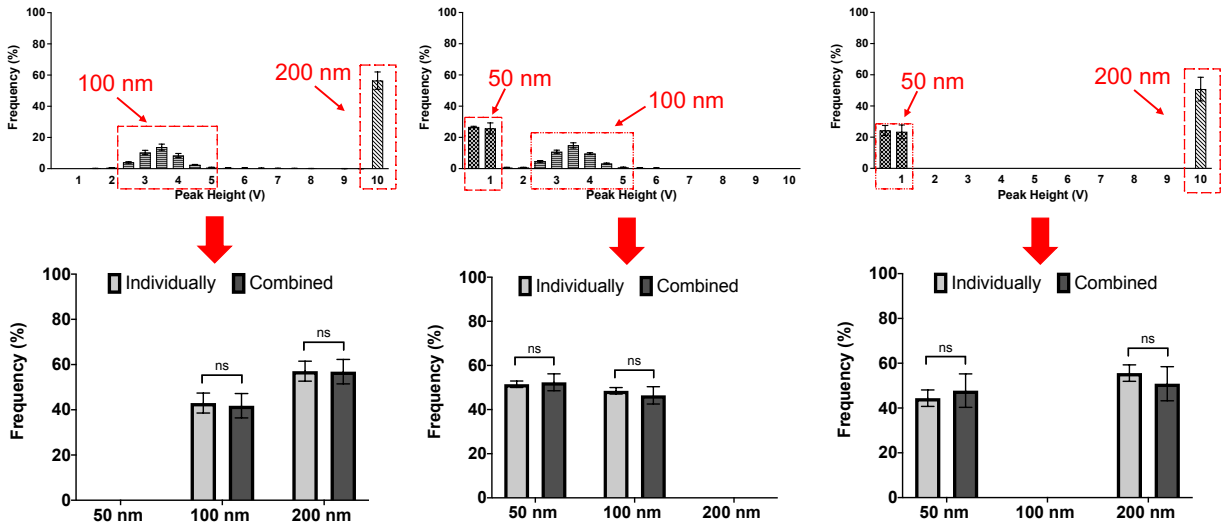


**Figure 4.13 - Peak Height Values in Mixture Samples of Two Nanoparticles.**

Furthermore, A mixture of all three nanoparticles (200, 100 and 50 nm) with the same concentrations was also tested (**Figure 4.14**). Similarly, observing three distinguished peaks in the histogram and no significant difference in quantitative analysis suggested that peak height can be used for determining the size of nanoparticles. It is important to note that the peak height value depends on the size of nanoparticles and the number of fluorescein dye molecules per particle.

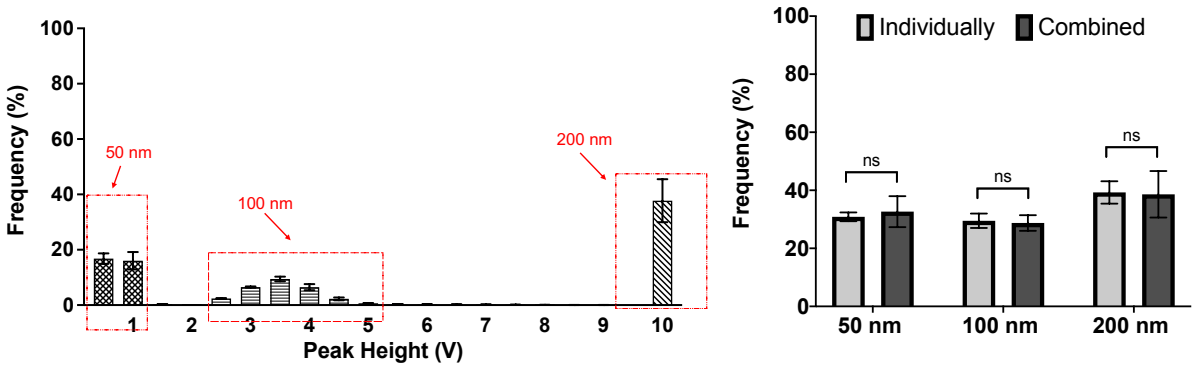


**Figure 4.14 - Peak Height Values in Mixture Samples of Three Nanoparticles.**

### 4.6.2.2 Peak Width

A better alternative to the peak height is the peak width. Peak width's unit is second which represents the amount of time that a particle spends in front of the laser (dwelling time). The bigger the nanoparticles, the broader the peaks are, therefore, peak width can directly represent the size of nanoparticles. Similar set of experiments was performed, and the peak width values were studied. The peak width is the amount of time that a particle travels in front of the laser. The peak width values in monodisperse samples of 50, 100, and 200 nm nanoparticles can be found in **Figure 4.15**.

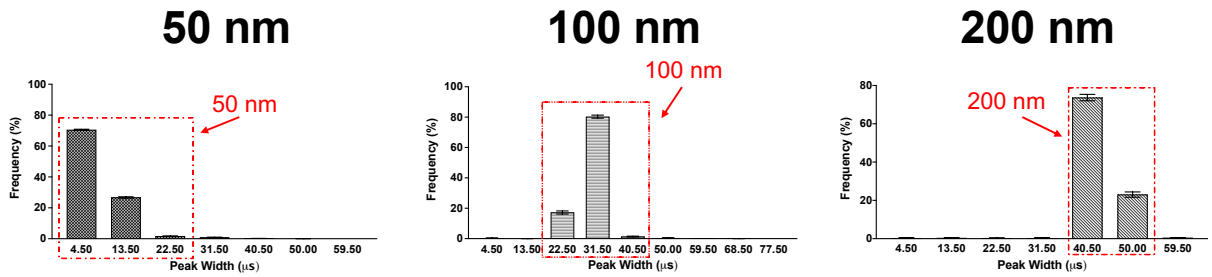


**Figure 4.15 - Peak Width Values in Monodisperse Samples of 50, 100, and 200 nm Nanoparticles.**

When mixtures of 2 nanoparticles were tested, different size of nanoparticles were easily distinguished based on their peak width values (**Figure 4.16**). Similarly, peak histogram and quantitative analysis of the mixture of all nanoparticles suggested that peak width values can be correlated to the size of nanoparticles.

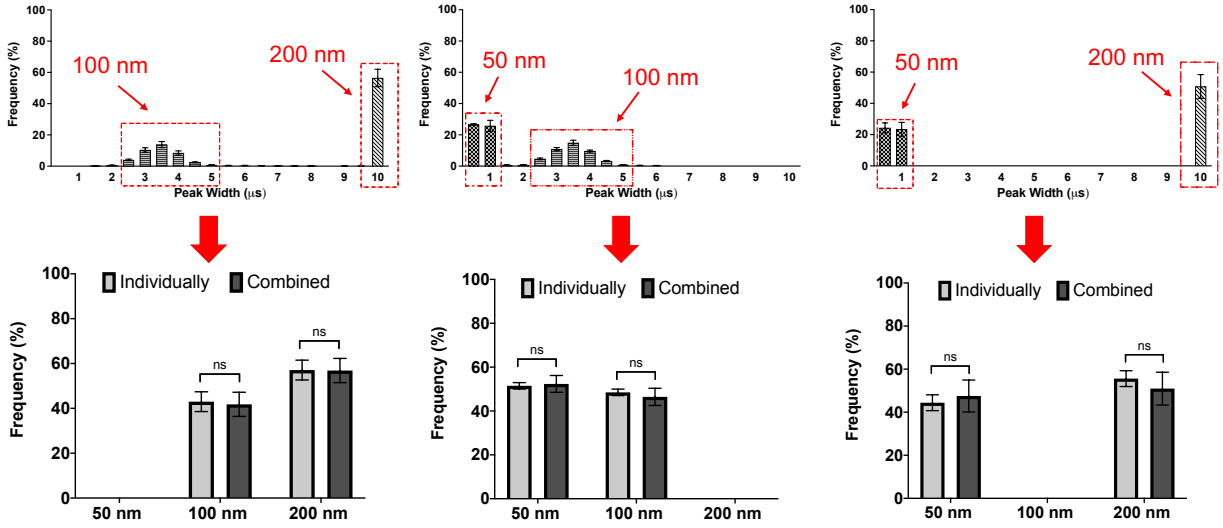


**Figure 4.16 - Peak Width Values in Mixture Samples of Two Nanoparticles.**

Similarly, the mixtures of 3 nanoparticles (50/100/200 nm) were made and tested by the VC3100. The peak width values in the mixtures were evaluated and different size of nanoparticles were distinguishable (**Figure 4.17**).

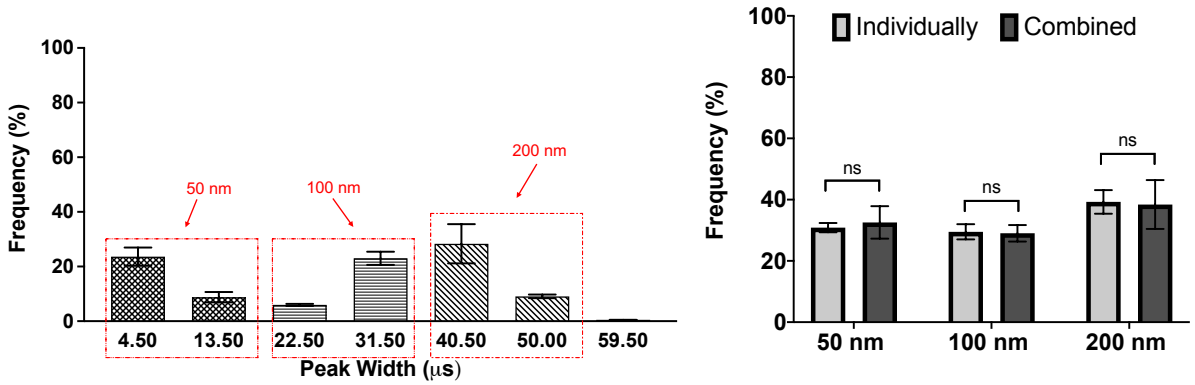


**Figure 4.17- Peak Width Values in Mixture Samples of Three Nanoparticles.**

### 4.6.2.3 Proposed Set of Experiments

To examine the performance of the VC3100 in identifying size of nanoparticles, a series of monodisperse silica fluorescent nanoparticles of different sizes ranging from 20 to 300 nm could be purchased and used as the size reference materials. The size of the nanoparticles will be first characterized by electron microscopy and NTA. Then, the fluorescent nanoparticle samples could be tested individually first, and their peak width and height could be determined. A calibration curve could be obtained by correlating the size of fluorescent nanoparticles to the peak height and width values. As the next step, different mixtures of these nanoparticles with known ratios could be made and tested by the VC3100. Comparing the peak height and width values of nanoparticles individually and combined, the feasibility of the VC3100 for sizing could be fully confirmed, as the preliminary results suggested.

Similar to this proposed set of experiment, Tian et al. recently developed a high sensitivity flow cytometry (HSFCM) which was used successfully for protein profiling and sizing of EVs [7]. The authors examined the performance of HSFCM for sizing of nanoparticles using a series of monodisperse silica nanoparticles (47, 59, 74, 94 and 123 nm). Since, the HSFCM is a scattering

based technique, the authors had to correct the deviation induced by the refractive index mismatch between silica nanoparticles and EVs to make the calibration curve. But this should not be a problem for sizing using the VC3100 since this technique is fluorescence based.

## 4.7 Conclusion

The missing element in current solutions used to enumerate and characterize EVs lies in the fact that there is no one platform that provides the holistic data required for full characterization. This would include the combined attributes of pan enumeration of EVs or exosomes, differential sizing and enumeration of those sub-populations within different preparations of EVs, multi-parametric phenotypic analysis, measures of cargo and, finally, controls to exclude cell fragments. Expanded probes and especially measure of cargo may represent the most pressing needs. Achieving this requires surmounting the challenges that are presented by the small size and heterogeneity of EVs. In this study, we tested the capability of the flow cytometry-based nanoparticle analyzer, Virus Counter 3100, in the combined areas of enumeration of particles as small as 50 nm (in the absence of scatter), compatibility with polydisperse samples, and compared this to the gold standard in the field, NTA. We expanded on this to include a pan EV stain as well as phenotypic measure of some of the more common exosome markers. First, the detection and enumeration of individual nanoparticles (50 to 200 nm) was confirmed by studying serially diluted samples. Appropriate sample dilution was shown to be critical to avoid coincidence and swarm detection caused by high sample concentration. The performance of the VC3100 was then compared to NTA and the former successfully demonstrated accurate quantification of nanoparticles in polydisperse samples such as EVs. NTA demonstrated issues for accurate measurements of mixture samples due to the masking effect of smaller nanoparticles from the presence of larger ones. In other studies, EVs from six different sources were fluorescently labeled by CellMask Orange and were successfully quantified by the VC3100

without a post labeling washing step. Additionally, the expression level of tetraspanins (CD9, CD63, and CD81) were effectively measured using the VC3100. Future work with alternative probes could potentially label cargo as well as surface antigens using this methodology. These results suggest that the VC3100 is an emerging technology that may be further refined to provide information on sizing, to expand on the number of parameters simultaneously measured, to ultimately emerge as a technology capable of simultaneously addressing a number of desired parameters.

## 4.8 Acknowledgments and Funding

I would like to acknowledge the Sartorius, Virus Analytics team (Arvada, CO) for providing technical advice and support, particularly, I would like to thank Dr. Rebecca K. Montange and Dr. Michael W. Olszowy. I would also like to thank Dr. David Pollard, the head of advanced materials and processing (corporate research, Sartorius) for his supervision during my internship.

## 4.9 References


[1] L. König, S. Kasimir-Bauer, A.K. Bittner, O. Hoffmann, B. Wagner, L.F. Santos Manvailer, R. Kimmig, P.A. Horn, V. Rebmann, Elevated levels of extracellular vesicles are associated with therapy failure and disease progression in breast cancer patients undergoing neoadjuvant chemotherapy, Oncoimmunology. 7 (2017) 1–9. doi:10.1080/2162402X.2017.1376153.

[2] A. Dickhout, R.R. Koenen, Extracellular Vesicles as Biomarkers in Cardiovascular Disease; Chances and Risks, Front. Cardiovasc. Med. 5 (2018) 1–9. doi:10.3389/fcvm.2018.00113.

[3] L.A. Mulcahy, R.C. Pink, D.R.F. Carter, Routes and mechanisms of extracellular vesicle uptake, J. Extracell. Vesicles. 3 (2014). doi:10.3402/jev.v3.24641.

[4] H. Kalra, G.P.C. Drummen, S. Mathivanan, Focus on extracellular vesicles: Introducing the next small big thing, Int. J. Mol. Sci. 17 (2016). doi:10.3390/ijms17020170.

[5] T.G. Kormelink, G.J.A. Arkesteijn, F.A. Nauwelaers, G. van den Engh, E.N.M. Nolte-'t Hoen, M.H.M. Wauben, Prerequisites for the analysis and sorting of extracellular vesicle subpopulations by high-resolution flow cytometry, Cytom. Part A. 89 (2016) 135–147. doi:10.1002/cyto.a.22644.

[6] E.J. van der Vlist, E.N.M. Nolte-'t Hoen, W. Stoorvogel, G.J.A. Arkesteijn, M.H.M. Wauben, Fluorescent labeling of nano-sized vesicles released by cells and subsequent quantitative and qualitative analysis by high-resolution flow cytometry., Nat. Protoc. 7 (2012) 1311–1326. doi:10.1038/nprot.2012.065.

[7] Y. Tian, L. Ma, M. Gong, G. Su, S. Zhu, W. Zhang, S. Wang, Z. Li, C. Chen, L. Li, L. Wu, X. Yan, Protein Profiling and Sizing of Extracellular Vesicles from Colorectal Cancer Patients via Flow Cytometry, ACS Nano. 12 (2018) 671–680. doi:10.1021/acsnano.7b07782.

[8] H.C. Inglis, A. Danesh, A. Shah, J. Lacroix, P.C. Spinella, P.J. Norris, Techniques to improve detection and analysis of extracellular vesicles using flow cytometry, Cytom. Part A. 87 (2015) 1052–1063. doi:10.1002/cyto.a.22649.

[9] K. Lee, K. Frase, B. Ghaddar, K. Yang, E. Kim, L. Balaj, E.A. Chiocca, X.O. Breakefield, H. Lee, Ralph Weissleder, Multiplexed Profiling of Single Extracellular Vesicles, Physiol. Behav. 176 (2017) 139–148. doi:10.1016/j.physbeh.2017.03.040.

[10] S.A. Stoner, E. Duggan, D. Condello, A. Guerrero, J.R. Turk, P.K. Narayanan, J.P. Nolan, High sensitivity flow cytometry of membrane vesicles, Cytom. Part A. 89 (2016) 196–206. doi:10.1002/cyto.a.22787.

[11] V. Pospichalova, J. Svoboda, Z. Dave, A. Kotrbova, K. Kaiser, D. Klemova, L. Ilkovics, A. Hampl, I. Crha, E. Jandakova, L. Minar, V. Weinberger, V. Bryja, Simplified protocol for flow cytometry analysis of fluorescently labeled exosomes and microvesicles using dedicated flow cytometer, J. Extracell. Vesicles. 4 (2015) 1–15. doi:10.3402/jev.v4.25530.

[12] E.N.M.N. t. Hoen, E.J. van der Vlist, M. Aalberts, H.C.H. Mertens, B.J. Bosch, W. Bartelink, E. Mastrobattista, E.V.B. van Gaal, W. Stoorvogel, G.J.A. Arkesteijn, M.H.M. Wauben, Quantitative and qualitative flow cytometric analysis of nanosized cell-derived membrane vesicles, Nanomedicine Nanotechnology, Biol. Med. 8 (2012) 712–720. doi:10.1016/j.nano.2011.09.006.

[13] P. Parisse, I. Rago, L. Ulloa Severino, F. Perissinotto, E. Ambrosetti, P. Paoletti, M. Ricci, A.P. Beltrami, D. Cesselli, L. Casalis, Atomic force microscopy analysis of extracellular vesicles, Eur. Biophys. J. 46 (2017) 813–820. doi:10.1007/s00249-017-1252-4.

[14] Y. Yuana, R.I. Koning, M.E. Kuil, P.C.N. Rensen, A.J. Koster, R.M. Bertina, S. Osanto, Cryo-electron microscopy of extracellular vesicles in fresh plasma, J. Extracell. Vesicles. 2 (2013) 21494. doi:10.3402/jev.v2i0.21494.

[15] S.T.Y. Chuo, J.C.Y. Chien, C.P.K. Lai, Imaging extracellular vesicles: Current and emerging methods, J. Biomed. Sci. 25 (2018) 1–10. doi:10.1186/s12929-018-0494-5.

[16] D. Bachurski, M. Schuldner, P.H. Nguyen, A. Malz, K.S. Reiners, P.C. Grenzi, F. Babatz, A.C. Schauss, H.P. Hansen, M. Hallek, E. Pogge von Strandmann, Extracellular vesicle measurements with nanoparticle

tracking analysis–An accuracy and repeatability comparison between NanoSight NS300 and ZetaView, J. Extracell. Vesicles. 8 (2019) 1596016. doi:10.1080/20013078.2019.1596016.

[17] C.Y. Soo, Y. Song, Y. Zheng, E.C. Campbell, A.C. Riches, F. Gunn-Moore, S.J. Powis, Nanoparticle tracking analysis monitors microvesicle and exosome secretion from immune cells, Immunology. 136 (2012) 192–197. doi:10.1111/j.1365-2567.2012.03569.x.

[18] V. Filipe, A. Hawe, W. Jiskoot, Critical evaluation of nanoparticle tracking analysis (NTA) by NanoSight for the measurement of nanoparticles and protein aggregates, Pharm. Res. 27 (2010) 796–810. doi:10.1007/s11095-010-0073-2.

[19] V. Sunkara, H.K. Woo, Y.K. Cho, Emerging techniques in the isolation and characterization of extracellular vesicles and their roles in cancer diagnostics and prognostics, Analyst. 141 (2016) 371–381. doi:10.1039/c5an01775k.

[20] A. Görgens, M. Bremer, R. Ferrer-Tur, F. Murke, T. Tertel, P.A. Horn, S. Thalmann, J.A. Welsh, C. Probst, C. Guerin, C.M. Boulanger, J.C. Jones, H. Hanenberg, U. Erdbrügger, J. Lannigan, F.L. Ricklefs, S. El-Andaloussi, B. Giebel, Optimisation of imaging flow cytometry for the analysis of single extracellular vesicles by using fluorescence-tagged vesicles as biological reference material, J. Extracell. Vesicles. 8 (2019). doi:10.1080/20013078.2019.1587567.

[21] N. Arraud, C. Gounou, D. Turpin, A.R. Brisson, Fluorescence triggering: A general strategy for enumerating and phenotyping extracellular vesicles by flow cytometry, Cytom. Part A. 89 (2016) 184–195. doi:10.1002/cyto.a.22669.

[22] A. Morales-Kastresana, B. Telford, T.A. Musich, K. McKinnon, C. Clayborne, Z. Braig, A. Rosner, T. Demberg, D.C. Watson, T.S. Karpova, G.J. Freeman, R.H. Dekruyff, G.N. Pavlakis, M. Terabe, M. Robert-Guroff, J.A. Berzofsky, J.C. Jones, Labeling extracellular vesicles for nanoscale flow cytometry, Sci. Rep. 7 (2017) 1–10. doi:10.1038/s41598-017-01731-2.

[23] J.P. Nolan, S.A. Stoner, A trigger channel threshold artifact in nanoparticle analysis, Cytom. Part A. 83 A (2013) 301–305. doi:10.1002/cyto.a.22255.

[24] S.F.W.M. Libregts, G.J.A. Arkesteijn, A. Németh, E.N.M. Nolte-'t Hoen, M.H.M. Wauben, Flow cytometric analysis of extracellular vesicle subsets in plasma: impact of swarm by particles of non-interest, J. Thromb. Haemost. 16 (2018) 1423–1436. doi:10.1111/jth.14154.

[25] L. De Rond, E. Van Der Pol, C.M. Hau, Z. Varga, A. Sturk, T.G. Van Leeuwen, R. Nieuwland, F.A.W. Coumans, Comparison of generic fluorescent markers for detection of extracellular vesicles by flow cytometry, Clin. Chem. 64 (2018) 680–689. doi:10.1373/clinchem.2017.278978.

[26] C.L. Stoffel, R.F. Kathy, K.L. Rowlen, Design and characterization of a compact dual channel virus counter, Cytom. Part A. 65 (2005) 140–147. doi:10.1002/cyto.a.20145.

[27] M.M. Ferris, P.C. Stepp, K.A. Ranno, W. Mahmoud, E. Ibbitson, J. Jarvis, M.M.J. Cox, K. Christensen, H. Votaw, D.P. Edwards, K.L. Rowlen, Evaluation of the Virus Counter® for rapid baculovirus quantitation, J. Virol. Methods. 171 (2011) 111–116. doi:10.1016/j.jviromet.2010.10.010.

[28] E.N. Hoen, T. Cremer, R.C. Gallo, L.B. Margolis, Extracellular vesicles and viruses: Are they close relatives?, Proc. Natl. Acad. Sci. U. S. A. 113 (2016) 9155–9161. doi:10.1073/pnas.1605146113.

[29] J.A. Welsh, E. Van Der Pol, G.J.A. Arkesteijn, M. Bremer, A. Brisson, F. Coumans, F. Dignat-George, E. Duggan, I. Ghiran, B. Giebel, A. Görgens, A. Hendrix, R. Lacroix, J. Lannigan, S.F.W.M. Libregts, E. Lozano-Andrés, A. Morales-Kastresana, S. Robert, L. De Rond, T. Tertel, J. Tigges, O. De Wever, X. Yan, R. Nieuwland, M.H.M. Wauben, J.P. Nolan, J.C. Jones, MIFlowCyt-EV: a framework for standardized reporting of extracellular vesicle flow cytometry experiments, J. Extracell. Vesicles. 9 (2020). doi:10.1080/20013078.2020.1713526.

[30] C. Gardiner, M. Shaw, P. Hole, J. Smith, D. Tannetta, C.W. Redman, I.L. Sargent, Measurement of refractive index by nanoparticle tracking analysis reveals heterogeneity in extracellular vesicles, 3 (2014) 25361.

[31] S. Valkonen, E. van der Pol, A. Böing, Y. Yuana, M. Yliperttula, R. Nieuwland, S. Laitinen, P.R.M. Siljander, Biological reference materials for extracellular vesicle studies, Eur. J. Pharm. Sci. 98 (2017) 4–16. doi:10.1016/j.ejps.2016.09.008.

[32] E. van der Pol, F.A.W. Coumans, A.E. Grootemaat, C. Gardiner, I.L. Sargent, P. Harrison, A. Sturk, T.G. van Leeuwen, R. Nieuwland, Particle size distribution of exosomes and microvesicles determined by transmission electron microscopy, flow cytometry, nanoparticle tracking analysis, and resistive pulse sensing, J. Thromb. Haemost. 12 (2014) 1182–1192. doi:10.1111/jth.12602.

[33] J. Gross, S. Sayle, A.R. Karow, U. Bakowsky, P. Garidel, Nanoparticle tracking analysis of particle size and concentration detection in suspensions of polymer and protein samples: Influence of experimental and data evaluation parameters, Eur. J. Pharm. Biopharm. 104 (2016) 30–41. doi:10.1016/j.ejpb.2016.04.013.

[34] J. Wang, R. Guo, Y. Yang, B. Jacobs, S. Chen, I. Iwuchukwu, K.J. Gaines, Y. Chen, R. Simman, G. Lv, K. Wu, J.C. Bihl, The Novel Methods for Analysis of Exosomes Released from Endothelial Cells and Endothelial Progenitor Cells, Stem Cells Int. 2016 (2016). doi:10.1155/2016/2639728.

[35] P. Pužar Dominkuš, M. Stenovec, S. Sitar, E. Lasič, R. Zorec, A. Plemenitaš, E. Žagar, M. Kreft, M. Lenassi, PKH26 labeling of extracellular vesicles: Characterization and cellular internalization of contaminating PKH26 nanoparticles, Biochim. Biophys. Acta - Biomembr. 1860 (2018) 1350–1361. doi:10.1016/j.bbamem.2018.03.013.

[36] E.N.M.N. t. Hoen, E.J. van der Vlist, M. Aalberts, H.C.H. Mertens, B.J. Bosch, W. Bartelink, E. Mastrobattista, E.V.B. van Gaal, W. Stoorvogel, G.J.A. Arkesteijn, M.H.M. Wauben, Quantitative and qualitative flow cytometric analysis of nanosized cell-derived membrane vesicles, Nanomedicine Nanotechnology, Biol. Med. 8 (2012) 712–720. doi:10.1016/j.nano.2011.09.006.

[37] M. Dehghani, S.M. Gulvin, J. Flax, T.R. Gaborski, Systematic Evaluation of PKH Labelling on Extracellular Vesicle Size by Nanoparticle Tracking Analysis, Sci. Rep. 10 (2020) 1–10. doi:10.1038/s41598-020-66434-7.

[38] and R.D. Pauline Carnell-Morris, Dionne Tannetta, Agnieszka Siupa, Patrick Hole, Extracellular Vesicles, Methods and Protocols - Chapter 13; Analysis of Extracellular Vesicles Using Fluorescence Nanoparticle Tracking Analysis., 2017. doi:10.1016/j.semcdb.2017.05.016.

[39] T. Tian, Y.L. Zhu, F.H. Hu, Y.Y. Wang, N.P. Huang, Z.D. Xiao, Dynamics of exosome internalization and trafficking, J. Cell. Physiol. 228 (2013) 1487–1495. doi:10.1002/jcp.24304.

[40] M. Mireles, C.W. Soule, M. Dehghani, T.R. Gaborski, Use of nanosphere self-assembly to pattern nanoporous membranes for the study of extracellular vesicles, Nanoscale Adv. (2020). doi:10.1039/d0na00142b.

[41] M. Dehghani, K. Lucas, J. Flax, J. McGrath, T. Gaborski, Tangential Flow Microfluidics for the Capture and Release of Nanoparticles and Extracellular Vesicles on Conventional and Ultrathin Membranes, Adv. Mater. Technol. 4 (2019) 1–11. doi:10.1002/admt.201900539.

[42] H. Li, Y. Liao, L. Gao, T. Zhuang, Z. Huang, H. Zhu, J. Ge, Coronary serum exosomes derived from patients with myocardial ischemia regulate angiogenesis through the miR-939-mediated nitric oxide signaling pathway, Theranostics. 8 (2018) 2079–2093. doi:10.7150/thno.21895.

[43] C.P. Lai, E.Y. Kim, C.E. Badr, R. Weissleder, T.R. Mempel, B.A. Tannous, X.O. Breakefield, Visualization and tracking of tumour extracellular vesicle delivery and RNA translation using multiplexed reporters, Nat. Commun. 6 (2015) 1–12. doi:10.1038/ncomms8029.

[44] K. Takov, D.M. Yellon, S.M. Davidson, Confounding factors in vesicle uptake studies using fluorescent lipophilic membrane dyes, J. Extracell. Vesicles. 6 (2017). doi:10.1080/20013078.2017.1388731.

[45] L. Chen, Z. Xie, T. Gan, Y. Wang, G. Zhang, C.A. Mirkin, Z. Zheng, Biomimicking Nano-Micro Binary Polymer Brushes for Smart Cell Orientation and Adhesion Control, (2016) 3400–3406. doi:10.1002/smll.201600634.

# 5 Conclusion and Contributions

**In the first aim**, we developed a filtration based microfluidic system termed as tangential flow for analyte capture (TFAC), which is a modified version of tangential flow filtration. we observed that normal flow filtration (NFF) of undiluted plasma on ultrathin nanomembranes leads to rapid formation of a protein cake which also stops the purification process. As opposed to NFF, we found that tangential flow filtration of plasma can be used to capture extracellular vesicle (EVs) on the pores of ultrathin nanomembranes with minimal contamination. We further found that ultrathin nanomembranes are ideally suited for purification of EVs using TFAC compared to conventional thickness membranes since, 1) ultrathin nanomembranes operate with two orders of magnitude lower pressure, which minimizes concerns of damaging EVs during filtration, and 2) the 1 -10 µm thickness of conventional nanomembranes can cause trapping the nanoparticles inside the pore channels which leads to loss of sample and low yield. The performance of TFAC on NPN needs to be further optimized to increase the purification yield and purity by coating the surface of membranes to minimize non-specific interactions, recirculating EV samples, and adjusting the operating condition and device design. This project titled “Tangential Flow Microfluidics for the Capture and Release of Nanoparticles and Extracellular Vesicles on Conventional and Ultrathin Membranes” was published in the journal of *Advanced Materials Technologies* in 2019.

In another study collaborating with Dr. James McGrath and his laboratory at the University of Rochester, we further studied and compared the critical flux behavior of the track-etch membrane and ultrathin nanomembrane microfluidic devices. Studying the critical flux

behavior of ultrathin nanomembranes is essential for TFAC purification of EVs from complex biological fluids with high concentrations of proteins. We found that the ultrathin nature of NPN membranes enables 10 times higher critical flux than conventional thickness membranes under the same operating condition. This study titled “Critical Flux Behavior of Ultrathin Silicon Nanomembranes” was published in 2020 in the journal of *Separation and Purification Technology*.

Additionally, in our lab, we recently reported the fabrication of ultrathin free-standing nanoporous membranes using nanosphere lithography (NSL) which offers a pore size control over large area at an affordable cost. We evaluated the performance of NSL nanomembranes for separating a subpopulation of EVs based on size. We found an effective size cut-off of 300 nm with the majority of EVs < 200 nm, suggesting potential for studying subpopulations of EVs. The NSL technique can be extended for fabrication of nanopocket membranes, a novel type of membranes with pores patterned as a bowl like structure with a hole at the bottom. Nanopocket membranes with different dimensions can be fabricated and employed in TFAC for separation of subpopulations of EVs. This study titled “Use of Nanosphere Self-Assembly to Pattern Ultrathin Membranes for the Study of Extracellular vesicles” was published in the journal of the *Nanoscale Advances* in 2020.

**Related to the second aim**, we systematically studied the effect of PKH labeling as the most commonly used fluorescent dye, on the size of extracellular vesicles. Nanoparticle tracking analysis (NTA) was employed to determine the size of EVs before and after labeling. We found that PKH labeling does not preserve the size of EVs which can alter the uptake and biodistribution studies. As opposed to the PKH labeling, CFSE dye (luminal labeling approach)

does not affect the size of EVs after labeling and is a more reliable technique for fluorescent labeling of EVs. Therefore, more attention needs to be paid to the effect of fluorescent labeling approaches on the size of EVs. In addition to preserving the size of EVs, an ideal generic fluorescent dye molecule must label all and only EVs, have minimal background signal, have a high signal to noise ratio, and preserve the native biological behavior of EVs. This project titled "Systematic Evaluation of PKH Labeling on Extracellular Vesicles Size Using Nanoparticles Tracking Analysis" was published in 2020 in the journal of *Scientific Reports*. In another contribution related to fluorescent labeling of extracellular vesicles, we were invited to write a book chapter on fluorescent labeling approaches of EVs. This book chapter titled "Fluorescent Labeling of Extracellular vesicles" was recently accepted for publication in *Methods in Enzymology*.

**In the third aim,** since EVs and viruses share many common features, we evaluated the efficacy of a virus detection technology for EVs. Virus counter 3100 (VC3100) is a fluorescence based approach with similar principles as flow cytometry and is purposely built for detection of nanoparticles such as viruses. We found that NTA, the most commonly used technique for determining size and concentration of EVs, is not capable of precise measurements of the concentration in heterogenous samples of nanoparticles such as EVs due to the masking effect. We showed that the virus counter is superior for accurate concentration measurements in heterogeneous mixtures of particles compared to NTA. We further observed that CellMask Orange can be used to successfully quantify EVs derived from different sources without a post-labeling washing step. We also found that the virus counter is capable of protein profiling of EVs to determine their expression level. The possibility of using the virus counter for

multiparametric analysis of EVs to investigate the co-expression of markers needs to be further explored. Furthermore, the capability of this technique for determining the size of nanoparticles based on the peaks characteristics of individual events needs to be studied in details. This study titled “An Emerging Fluorescence-Based Technique for Quantification and Protein Profiling of Extracellular Vesicles” is submitted in the journal of *SLAS Technology* and is currently under review.

## 5.1 List of Publications

1. **Dehghani M**, Lucas K, Mcgrath J, Gaborski TR. Tangential Flow Microfluidics for the Capture and Release of Nanoparticles and Extracellular Vesicles on Conventional and Ultrathin Nanomembranes. Advanced Materials Technologies. 2019. 4; 1900539.
2. Lucas K, Ahmad D, **Dehghani M**, Gaborski TR, McGrath J. Critical Flux Behavior of Ultrathin Silicon nanomembranes. Separation and Purification Technology. 2020. 117342
3. mirez MM, Soule CW, **Dehghani M** and Gaborski TR. Use of Nanosphere Self-Assembly to Pattern Ultrathin Membranes for the Study of Extracellular Vesicles. Nanoscale Advances. 2020.
4. **Dehghani M**, Gulvin SM, Flax J and Gaborski TR. Systematic Evaluation of PKH labelling on Extracellular Vesicles Size Using Nanoparticles Tracking Analysis. Scientific Report. 2020. 10 (1), 1-10.

5. **Dehghani M,** Gaborski TR. Fluorescent Labelling of Extracellular Vesicles (Book Chapter). Methods in Enzymology. 2020. *(Accepted)*
6. **Dehghani M**, Montange R, Olszowy M, Pollard D. An Emerging Fluorescence-Based Technique for Quantification and Protein Profiling of Extracellular Vesicles. SLAS Technology. *(Submitted on 09/02/2020)*
7. RaPiazza N, **Dehghani M**, Gaborski TR, Wuertz-Kozak K. Therapeutic Potential of Extracellular Vesicles in Degenerative Diseases of Intervertebral Disc. Frontiers in Bioengineering and Biotechnology. 2020. 8; article 311.